Optical detection of laser-induced shock waves : investigating the physical mechanism of laser lithotripsy

Zwegers, Johnny

Award date:
1991

Technische Universiteit
Eindhoven

Faculteit der
Technische Natuurkunde

Optical detection of laser-induced shock waves

- investigating the physical mechanism of laser lithotripsy -

Johnny Zwegers July 1991

Report of a training performed at the Laser Centre of the Academic Medical Centre in Amsterdam (1990 - 1991), as graduate in physical engineering at the University of Technology in Eindhoven.

coach (Laser Centre) : dr.ir. H.J.C.M. Sterenborg
mediator (TUE) : dr.ir. C.H. Massen
supervisor (TUE) : prof.dr.ir. H.L. Hagedoorn

SAMENVATTING

De klinische relevantie van deze stage betreft de toepassing van lasers in lithotripsie, fragmentatie *in situ* van stenen in het menselijk lichaam met behulp van een laser. Er wordt verwacht dat deze techniek zich zal ontwikkelen tot een waardevolle mogelijkheid om stenen in de urine- of galwegen of in de speekselklieren te behandelen. In principe wordt met behulp van een kwarts fiber die via een endoskoop is ingebracht gepulst laser licht met een hoge intensiteit op de steen gericht. Omdat het fysisch mechanisme dat uiteindelijk leidt tot fragmentatie slecht bekend is wordt op het Laser Centrum in Amsterdam onderzoek verricht aan dit onderwerp.

De interaktie tussen laserpuls en het steenmateriaal induceert drukgolven waaraan het gewenste effect, namelijk fragmentatie, wordt toegeschreven. Een eenvoudig één dimensionaal model wordt voorgesteld om de afhankelijkheid van de drukgolven van de laserpulsenergie, van geometrische parameters zoals afstand tussen fibertip en steenoppervlak en fiberdiameter en de vloeistof waarin steen en fiber zijn ondergedompeld te verklaren.

Een optische Schlieren techniek wordt ontwikkeld om de dichtheidsgradienten in de drukgolven in de omringende vloeistof te detekteren. De waarnemingen zijn gebruikt om twee karakteristieke parameters te definieren: een drempelwaarde voor de pulsenergie en een helling, in feite een rendement.

De helling blijkt afhankelijk te zijn van de geometrische parameters en de vloeistof voor metingen in water, siliconenolie en glycerol.

In siliconenolie en glycerol blijkt de drempelenergie niet signifikant af te hangen van de geometrische parameters. Gemiddelde waarden voor de drempelenergie zijn 4.0 ± 0.3 mJ ($p = 0.95$) in siliconenolie en 5.3 ± 0.6 mJ ($p = 0.95$) in glycerol. In water is mogelijk een trend als funktie van geometrische parameters te onderscheiden maar de grote spreiding in de resultaten bemoeilijkt de interpretatie.

Het voorgestelde model kan de experimentele resultaten niet fitten. Ten eerste is het de vraag of lineaire akoestische theorie toegepast kan worden in geval van de grote viskositeit van siliconenolie en glycerol. Bovendien bestaat het vermoeden dat het fysisch mechanisme zelf afhangt van de betreffende parameters.

ABSTRACT

The clinical relevance of this work concerns the application of lasers in lithotripsy, laser-aided fragmentation *in situ* of stones in the human body. It is expected that this technique will become a valuable possibility for treatment of stones in the urinary and biliary tract and in the salivary glands. In principle a quartz fibre that is introduced via an endoscope guides pulsed laser light of high intensity onto the stone. As the physical mechanism that eventually leads to stone fragmentation is not fully understood basic research on this subject is being performed at the Laser Centre in Amsterdam.

The interaction between laser pulse and stone material induces pressure waves which are held responsible for the destructive effect. A simple one dimensional acoustic theory is proposed to predict the dependence of the pressure waves on laser pulse energy, geometrical parameters as the distance between fibre tip and stone surface and the fibre diameter, and the surrounding liquid wherein stone and fibre are immersed.

An optical Schlieren technique is developed for detection of the density gradients of the pressure waves in the surrounding liquid. From the observations two characteristic parameters are defined: a threshold for the laser pulse energy and a slope efficiency.

The slope efficiency shows to be dependent on geometrical parameters and liquid properties for measurements in water, silicone oil and glycerol.

In silicone oil and glycerol the threshold energy shows no significant dependency on geometrical parameters. Average threshold energies are 4.0 ± 0.3 mJ ($p = 0.95$) in silicone oil and 5.3 ± 0.6 mJ ($p = 0.95$) in glycerol. In water a trend with geometrical parameters might be distinguished but the large spread in results makes proper interpretation difficult.

The proposed theory cannot fit the experimental results. First the large viscosity of silicone oil and glycerol makes the applicability of linear acoustic theory questionable. Further the presumption arises that the physical mechanism itself depends on the parameters under consideration.

TABLE OF CONTENTS

SYMBOLS

Symbol	Quantity	Unit
ρ	density	kg/m^3
ρ_v	vapor density	kg/m^3
ρ_l	liquid density	kg/m^3
ρ_∞ or ρ_0	ambient density	kg/m^3
c_v	specific heat at constant volume	J/kg·K
c_p	specific heat at constant pressure	J/kg·K
γ	ratio of specific heats c_p/c_v	-
T	absolute temperature	K
T_d	dissociation temperature	K
ΔT	temperature change	K
t	time	s
t_L	laser pulse duration	s
τ_d	time needed to reach T_d	s
τ_{vbr}	time needed for vapor breakdown	s
p	pressure	Pa
p' or Δp	pressure change	Pa
p_∞ or p_0	ambient pressure	Pa
p_{ref}	reference pressure	Pa
V	volume	m^3
P	power	W
P_a	absorbed power	W
P_r	reradiative power	W
P_0	total beam power	W
P_{tr}	transmitted power	W
Φ_0	irradiance or flux	W/m^2
F	fluence	J/m^2
μ	mean molar mass	kg/mol
N	number of particles	mol
L	latent heat	J/kg
L_d	latent heat of dissociation	J/kg
λ	heat conductivity	W/m·K
κ	(thermal) diffusivity	m^2/s

c	sound velocity	m/s
δ	optical absorption length	m
λ_0	wavelength	m
α	ratio of thermal properties	-
u	(medium) velocity	m/s
a_T	thermal expansion coefficient	1/K
Z_i	acoustic impedance of medium i	$kg/m^2 \cdot s$
ϕ	velocity potential	m^2/s
$\underline{v}$	velocity	m/s
r	radial distance	m
a	bubble interface distal parameter (e.g. radius)	m
R_i	acoustic impedance per unit area	$kg/m^4 \cdot s$
h	distance between fibre and stone	m
r_f	fibre radius	m
D	fibre diameter	m
f_i	focal length of lens i	m
w	Gaussian beam radius	m
w_0	beam waist	m
α_0	beam divergence	rad
L_w	beam waist length	m
I	intensity	W/m^2
d	beam translation at razor blade	m
d	thickness of an one dimensional vapor layer	m
v_i	object distance	m
φ	deflection angle	rad
S	measured signal	-
η_{vis}	dynamic viscosity	$kg/m \cdot s$
ζ	second viscosity (coefficient)	$kg/m \cdot s$
ν	kinematic viscosity	m^2/s
E	energy	J
E_{thr}	threshold energy	J
η	slope (conversion efficiency)	J^{-1}
$(\Delta)n$	(change in) refractive index	-
$(\Delta)OPL$	(change in) optical path length	m
L	shock thickness	m
β	normalized shock thickness	-
u_s	shock velocity	m/s
u_p	particle velocity	m/s

1 INTRODUCTION

1.1 Lasers in medicine - clinical background

At the Laser Centre in Amsterdam applications and applicability of lasers in medicine are being investigated.

The characteristic features of a laser sometimes combined with the enthusiasm of clinicians enabled its introduction as a therapeutic instrument in various medical fields. One can discriminate between these applications by their basic physical mechanism that determines the light-matter interaction ([23,26,72]).

In the photo- or electromechanical regime irradiation of matter eventually leads to selective mechanical or acoustic damage. A clinical example can be found in ophtalmology where returning cataract after implantation of an artificial lens can be treated very easily with a focussed infrared laser (Nd:YAG). Another example of a reasonably accepted application is laser induced stone fragmentation, so called laser lithotripsy. The latter is subject of the present report.

Obstructive stones can occur in various sites in the human body.

The most unknown group consists of the salivary stones that develop in the salivary glands and consequently resort under maxillofacial surgery. At present the only possible therapy is surgery.

Gastroenterology is responsible for the treatment of biliary stones that appear in gall bladder and biliary duct. Sufficient treatment of these stones apart from surgery as a final option is relatively difficult. Possibilities are extracting the stone or placing a stent - a kind of bypass - with the aid of an endoscope, a device that provides the surgeon with sight *in situ*. However endoscopy, in this case insertion of the device via mouth and digestive tract, requires great skill of the endoscopist. For this reason applying laser lithotripsy leads to relatively poor success rates although *in vitro* experiments showed that biliary stones are easily fragmented with a laser ([10,26]).

The last category of stones is formed by the urinary stones which appear along the urinary tract, inside the kidney, ureter and the bladder. Possible treatments are numerous but the most common option is extracorporeal shock wave lithotripsy - ESWL. In this technique the patient is immersed in, or lies in contact with a water container. A shock wave is generated in this container and focussed onto the stone. The great resemblance of acoustic properties of water and tissue (which exists mainly of water) ensures optimal transmittance of

the shock wave. Some kind of monitoring commonly x-ray or ultrasound imaging is required in order to focus the shock onto the stone properly. The main advantages of this technique are the non-invasivity and the fact that hospitalisation is usually not required. However structures in the path of the acoustic wave with different acoustic properties like bone from the pelvis reduce the effectiveness of ESWL dramatically.

Endoscopy by insertion of a ureteroscope offers several alternative ways of treatment. The surgeon can attempt to extract the stone with a trapping device (Dormia basket or Zeiss loop) or fragment it *in situ*. In the latter case he can use an electro-hydraulic lithotripter (EHL) probe or an ultrasonic device. In both cases the stone is pushed back rather easily so one still has to trap (with a basket) or block it (with a balloon) which can be difficult for tightly impacted stones. Besides in order to pass all equipment these methods require relatively great lumina of the ureteroscope which is more traumatic to the surrounding tissue. Moreover both techniques themselves have frequently resulted in severe ureter damage.

A promising alternative is offered by laser therapy which is becoming a widely accepted treatment as an addition to ESWL. At present two laser systems have proven their applicability and reliability in clinical use. Recently the alexandrite laser has been introduced as a third option that holds great promise. A comparison of the relevant parameters can be found in table 1.1.

laser	Q-switched Nd:YAG	dye laser	alexandrite
wavelength pulse length pulse energy	1064 nm 12 ns 0 - 80 mJ	509 / 590 / 720 nm 0.5 - 3.0 µs 0 - 120 mJ	740 nm 200 ns 0 - 200 mJ
energy density at fibre tip	(600 µm fibre) 25 - 50 GW/cm^2	(200 µm fibre) 0.1 - 1.0 GW/cm^2	(...)
laser induced breakdown induction	* optomechanical (metal tip) * spherically polished fibre * optical focussing device	NO coupler needed, bare fibre contact	NO coupler needed, bare fibre contact
fibre surface	critical	uncritical	uncritical

Table 1.1. Laser systems ([8]).

The fundamental difference between the first two is obvious: contrary to the dye laser the Nd:YAG laser operates at a low absorbed wavelength and consequently some kind of coupling device and a neat fibre surface are required. Thomas et al. ([8]) reports on an optical feedback system for the dye laser which enables blind application[1]. The alexandrite laser combines the advantages of both systems: a directly absorbed wavelength and a reliable and user friendly system.

1.2 Physical background - a review

1.2.1 Observations

An overview of experimental observations including those obtained by others is given by Teng et al. ([9]). One of the observations is that laser lithotripsy appears to be very energy efficient. Sterenborg et al. ([10]) reports a fragmentation energy value of 127 ± 14 J/g for biliary stones (laser pulse length: 1.5 μs; wavelength: 504 nm; various fibre diameters ranging from 0.2 to 0.6 mm). Teng gives an indicative value of 40 J/g for one biliary stone (laser pulse length: 0.8 μs; wavelength: 690 nm; fibre diameter: 0.324 mm). The energy needed to increase the temperature of the stone material, mainly cholesterol, from room temperature to its boiling point (360 ^{0}C; specific heat: 1 J/g·K) is estimated to be 340 J/g. Even when neglecting latent melting and vaporization heat this value exceeds the fragmentation efficiency by far. Thus fragmentation is not likely to occur by simple heating and vaporization.

Teng and Nishioka ([6,9,11]) paid special attention to the observed white flash that seemed to be of major importance to the fragmentation process. Time-resolved measurements of the emission spectra led to the interpretation that the flash was caused by emission of a rapidly evolving plasma[2].

---

1 This feedback system is based on the fact that there is a difference in temporal profile of the backscattered light (at the laser wavelength) from tissue versus stone material. In this way aiming at healthy tissue is directly followed by shutting off most of the laser pulse. ([8])

2 The measurements of the emission spectra yielded the following general impression: at time $t \approx {}^1/_4 t_L$ (t_L is the laser pulse length (full width half maximum)) the spectra consist of an intense continuum with superimposed absorption lines. Slightly later ($t \approx {}^1/_2 t_L$) the continuum persists but the absorption lines are replaced by poorly resolved emission lines. Later on ($t \approx 2t_L$), the continuum has totally disappeared but the line spectra persist and are better resolved. Temporal and emissive behaviour shows to be very reproducible for different stones. The line spectra are strongly dominated by calcium emission because of its relatively low ionization level which is confirmed by modelling calculations ([28]). These emission

Lastly we mention the observation of an expanding and collapsing bubble at the surface of a stone or a stone phantom with the aid of high speed photography ([7,22]).

1.2.2 Interpretations

The most popular interpretation of observations as listed above points out a central role to a presumed plasma ([11,27]). A weak point in this approach, from now on referred to as the plasma-mediated mechanism, is the almost total neglect of any preceding process responsible for plasma initiation. The only thorough mathematical analysis of this mechanism performed by Lo et al.([27]) also fails in this respect. Mostly one simply assumes that a certain amount of energy, the threshold energy, is needed for plasma initiation.

Rapid expansion of the plasma bubble is held responsible for generation of strong pressure effects which eventually lead to stone damage. Therefore it seems reasonable to assume that the plasma initiation threshold coincides with the threshold for acoustic effects. Acoustic threshold measurements based on this assumption ([23,38]) did yield the expected dependence on stone colour and laser fluence (energy per unit area) however not in detail. Therefore an alternative mechanism was formulated considering an eventual plasma a side effect.

This alternative approach called the hot particle (flux) mechanism supposes explosive ablation of stone fragments to be the driving mechanism behind pressure build-up. Numerical analysis of the experimentally observed evolution of the previously mentioned bubbles ([22]) did not yield any distinction between the two hypotheses: both models can account for experimentally obtained bubbles after correction of the net deposited energy with a certain threshold. The energy threshold values appear to agree with those found in the acoustic threshold experiments described in the previous paragraph ([22,23]).

A more likely suggestion is outlined by Weyl et al. ([28,39]) who presents a synthesis of the two former possibilities. Absorption of the laser light by the stone material causes its vaporization at temperatures high enough for partial ionization of present alkali atoms like calcium. Further inverse Bremsstrahlung absorption by the liberated electrons will be the source of direct vapor heating eventually leading to electrical breakdown. First this

---

spectra are interpreted by Nishioka et al. as specific plasma radiation. The spectra observed at $t \approx {}^{1}/_{2\tau_L}$ also show a main absorption line of neutral calcium which can be indicative of colder calcium vapor surrounding a hot plasma which absorbs some of the emitted plasma radiation ([28]).

allows a gradual shift from ablation of hot stone fragments towards direct vapor heating as the main contribution to the required energy increase. Second this again implies some kind of threshold effect for plasma initiation. Direct absorption by an almost totally opaque vapor/plasma is far more efficient than administration of latent heat and subsequent ablation for the latent heat can never add to the energy contents of the vapor.

1.2.3 Mathematics

For completeness we will reproduce the results of the respective analyses on plasma-mediated ([27]) and hot particle ([22]) mechanism. A few conditions are identical for both cases:

* the energy is equated by putting the time rate of change of the bubble energy equal to the energy deposition by either direct absorption or a flux of hot particles minus the work done on the surrounding fluid;
* the pressure p, temperature T and vapor density ρ_v are taken to be uniform within the bubble. This requires the sound velocity to be large compared to the expansion speed;
* the vapor/plasma is treated as an ideal gas of constant heat capacities c_v and c_p;
* a relatively small amount of the laser pulse energy is required for either plasma initiation or heating the stone material to its dissociation temperature respectively;
* a small spherical vapor or plasma bubble is taken to be the initial volume.

These conditions imply for a fully absorbing plasma/vapor bubble ([27])

$$\frac{d}{dt}(\rho_v c_v T V) = P_a - P_r - p\frac{dV}{dt} \qquad (1.1)$$

where V is the volume and P_a the absorbed laser power. In addition the reradiative energy loss from the surface of the high temperature expanding bubble is incorporated by putting in the term P_r. The calculation of the reradiation losses requires knowledge of composition, density and temperature of the bubble. The method for doing so is beyond the scope of this research. Suggested reading for those especially interested in this theoretical part: the publications of Lo ([27]) and Weyl ([28]). Assuming this loss negligible with respect to the total absorbed power and rearranging leads to

$$\frac{dp}{dt} = (\gamma - 1)\frac{1}{V}P_a - \frac{\gamma p}{V}\frac{dV}{dt} \qquad (1.2)$$

where γ is the ratio of the specific heats c_p/c_v.

On the other hand when expecting a flux of hot particles to be responsible for the energy rise of the bubble we find ([22]; modified)

$$\mu N c_v \frac{dT}{dt} = \mu c_p T_d \frac{dN}{dt} - p\frac{dV}{dt} \tag{1.3}$$

where μ denotes an average molar mass accounting for the possibility of large molecules breaking up in smaller fragments, T_d is the dissociation temperature of the stone material and N the number of particles. Reworking equation (1.3) again yields a relation between p(t) and V(t)

$$\frac{dp}{dt} = \frac{(\gamma - 1)}{V} \mu c_p T_d \frac{dN}{dt} + \frac{p}{N}\frac{dN}{dt} - \frac{\gamma p}{V}\frac{dV}{dt} \tag{1.4}$$

Assuming steady state ablation enables coupling of the particle production rate dN/dt to the absorbed laser power $P_a(t)$ via ([32])

$$\begin{aligned} \frac{dN(t)}{dt} &= \varepsilon P_a(t) \\ \varepsilon &= \frac{1}{\mu\left(c_v \Delta T + L_d\right)} \end{aligned} \tag{1.5}$$

where $\mu c_v \Delta T$ is the heat needed to raise the temperature to its dissociation value T_d, μL_d is the latent heat of dissociation. Both are implicitly supposed to be constant by Wiersma ([22]). Straightforward integration leads to the particle amount N itself.

Both models yield a relation between pressure p(t) and volume V(t) by evaluating the bubble energetics. A second relation can be acquired by developing the acoustic flow of the surrounding liquid.

1.3 This work

As mentioned earlier the work reviewed above does not include the initial stage of interaction between laser light and stone surface. In that interval thermal effects are expected to be essential. Therefore some basic considerations on simple heating and vaporization are worked out for the case of lithotripsy. In this manner we intend to obtain a better idea of what effects and parameters are important in the evolution and energetics of the bubble. The mathematical modelling is presented in the next chapter.

Besides the acoustic flow of the surrounding liquid is an essential factor in the total mechanism. Its evaluation is usually worked out for spherical symmetry which obviously does not exist in the initial part of bubble formation. Apart from the mechanism that induces the vapor bubble expansion the geometry is reconsidered. A simplified one dimensional

alternative to the spherical case is proposed and is taken as a starting point for the experimental work. The model as well as a detailed experimental objective is described in chapter three.

Chapter four contains a detailed description of the experimental method and its characteristic features. Thereafter the results are presented. The report concludes with discussion and evaluation of results, method and physical mechanism.

2 CONSIDERATIONS ON THERMAL EFFECTS

2.1 Thermal properties

As argued before in section 1.3 of the previous chapter thermal effects are assumed essential in the initial stage of the interaction between laser light and stone material. The poor knowledge on this aspect is a little embarrassing for rather simple calculations provide not only order of magnitude estimate values of relevant parameters but also arguments for interpretation and assessment of experiments and theory. Therefore we did some basic calculations on possible processes that are extensively presented in appendix C or can be found in the standard work of Carslaw & Jaeger ([31]). Here only the results are presented and discussed.

All calculations can only yield numerical values when the thermal properties of the media, i.e. stone and water, are known. Values for density ρ, specific heat c_p and thermal conductivity λ and sound velocity c are needed. Here the following values will be used:

	ρ (kg/m^3)	c_p (J/kg.K)	λ (W/m.K)	c (m/s)
water	1000	4200	0.60	1500
stone	2500	920	2.60	3000

Table 2.1. Thermal properties ([31,36,37])

The numbers for stone material are the mean of values for marble, granite, sandstone and gypsum found in references [31], [36] and [37], except for the sound velocity which value is an estimate based on reference values.

Furthermore the following three general assumptions are made throughout the following sections:

* The problem can be described in one dimension;
* The media are considered to be semi-infinite, with their boundary plane located at $x = 0$;
* The dissipated energy per unit area per unit time, the so called irradiance or flux Φ_0, is considered constant during the nominal laser pulse time t_L.

2.2 Heat dissipation

For simplicity we restrict ourselves to evaluating the surface temperature of the stone material at x = 0 in a few cases.

First we consider the case where all heat is dissipated at the stone surface which is also thermally insulated, in other words the thermal contact with water is neglected. Then the temperature change of the surface is given by ([30,31])

$$\Delta T(t) = \frac{2\Phi_0}{\lambda}\sqrt{\frac{\kappa}{\pi}}\left(\sqrt{t} - \sqrt{t - t_L}\, H(t - t_L)\right) \tag{2.1}$$

where κ is the thermal diffusivity defined as $\kappa = \lambda/\rho c_p$ and H denotes the Heaviside or unit step function $H(z-z_0)$

$$H(z - z_0) = \begin{cases} 0 & , z < z_0 \\ 1 & , z \geq z_0 \end{cases} \tag{2.2}$$

If we neglect changes in thermal properties and eventual phase transitions we find after a pulse with $t_L = 1.5$ µs and moderate laser irradiances the following peak temperatures

fibre diameter (µm)	pulse energy (mJ)	irradiance ($\cdot 10^{10}$ W·m^{-2})	ΔT (t = 1.5 µs) ($\cdot 10^3$ K)
600	10	2.4	14
300	10	9.6	56
600	25	6.0	35

Table 2.2. A few examples of peak temperatures.

Thermal contact with water is easily added to this solution by putting in a certain factor that accounts for the fraction of the heat diffusing into the stone

$$\Delta T_2(t) = \left(\frac{\alpha}{1+\alpha}\right)\frac{2\Phi_0}{\lambda_2}\sqrt{\frac{\kappa_2}{\pi}}\left(\sqrt{t} - \sqrt{t - t_L}\, H(t - t_L)\right) \tag{2.3}$$

where subscript 2 denotes the stone medium. It follows from the boundary conditions that

$$\alpha = \left(\frac{\lambda_2}{\lambda_1}\right)\sqrt{\frac{\kappa_1}{\kappa_2}} \tag{2.4}$$

Subscript 1 denotes the liquid medium, water. With the values as tabulated in section 2.1 a value for $\alpha/(\alpha+1)$ of about 0.6 is found. In other words, the thermal contact with water leads to a decrease in temperature of 40 %. However one has to realize that this case is rather pathological as the water will start to evaporate at 100 ^{0}C or a temperature change of approximately 80 K. With an irradiance of $6.0 \cdot 10^{10}$ W/m^2 this will only take about 20 ps. When a vapor layer has been formed between stone and water it behaves as an almost perfect insulator compared to water and the solution of the surface temperature will approximate the one given in equation (2.1).

It is far more interesting to consider the influence of a finite optical absorption length δ which equals $1/\mu_a$, μ_a being the absorption coefficient. When instead of total absorption at the surface the irradiance is assumed to obey Beer's law

$$\Phi(x) = \Phi_0 e^{-(x/\delta)} \tag{2.5}$$

the change in surface temperature is a little more complicated

$$\Delta T(t) = \frac{\Phi_0 \delta}{\lambda} \left\{ \frac{2}{\sqrt{\pi}} \frac{\sqrt{\kappa t}}{\delta} + e^{(\kappa t/\delta^2)} \operatorname{erfc}\left(\frac{\sqrt{\kappa t}}{\delta}\right) - 1 \right\} \tag{2.6}$$

where only the heating stage is written down. The introduced function erfc(z) is explained in appendix C (equation (C.7)). The first term is recognized as the solution to surface dissipation, relation (2.1). Besides it is obvious from equation (2.6) that the surface temperature is strongly dependent on the ratio of the thermal diffusion length $\sqrt{(\kappa t)}$ and the optical absorption length δ. It is therefore illustrative to examine the two extremes of this ratio.

First, if $\sqrt{(\kappa t)}$ becomes much larger than δ equation (2.6) reduces to

$$\Delta T(t) = \frac{2\Phi_0}{\lambda} \sqrt{\frac{\kappa t}{\pi}} \tag{2.7}$$

which is the solution for surface heating again. When on the other hand $\sqrt{(\kappa t)} \ll \delta$ we get

$$\Delta T(t) = \frac{\Phi_0 \kappa t}{\lambda \delta} = \frac{\Phi_0 t}{\rho c_p \delta} \tag{2.8}$$

which agrees with the range where heat losses due to thermal conduction are negligible. As both van Swol ([23]) and Weyl ([39]) argue that this range is valid throughout the laser pulse it is interesting to express the related criterium for δ

$$\delta \gg \sqrt{\kappa t_L} = 1.30\ \mu m \qquad (2.9)$$

Conclusively the dependence of the surface temperature on optical absorption length δ is illustrated in figure 2.1.

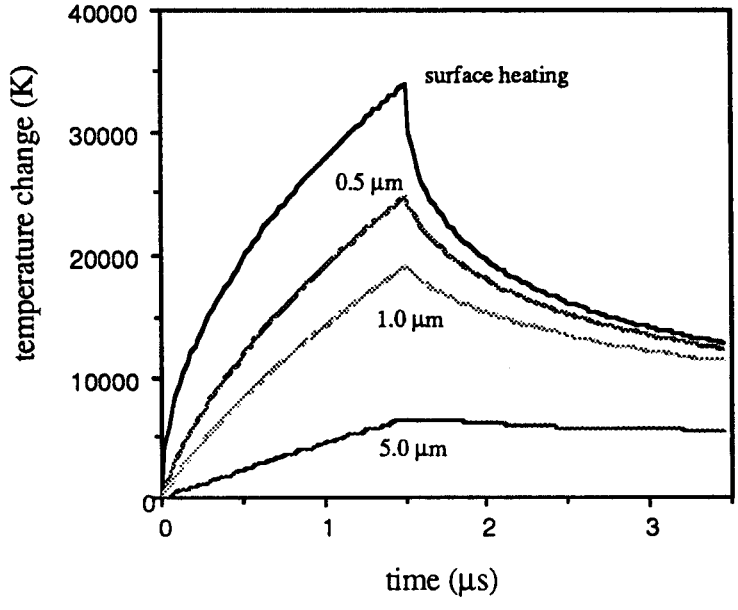

Figure 2.1. Temperature change as a function of time for different optical absorption lengths. Irradiance $\Phi_0 = 6.0 \cdot 10^{10}$ W/m^2 which corresponds to a 25 mJ laser pulse out of a 600 μm diameter fibre.

Another conclusion that can be made up from these results concerns the values for δ as found by van Swol ([23]). His resulting values are physically impossible for the stone will hardly reach its evaporation temperature. Moreover, when the temperature rise is relatively slow the thermal losses to water will play a more important role in suppressing the thermal effects. These errors are due to a misinterpretation of the experimental method. When his measurements are worked out correctly values for the optical absorption length range from 0.7 to 3.2 μm ([38]).

2.3 Pressure changes

Our interest mainly concerns pressure changes: which amplitudes and time scales can be expected? One effect that gives rise to pressure change is thermal expansion caused by heating. A method to obtain values of pressure changes solely due to thermal expansion is explained in appendix C. The expansion of stone and water neglecting compressibility effects leads to a pressure increase of

$$p' = (3.3 \cdot 10^{-4}) \cdot \Phi_0 \quad [\text{Pa}] \qquad (2.10)$$

which means a pressure change of approximately 20 bar for the earlier applied incident irradiance Φ_0 of $6.0 \cdot 10^{10}$ W/m^2.

It is evident that other effects are more dominant. The first change of state that is bound to occur is the vaporization of water. A strongly simplified model is evaluated to obtain thickness, expansion speed, vapor pressure and temperature of a vaporized water layer. Again the extended analysis of the problem can be found in appendix C. The problem is schematically depicted in figure 2.2.

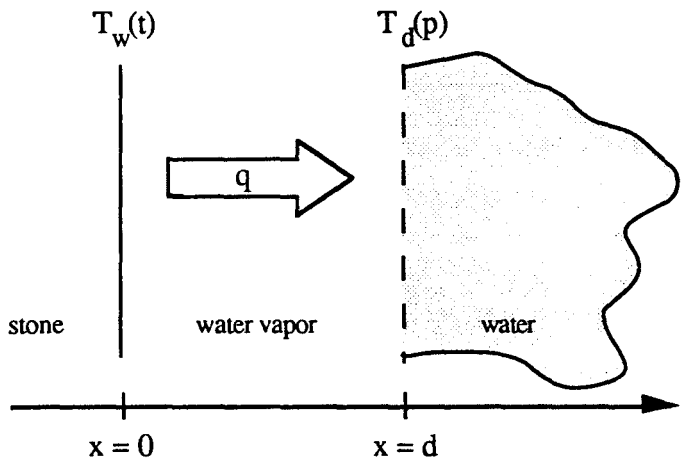

Figure 2.2. Model for calculation of an expanding water vapor layer.

The assumptions and conditions are :

* The vapor layer is supposed to be mainly insulating. We therefore take semi-infinite liquid water at 373 K (100 °C) and force a temperature change ΔT_w as calculated in section 2.2 at its boundary. The optical absorption length δ and irradiance Φ_0 are taken to be 1 μm and $6.0 \cdot 10^{10}$ W/m^2 respectively.

* Still a small heat flux q exists. This heat flux is assumed homogeneous over the layer and described by

$$|q| = \lambda_v \frac{dT}{dx} = \lambda_v \frac{|T_w(t) - T_d(p)|}{d} \qquad (2.11)$$

where λ_v is the supposed constant heat conductivity of the vapor, d the thickness of the vapor layer and $T_d(p)$ the vapor temperature at $x = d$. The dependency of T_d on pressure is linearized based on data from steam tables ([40]).

* At the vapor-liquid interface the flux q supplies the latent heat L required for vaporization. The energy needed to heat the liquid is neglected. The vapor is supposed to expand instantaneously by a factor ρ_l/ρ_v which is the ratio of liquid and vapor density. This yields a second relation for q

$$|q| = L\rho_v \frac{d}{dt}(d) \qquad (2.12)$$

The dependency of vapor density ρ_v, latent heat L and their product on pressure can also be derived from steam tables ([40]). Their product is again linearized.

* Equating q from relations (2.11) and (2.12) yields a relation between pressure p and layer thickness d. A second differential equation of p and d is found from basic acoustic theory

$$p - p_{ref} = \rho_l c \frac{d}{dt}(d) \qquad (2.13)$$

The coupled set of differential equations is solved by a computer code. The results are shown in figures 2.3. and 2.4. The major problem in the algorithm design consists of describing the initial evolution of the parameters. Because of the simplifications heat flux q, layer velocity and pressure p tend to approximate infinity at small values for time t and layer thickness d. The solution to this problem mainly induced by series expansion is explained in detail in appendix C.

A few details from the resulting graphs should be noticed. The pressure never exceeds a value of 50 bar. However it takes only about 20 ns to reach the peak pressure. The mean rise is $0.23 \cdot 10^6$ bar/ns and the peak value at $t \approx 0$ is even $1.5 \cdot 10^6$ bar/ns. The stone surface reaches its dissociation temperature of 2 to 3000 K after 100 to 150 ns. The heat flux over the vapor layer can also be studied as a function of time. It appears to be less than 2.5 ‰ of the incident laser flux Φ_0 except within the first 15 ps. So the assumption of almost total insulation holds.

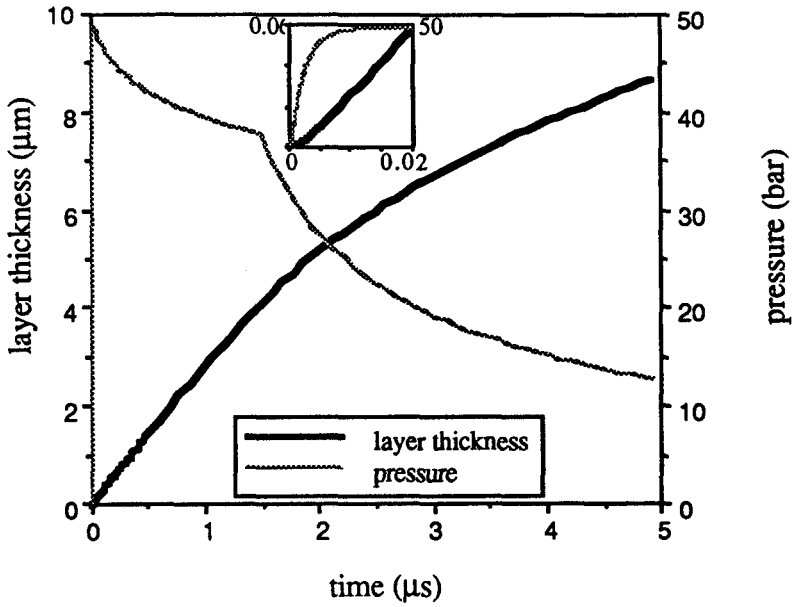

Figure 2.3. Thickness and pressure of an expanding water vapor layer.

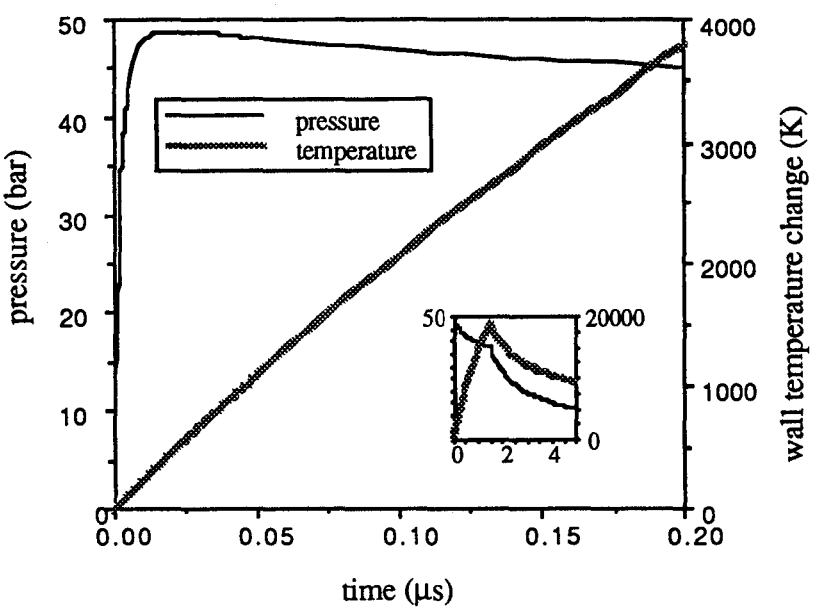

Figure 2.4. Boundary temperature $T_w(t)$ and pressure.

3 DESCRIPTION OF THE ACOUSTIC FLOW & EXPERIMENTAL OBJECTIVE

3.1 Introduction

A mathematical description of a fragmentation mechanism also requires developing the acoustic flow field of the surrounding liquid. In section 1.2.3 only the bubble energetics were evaluated resulting in a differential equation relating bubble volume V(t) and pressure p(t). The solution of the exterior acoustic flow can also be expressed as a relation between these two quantities. Finally the two resulting equations are coupled by imposing continuity of velocity and pressure at the gas/liquid interface of the bubble boundary (hereafter indicated as bubble interface).

First the method as followed by both Lo et al.([27]) and Wiersma ([22]) is outlined in short. Detailed mathematics can be found in appendix B, Lo ([27]) and the basic work of Landau & Lifshitz ([21]).

3.2 Acoustics

The flow of an ideal, inviscid and compressible fluid can be described by equating the conservation of mass and momentum. If the flow is also irrotational the velocity $\underline{v}$ can be expressed in a velocity potential ϕ by putting $\underline{v} = \text{grad}\ \phi$. When the acoustic approximation is applied the two conservation laws can be reduced to the following wave equation

$$\frac{\partial^2 \phi}{\partial t^2} - c^2 \Delta\phi = 0 \qquad (3.1)$$

where Δ is the Laplace operator and c the acoustic velocity defined as $\sqrt{(\partial p/\partial \rho_\infty)_S}$ subscript s denoting the fact that acoustic waves in an ideal fluid are adiabatic. Pressure p is simply related to ϕ by

$$p(\underline{r},t) = -\rho_\infty \frac{\partial \phi}{\partial t} + p_\infty \qquad (3.2)$$

where subscript ∞ denotes ambient values of the respective quantities. These equations can be considered further by taking the specific symmetry of the problem into account.

3.3 Spherical symmetry

Because the experimental bubbles appear to be approximately hemispherical ([22]) it seems reasonable to work out the spherical geometry. Then here the general solution of equation (3.1) of interest is an outwardly propagating wave

$$\phi = \frac{f(ct - r)}{r} \tag{3.3}$$

Next in order to couple the bubble dynamics with this general solution we impose continuity of pressure and velocity at the bubble interface, r = a(t). This rather tedious derivation can be found in appendix B. Now we skip directly to the result

$$\frac{d^2a}{dt^2} + \frac{2}{a}\left(\frac{da}{dt}\right)^2 = \frac{(p - p_\infty)}{\rho a} + \frac{(p - p_\infty)}{\rho c}\frac{da}{dt} + \frac{1}{\rho c}\frac{dp}{dt} \tag{3.4}$$

which is related to V by $V = (4/3)\pi a^3$. Substitution for dp/dt of either relation (1.2) or (1.4) leads to a differential equation of a(t) alone which can be solved numerically. The respective solutions appear to yield results that agree well with experimentally observed bubbles. As both models plasma-mediated and hot particle flux give the same results, the physical process responsible for the energy deposition in the bubble can not be discriminated.

3.4 One dimensional geometry

An obvious shortcoming is the assumption of a spherical starting volume. It is more likely that the expansion is developing from one dimensional, when the expansion is small compared to both fibre diameter and distance between fibre and stone, to cylindrical, when the expansion is only small compared to the fibre diameter and conclusively to hemispherical. The total configuration of fibre, stone and liquid may play an essential role in the coupling of acoustic effects into the media involved. We therefore propose a different description of the initial stage of expansion ([42]).

First the distance between fibre and stone is assumed to be large relative to the fibre diameter. In this way only the stone and liquid are involved in the initiation and evolution of the bubble. The configuration is shown in figure 3.1a. Both media are assumed to be semi infinite so that the bubble can only expand by compressing liquid and/or stone. Especially in

the early stage the expansion is essentially one dimensional along the hereby defined x axis. The general solution of equation (3.1) is then given by

$$\phi\,(x,t) = f\,(ct - x) \tag{3.5}$$

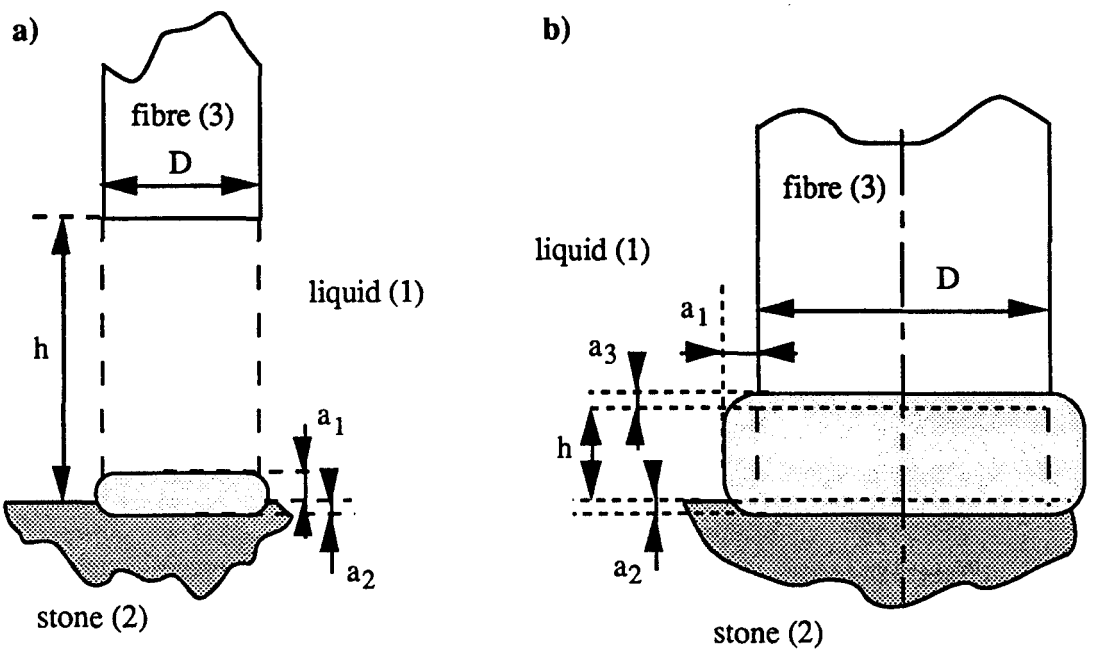

Figure 3.1. Configuration models for one dimensional acoustic flow. a) fibre far away; b) fibre near stone surface.

The involved quantities need not be identical for the different media so indices for each medium are introduced as defined in figure 3.1a. This implies for the velocity $u_i(x,t) = \partial x_i/\partial t$

$$u_i(x,t) = -f' \tag{3.6}$$

and pressure

$$p(x_i,t) = -\rho_i c_i f' + p_\infty \tag{3.7}$$

where the accent denotes derivation with respect to the total argument (ct - x). Again we impose continuity of velocity and pressure at the bubble interface $a_i(t)$ where x and t are no longer independent

$$p(a_i,t) - p_\infty = \rho_i c_i \frac{\partial a_i}{\partial t} - \rho_i \left(\frac{\partial a_i}{\partial t}\right)^2 \tag{3.8}$$

Recalling from section 1.2.3. the condition that the expansion speed is small compared to the sound velocity, $\partial a_i/\partial t \ll c$, reveals the normal acoustic relation $p' = \rho c u$. The same

condition also allows considering the pressure to be uniform so that the ratio of expansion velocities is given by the inverse ratio of their acoustic impedances $\rho_i c_i$

$$\frac{(\partial a_1/\partial t)}{(\partial a_2/\partial t)} = \frac{\rho_2 c_2}{\rho_1 c_1} \tag{3.9}$$

Alternatively the distance between fibre and stone is supposed to be comparable to the fibre diameter as shown in figure 3.1b. Then the expansion is cylindrically symmetric and consequently difficult to solve. The additional assumption that all expansions are small compared to the fibre radius, $a_i \ll r_f$, again enables one dimensional treatment of the three individual expansions. Direct enclosure of the condition of expansion velocities being small compared to the respective acoustic speeds then leads to

$$p - p_\infty = \rho_i c_i \frac{\partial a_i}{\partial t} \qquad (i = 1..3) \tag{3.10}$$

Next we introduce the following quantities

$$R_1 = \frac{\rho_1 c_1}{\pi D h} \tag{3.11a}$$

$$R_i = \frac{\rho_i c_i}{(\pi D^2/4)} = \frac{\xi_{i1}\rho_1 c_1}{(\pi D^2/4)} \qquad (i = 2,3) \tag{3.11b}$$

where h is the distance between fibre end and stone surface and D is the fibre diameter as shown in figure 3.1b. In fact R_i represents the acoustic impedance per unit area for each medium. Thus analogous with an electrical circuit of three parallel impedances the total impedance R_{tot} of the volume $\pi D^2 h/4$ is described by

$$\frac{1}{R_{tot}} = \frac{1}{R_1} + \frac{1}{R_2} + \frac{1}{R_3} \tag{3.12a}$$

$$R_{tot} = \frac{4\rho_1 c_1}{\pi D^2}\left(\frac{\xi}{4\xi h/D + 1}\right) \tag{3.12b}$$

where the parameter ξ is defined as

$$\frac{1}{\xi} = \frac{1}{\xi_{21}} + \frac{1}{\xi_{31}} \quad ; \quad \xi = \frac{\xi_{21}\xi_{31}}{\xi_{21} + \xi_{31}} \tag{3.13}$$

3.5 Definition of the experimental objective

In order to investigate this theorem of acoustic impedances an experimental method for measuring shock wave effects in the liquid was developed. We restrict ourselves to determination of pulse energy threshold values for shock wave generation as a function of the relevant parameters: distance h, fibre diameter D (= $2 \cdot r_f$) and parameter ξ which contains the acoustic impedance $\rho_1 c_1$ of the liquid. We can distinguish two phenomena.

Qualitatively spoken there will appear a certain critical ratio of h and D that marks the transition of the cylindrical situation with three involved media to the one dimensional situation that concerns only two media. In the latter regime depicted in figure 3.1a. R_{tot} of the initial volume transforms to

$$R_{tot} = \frac{4\rho_1 c_1}{\pi D^2}\left(\frac{\xi_{21}}{\xi_{21}+1}\right) \tag{3.14}$$

which is naturally no longer dependent on h. We suppose a dependence of the experiments on the total impedance R_{tot} and simultaneously a transition with increasing h from one regime described by relation (3.12b) to another described by (3.14). Intuitively this point is expected to arise when h approximately equals diameter D.

A second consideration only relates to the regime where equation (3.12) accounts for the total acoustic impedance. At a certain value of h/D the impedance R_1 of the liquid equals that of both solids taken together. This point can be calculated to be

$$\frac{h}{D} = \frac{1}{4\xi} \tag{3.15}$$

For distances h below this point the impedance of the bubble interface with medium 1 is much higher than with the other two media. Hence most expansion and subsequent emission of acoustic energy is coupled into both solid media which is supposed to be the clinically desirable effect. In the reverse situation an essential part of the acoustic energy disappears into the liquid.

4 SHOCK WAVE DETECTION IN THE LIQUID A SCHLIEREN SET-UP

4.1 The experimental set-up

The pressure waves evolving from the interaction between laser light and stone material are commonly referred to as shock waves regardless of their physical properties. In fact there is hardly any knowledge about these properties. Nevertheless the widespread conviction that these pressure waves are in some way responsible for stone fragmentation justifies their direct study.

The difficulty in measuring pressure within the stone material itself is obvious. For this reason the choice is made to conduct optical detection in the surrounding usually aqueous liquid. A Schlieren method is developed which in principle is applicable for measurement of the density gradient in any comparable pressure wave in liquids, e.g. in the study of oscillating vapor or cavitation bubbles (e.g. [1,5,24,35]). The density variations in pressure waves induce subsequent variations in the refractive index. In an ideal Schlieren set-up the deflection of a probe light beam caused by a gradient in the refractive index is measured.

In principle the set-up is constructed as follows

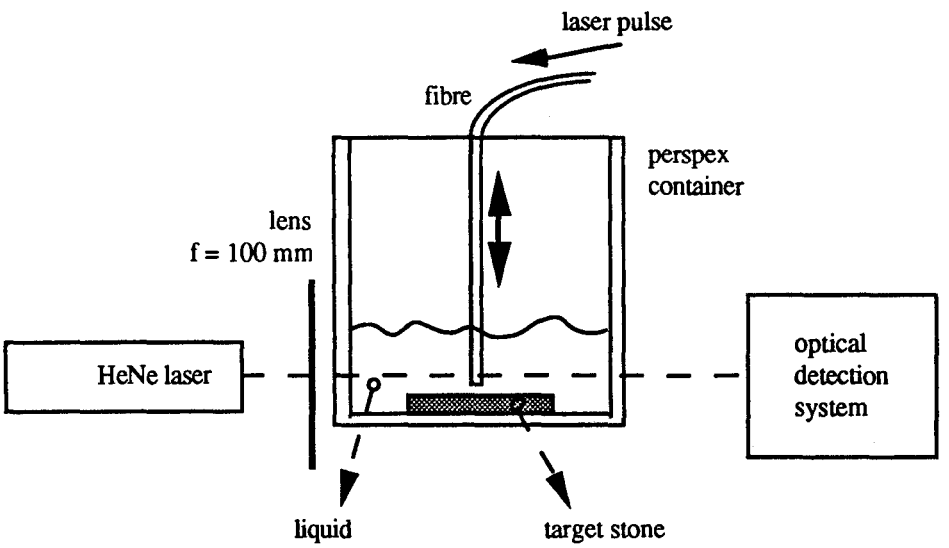

Figure 4.1. The experimental set-up.

The pulsed laser used in all experiments is a dye laser (Candela type LFDL-3) operating at a wavelength of 504 nm (Coumarin 504 dye) and a nominal pulse duration of 1.5 μs (full width half maximum). The laser output is coupled into a quartz fibre. Various

fibre diameters were applied. Either laser or fibre output as a function of the power supply settings can be determined by putting the laser to a pulse repetition rate of 10 Hz and obtaining the power with a power measuring device (Ophir 30A-P). The fibre enables guidance of the light to a perspex container partially filled with a liquid. The fibre tip is placed above a stone phantom viz. a polished piece of sandstone (i.e. black stone material used for tombstones) which is immersed in the liquid. The fibre is mounted on a micromanipulator in order to control the distance between fibre end and stone surface.

The probe beam of the Schlieren set-up from a helium-neon (HeNe) laser (Uniphase type 105-2) is focused into the perspex container which has an internal length of 200 mm and wall thickness of approximately 5 mm. Though the desired position of the beam focus was the central plane of the container a positive lens with a focal length of 100 mm in air is sufficient to achieve this as is explained in appendix D. This is due to the beam transformations as a consequence of the different media which lead to a displacement of the focal plane but leave the beam radius at the focal plane undisturbed.

In laser or Gaussian optics the beam radii w(z) correspond to the distances from the beam axis where the intensity has dropped off to $1/e^2$ of its axial value. The intensity profile of the beam is described by ([34])

$$I(r,z) = \frac{2P_0}{\pi w^2(z)} e^{-2(r/w(z))^2} \tag{4.1}$$

where P_0 is the total laser power. The z axis is parallel to the propagation direction of the beam. The minimal value of w(z) is defined as the beam waist w_0. Considering the outcoming beam of the HeNe laser parallel the waist behind a lens with focal length f is given by

$$w_0 = \frac{\lambda_0 f}{\pi w} \tag{4.2}$$

where w is the original beam radius and w_0 the waist behind the lens. With a wavelength of $\lambda_0 = 632.8$ nm and an experimentally determined value for $w = (0.42 \pm 0.01)$ mm a waist $w_0 = (48 \pm 1)$ µm is expected. This agrees well with experimental values of (51 ± 2) µm.

Behind the container the actual detection system is placed. The aim of the detection system is to measure the deflection angle of the probe beam. It consists of three lenses, a razor blade and a fast photodiode (type BPW34) loaded with 50 Ω and connected to a digital 500 MHz oscilloscope (Tektronix 2440). The optical part is shown in figure 4.2.

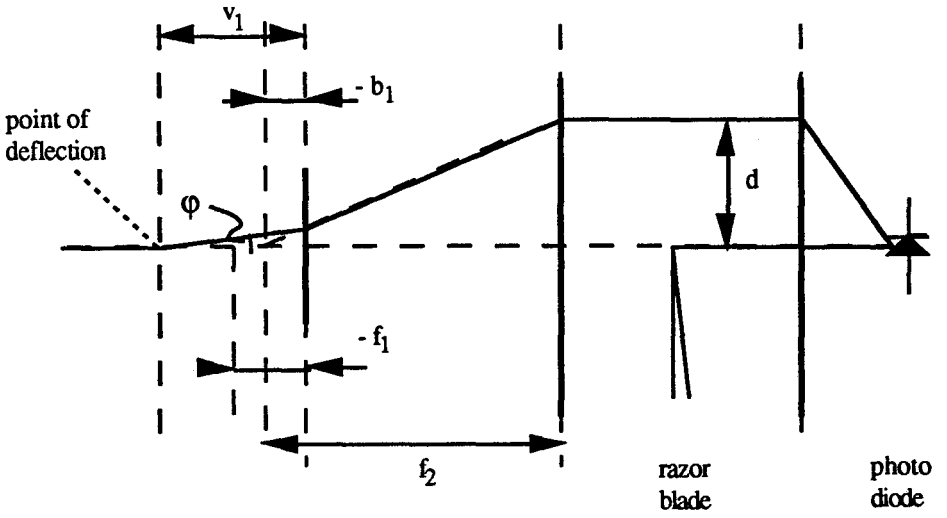

Figure 4.2. Optical detection system.

We prefer to convert the divergent beam that leaves the container to a parallel one of relatively large diameter. Therefore the negative lens (f_1 = -40 mm) and a positive lens (f_2 = 300 mm) are positioned in such a way that in the static situation a perfectly parallel beam impinges on the razor blade. The only advantage of the enlargement of the beam diameter is that it facilitates placing the razor blade in its desired position as any beam deflection will be enlarged with the same factor as the beam diameter itself. The intensity profile and parallellism of the beam are checked by translating the razor blade through the extended beam at two positions on the optical axis 200 mm apart. The result is shown in figure 4.3.

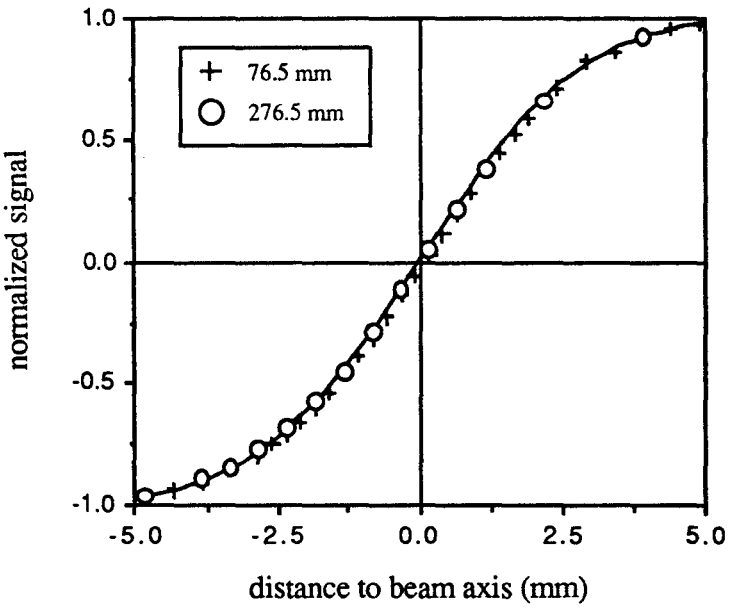

Figure 4.3. Intensity profile at two positions behind the 300 mm lens. Straight line represents fit to data at 76.5 mm.

4.2 Signal interpretation

Assuming that the first order effect of a pressure wave on the probe beam viz. deflection takes place at the waist implies that such a deflection only leads to a beam translation at the razor blade. We can deduce from figure 4.2. that this translation d depends on the deflection angle φ as

$$d = f_2\left(1 - \frac{v_1}{f_1}\right)\varphi \tag{4.3}$$

This displacement d need not be perpendicular to the razor blade edge. Consequently an unknown constant (co)sine factor has to be inserted in relation (4.3). Alternatively we can keep in mind that only the horizontal displacement and deflection can be obtained from experiments and continue this analysis. Hence we measure only the horizontal density gradients.

The transmitted power P_{tr} of an (approximately) Gaussian beam partially shielded by e.g. a razor blade is described by

$$P_{tr} = \frac{P_0}{w(z)}\sqrt{\frac{2}{\pi}}\int_{-\infty}^{d} e^{-2(x/w(z))^2}dx = \frac{P_0}{2}\left\{1 + \mathrm{erf}\left(\frac{\sqrt{2}d}{w(z)}\right)\right\} \tag{4.4}$$

where the error function is introduced of which a graphical representation is displayed in figure 4.3.. Its mathematical definition is written down in appendix C-equation (C.7b). For displacements relatively small to w(z) equation (4.4) can be linearized and rearranged to give

$$S = \frac{P_{tr} - (P_0/2)}{(P_0/2)} = 2\sqrt{\frac{2}{\pi}}\left(\frac{d}{w(z)}\right) \tag{4.5}$$

where signal S is the actual quantity that is obtained from the experiments. Combination of relations (4.3) and (4.5) shows that S is proportional to deflection angle φ for small signals. Plotting equations (4.4) and (4.5) in one graph (figure 4.4) shows that this is valid within 10 % for signals up to 0.6. Calibration of the set-up is conducted by determination of the beam radius w(z) at the razor blade from experimentally obtained intensity profiles (figure 4.3).

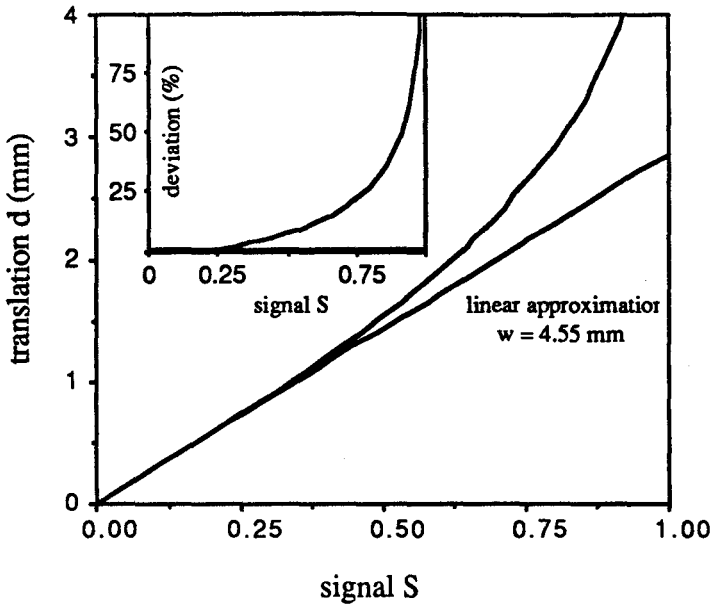

Figure 4.4. Considering the linearization of the error function.

4.3 Light passing refractive index variations of spherical symmetry

The following step in quantitative interpretation of the experiments is relating the deflection angle φ to a certain time-dependent refractive index variation at a fixed position. Because of the complexity of this problem we will restrict its theoretical treatment to the field of geometrical optics which implies neglecting diffraction. We will discuss if this gives a good approximation of the physical situation in a later section.

The starting point for ray tracing is the principle of Fermat ([17]). It states that the integral of the refractive index along the light path

$$\int_{P_1}^{P_2} n(x,y,z)\, ds \tag{4.6}$$

is minimal with respect to alternative paths in its direct surroundings. Marchand ([13]) worked out the exact solution of the spherically symmetric case in polar coordinates. As a consequence of the geometry of the set-up choosing cartesian coordinates is more convenient. Here we only reproduce the results of this analysis as given by Drees ([12]) and Hirschberg ([29]). The path of the light ray in the paraxial approximation is fully described by

$$\frac{d^2x}{dz^2} = \frac{1}{n}\frac{\partial n}{\partial x}$$
$$\frac{d^2y}{dz^2} = \frac{1}{n}\frac{\partial n}{\partial y} \qquad (4.7)$$

when the z-axis is parallel to the incoming ray. The paraxial approximation supposes both deflection angle and translation terms of the light ray to be relatively small ([12]). It also implies negligibility of $\partial^2 n/\partial z^2$ which is applicable for a single ray but has to be reconsidered in case of a beam. Then the second derivative can lead to undesired shadow effects which are in fact distortions of the wave front. These effects can be minimized by focussing the beam. Another advantageous consequence of focussing is the minimalization of a second wave front distorting effect viz. the lens effect of the spherical disturbance which affects the beam radius and subsequently the experimental signal.

In the case of spherical symmetry the spatial part of the refractive index is a function of r alone, r being $\sqrt{(x^2+y^2+z^2)}$

$$n = n(r) \qquad (4.8)$$

This implies that given the fact that the sound velocity is negligible compared to the light speed the light path will lie in a flat plane. Consequently the problem can be treated two-dimensional by rotating the coordinate system and demands solving only one equation of the form (4.7). Integrating leads to the integral angle of deflection

$$\varphi = \frac{dx}{dz} = \int \frac{1}{n}\frac{\partial n}{\partial x}\,dz \qquad (4.9)$$

By assuming a certain radial profile for the refractive index relation (4.9) can be solved numerically.

A second method for an approximate calculation of the deflection is more illustrative. We therefore consider a parallel light beam of finite width being crossed by an assumed radial pressure function. Comparison of the optical path length OPL at the beam edges provides us with an approximate measure of the deflection. Main assumptions are negligibility of the wave front distortion (i.e. effects due to $\partial^2 n/\partial z^2$) or diffraction and small deflection angles. This method is shown schematically in figure 4.5.
The resulting equation of this method is

$$\varphi = \frac{\Delta OPL}{2n_0 w_0} = \frac{1}{2n_0 w_0}\left\{\int_{P_1} n(r(z))\,dz - \int_{P_2} n(r(z))\,dz\right\} \qquad (4.10)$$

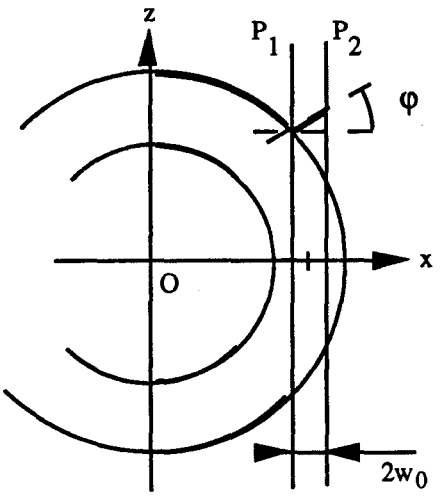

Figure 4.5. Simple geometrical method for calculating the beam deflection taking the beam width into account.

Equation (4.9) is evidently a differential form of relation (4.10).

Indeed assuming a certain pressure profile travelling outward with the acoustic velocity c_0 (in water approximately 1500 m/s) yields numerical solutions to both relations (4.9) and (4.10). In figure 4.6 two simple pressure wave models are depicted, the resulting deflection can be found in figure 4.7.

4.4 Discussion of the method

From the previous section it appears that only the integral effect φ as a function of time is obtained from experiments. As the argument of the integral contains the refractive index and its first derivative along the light path it is fairly impossible to obtain the refractive index as a function of time from the deflection angle φ alone. As one has to assume a certain radial profile with too many unknown parameters this method will yield a set of possible solutions. Notwithstanding these complications one can certainly get a coarse idea of the actual profile and amplitude of the pressure wave.

A few remarks on the applicability of the paraxial approximation of geometrical optics

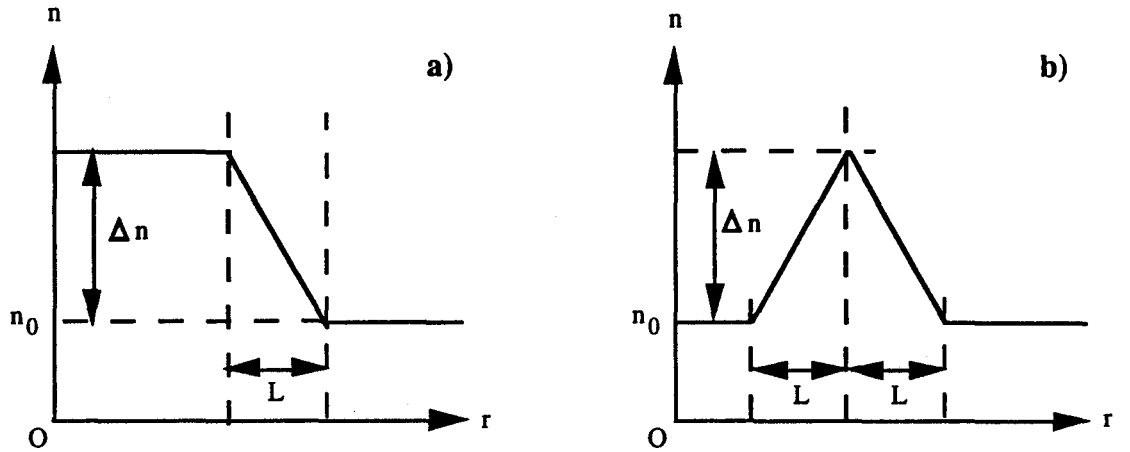

Figure 4.6. *a): single slope of constant gradient model (Δn = increase in refractive index with respect to ambient index of refraction n_0; L = shock thickness); b): double slope of constant gradient model.*

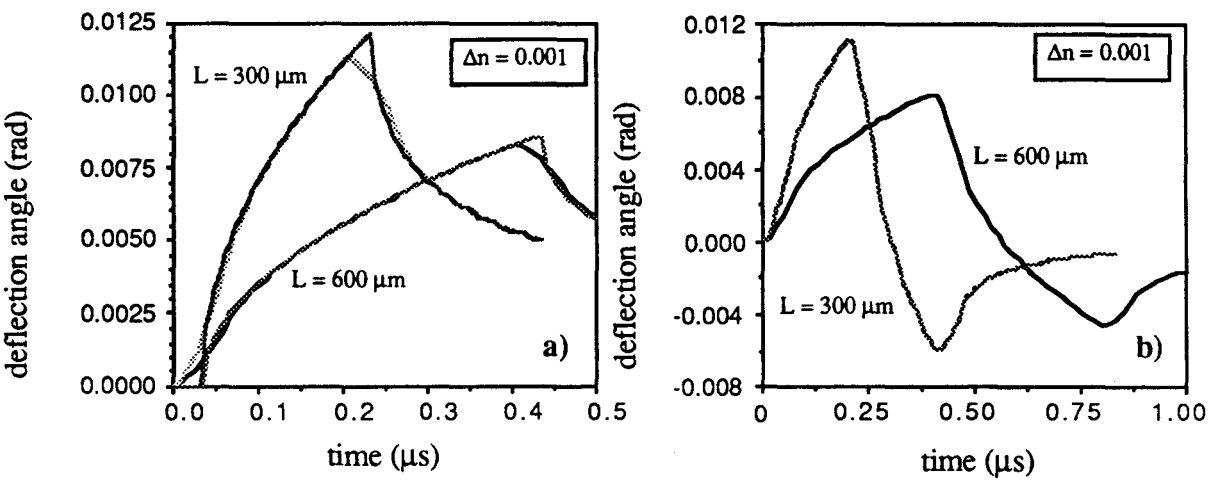

Figure 4.7. *a): Result on single slope model (fig. 4.5a) of both formulae (4.9) and (4.10); b) result on double slope model of only equation (4.10).*

have to be made. A commonly used criterium to get an idea if this simplification is allowable is looking at the waist length L_w of the detection beam. L_w is defined as ([19,34])

$$L_w = \frac{n\pi w_0^2}{\lambda_0} \tag{4.11}$$

If the detection system is placed within one waist length from the point of deflection diffraction can be neglected and geometrical optics can be applied. The waist length (w_0 = 50 μm) is approximately 12 mm which is much smaller than the 100 mm distance to the detection system. Alternatively if the positive lens in front of the container is removed the beam radius of 0.4 mm at the deflection point leads to a waist length of 0.8 m which satisfies the criterium. Comparison of experimental signals obtained with either focused or non-focused set-up contains therefore information on the negligibility of diffraction and shadow effects. For the sensitivity of the set-up also changes while the beam radius at the razor blade changes the signals are converted to deflection angles with the method outlined in section 4.2. and appendix D. Such a comparison was made in a small pilot experiment. Under identical conditions deflection angles for the focused and non-focused set-up were found to be (1.0 ± 0.2) and (0.9 ± 0.2) mrad respectively so no significant difference was found. Two examples of signals are shown in figure 4.8.

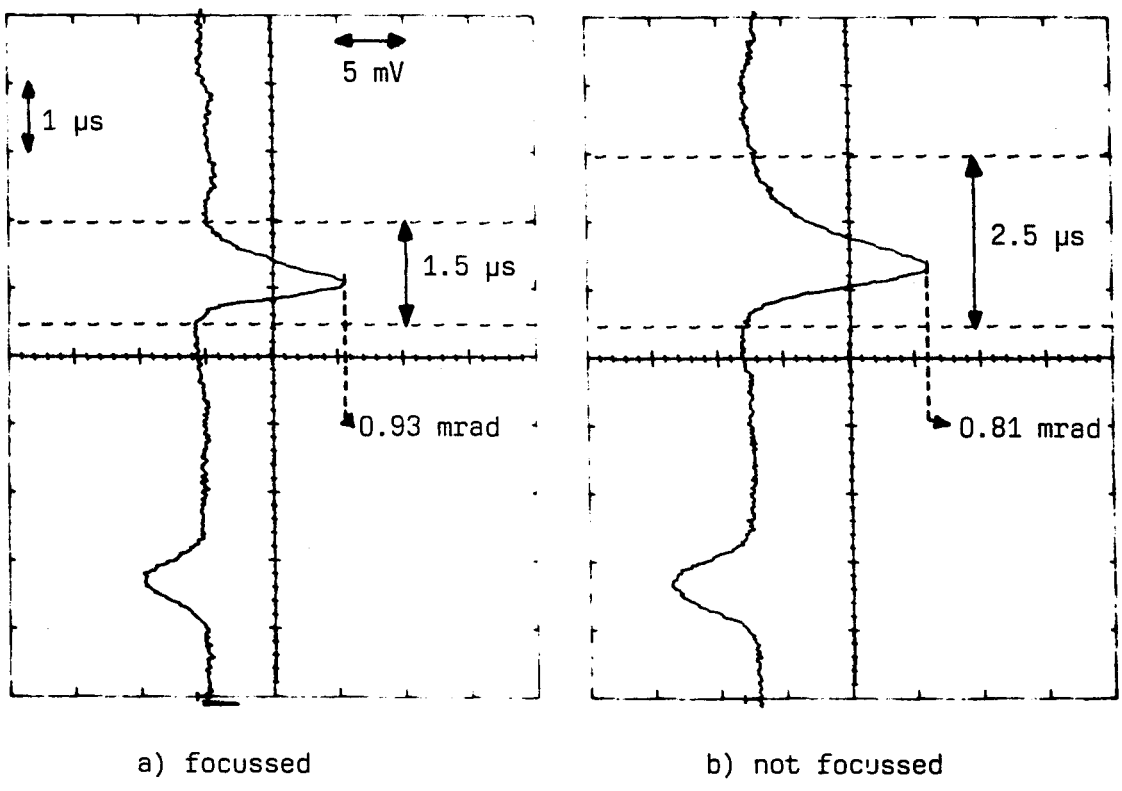

Figure 4.8. Focused compared with non-focused detection. (in water; 320 μm fibre; pulse energy unknown).

The observed difference in temporal width can largely be explained by the difference in

diameter of the respective detection beams which subsequently causes a difference in the time required for wave passage. Secondary effects as the curvature of pressure wave and probe beam are difficult to interpret but may also account for this effect.

The razor blade was also totally removed from the beam in both cases to investigate whether the total signal decreases as a consequence of absorption (which is unlikely to occur) or diffraction (in case the shock wave dimensions are small compared to the probe beam diameter) or beam distortion. Two examples of the resulting signals are depicted in figure 4.9.

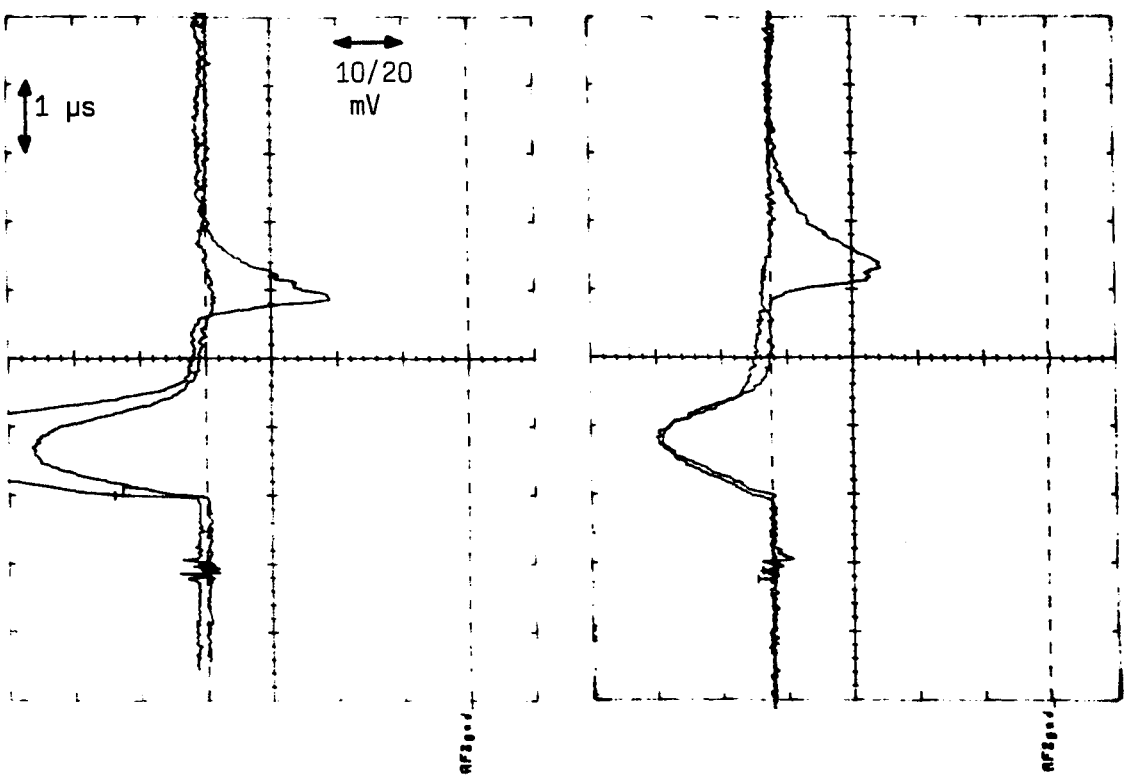

Figure 4.9. Comparison of signals with and without the razor blade placed in the set-up. The total power increases with a factor 2 upon removal of the razor blade. (in water; 320 µm fibre; pulse energy unknown).

We summarize this discussion with three conclusions. First no indications are found that effects other than beam deflection play an important role. Nevertheless these pilot studies have to be carried out more extensively to justify this conclusion completely. Comparison of the modelling calculations in figures 4.6. and 4.7. with the obtained

experimental signals (Figures 4.8. and 9) justifies the presumption that the pressure profile looks like

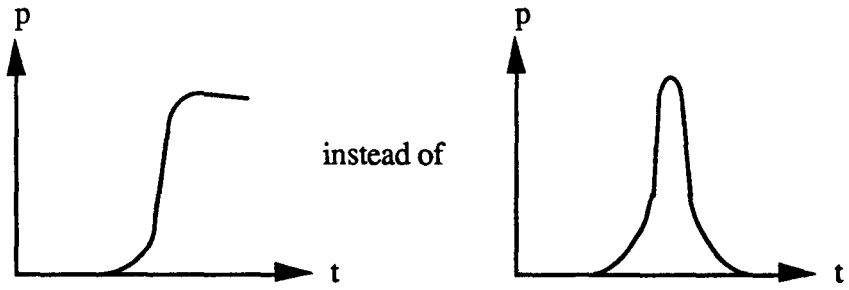

Finally the pressure is not expected to exceed a value of 200 bar.[1]

4.5 Equation of state for water

The last stage in obtaining shock wave characteristics from experiments is essentially linking the refractive index to the pressure. This is performed in two steps. First the refractive index is coupled to density variations and second an equation of state in order to relate density to pressure is derived.

The dependence of the refractive index on density is unknown for most liquids. As far as water is concerned several semi-empirical relations are deduced from experiments (which is also the case for its equation of state). Here the following relation of Zel'dovich et al. ([39]) is chosen

$$\Delta n = 0.334\,(\rho - 1) \qquad (4.12)$$

where density ρ has the unit g/cm^3 and Δn denotes the change in refractive index.

---

1 From experiments can be found that the maximum angle of deflection $\varphi \approx 2.5$ mrad. It follows from relation (4.7) that

$$\varphi \cong \frac{1}{n}\left(\frac{\partial n}{\partial x}\right)\Delta z \;\Rightarrow\; \Delta n \approx \frac{n\cdot\varphi}{\Delta z}\Delta x$$

Δx is estimated to be the temporal width of the signal times the acoustic velocity c_0. Δz is estimated from the temporal interval between onset of the laser pulse and shock signal on one hand and the the interval between onset of the shock signal and its extreme. We then find $\Delta x \approx 2$ mm and $\Delta z \approx 2$ mm at its minimum value so that Δn reduces to $n\cdot\varphi$. Using relations (4.12) and (4.18) we finally find

$$\Delta p = c_0^2 \frac{\Delta n}{0.334}\cdot 10^3 \cong c_0^2 \cdot 4\varphi \cdot 10^3 \approx 2\cdot 10^7 = 200 \text{ bar}$$

Using equation (4.12) and an equation of state enables direct linking of the refractive index to pressure changes in the liquid. A widely accepted equation of state for water is the Tait equation, modified by Kirkwood ([14])

$$p' = B\left\{\left(\frac{\rho}{\rho_\infty}\right)^a - 1\right\} \tag{4.13}$$

where B equals $\rho_\infty c_0^2/a$, c_0 being the acoustic velocity. Pressures p' and B are the changes with respect to static pressure. Here the suggested values a = 7.415 and B = 2961 bar (c_0 = 1481.7 m/s) will be used. Rearrangement of (4.13) gives us

$$\Delta\rho = \rho_\infty\left\{\left(\frac{p' + B}{B}\right)^{\frac{1}{a}} - 1\right\} \tag{4.14}$$

Another suggestion is worked out by Harris & Presles ([2]) who use the experimental data of Rice & Walsh ([16]) on shock and particle velocities, u_s and u_p respectively, to fit the relation

$$u_s = P + Q\,u_p \tag{4.15}$$

where P stands for the acoustic velocity c_0 with a value of 1483 m/s which implies 2.07 for Q. Obtaining both constants by averaging the mentioned experimental data yields values of 1519 m/s and 1.954 respectively. The second pair of parameters was applied here. Combination of relation (4.15) with the so called jump conditions for shock waves ([4])

$$\Delta p = \rho_\infty u_s u_p \tag{4.16a}$$

$$\rho_\infty u_s = \rho\,(u_s - u_p) \tag{4.16b}$$

leads to another semi-empirical equation of state

$$\begin{aligned} a\rho^2 + b\rho + c &= 0 \\ a &= (Q-1)^2\Delta p - \rho_\infty P^2 \\ b &= \rho_\infty^2 P^2 - 2\rho_\infty Q(Q-1)\Delta p \\ c &= \rho_\infty Q^2 \Delta p \end{aligned} \tag{4.17}$$

Comparison learns us that both relations yield the same values for ρ within 5 % over a large range of pressure changes. Thus having found a reliable equation of state we can express the change in refractive index as a function of pressure variations. The result is shown in figure 4.10. For comparison the acoustic approximation which is described as

$$\Delta p = c_0^2 \cdot \Delta \rho \tag{4.18}$$

is also depicted in this figure.

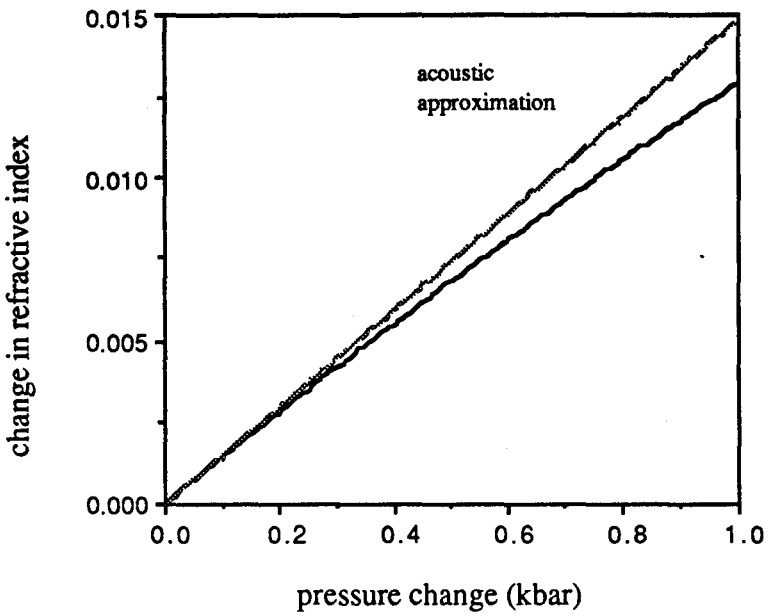

Figure 4.10. Change in index of refraction (Δn) as a function of pressure changes for water.

The acoustic approximation of the equation of state leads to a deviation of 8 % for a pressure change of 1 kbar and can thus be considered an applicable linearization for the experimental regime of pressures.

This still leaves us with the same problem, i.e. formulation of an equation of state, for the other liquids so that the respective experiments cannot be interpreted in terms of pressure values.

5 EXPERIMENTS & RESULTS

5.1 Experimental criterium & protocol

In this section the method developed to achieve the objective as described in section 3.5 is outlined in short.

Before experiments are performed the relative fibre to laser power throughput and the fibre output as a function of the power supply settings are determined. Therefore we set the laser to a pulse repetition rate of 10 Hz and obtain the power with a power measuring device. The fibre output is checked in the same manner after the experiments. As already can be seen in figures in the previous chapter the experimental signals essentially look like this

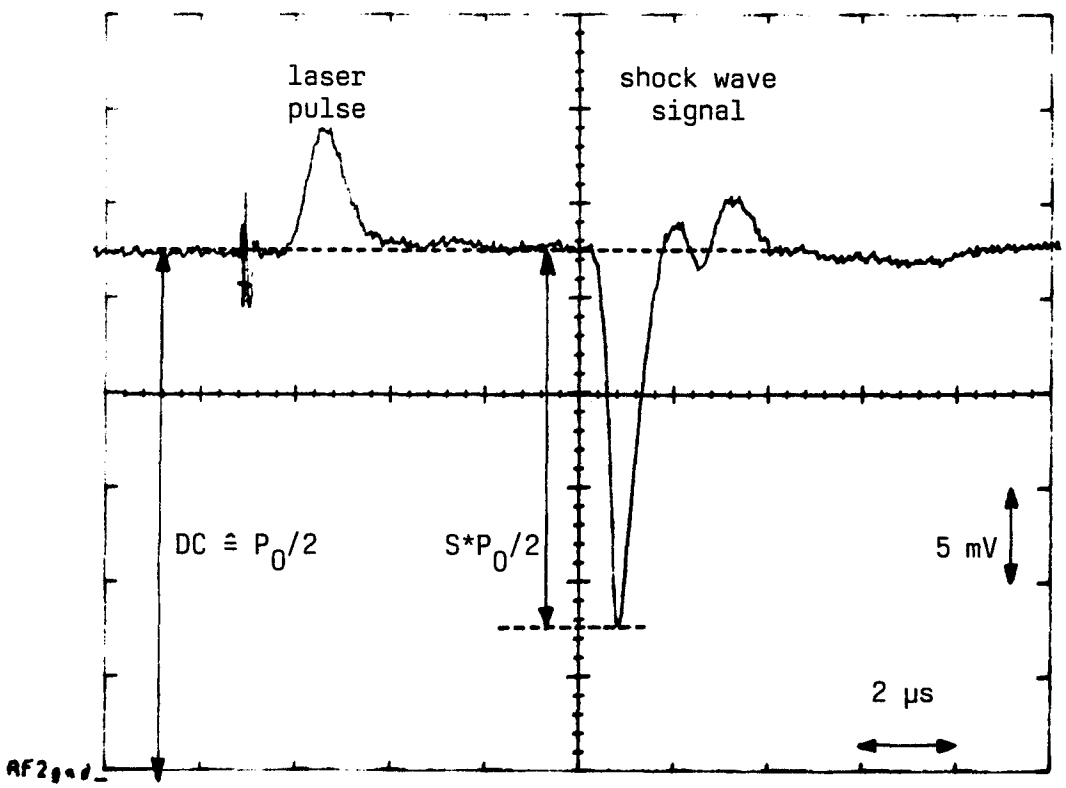

Figure 5.1. Experimental signal and explanation of relevant parameters . (in silicone oil; 320 µm fibre; pulse energy unkown).

The first peak is a consequence of scattering of the laser pulse and can be removed by putting in an appropriate filter that stops 504 nm. The second peak is the deflection signal. The decrease in the DC baseline voltage is arbitrary for this depends on which side the razor blade

is positioned (see figure 4.1). The signal decreases when the beam is deflected towards the origin of the pressure effects.

Because we do not succeed in relating the signal to the pressure it is impossible to calculate the shock wave energy. Therefore the amplitude voltage relative to DC is taken to be characteristic and determined in the experiments. As the spread in signals is large these relative amplitudes S are averaged over ten identical measurements for each set of parameters - pulse energy, distance between fibre and stone, fibre diameter and liquid. Keeping the latter three parameters constant enables definition of a criterium for an acoustic threshold energy. This is illustrated with an example shown in figure 5.2a.

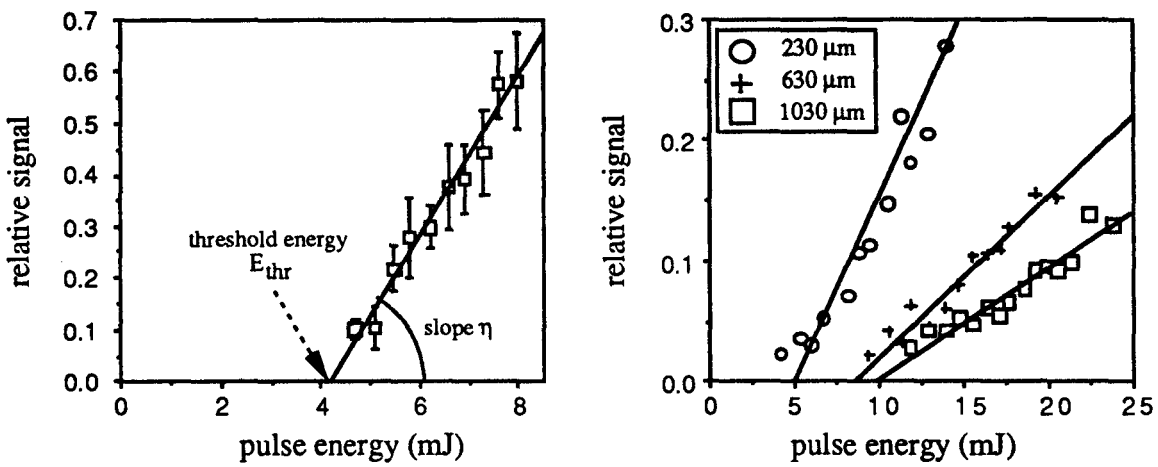

Figure 5.2. Example of an experimental series for constant distance between fibre and stone, fibre diameter and surrounding liquid and a comparison of different series for altered values of h.

We see that from a certain pulse energy on the signal S increases linearly with increasing pulse energy. Each data point in figure 5.2. represents an average value $\overline{X}$ of ten measurements X_i. The error bars denote the mean deviation σ_m defined as ([20])

$$\sigma_m = \frac{\sigma}{\sqrt{n}} = \sqrt{\frac{\sum (X_i - \overline{X})^2}{n\,(n-1)}} \qquad (5.1)$$

where σ denotes the standard deviation. Application of weighted linear regression (see appendix E) yields a straight line that intersects the ordinate axis at a certain pulse energy. We hereby define this energy as the threshold energy, E_{thr}. It can be seen from figure 5.2b. that the slope η also changes with varying parameters and therefore will η also be studied. The straight line is thus described by

$$S = \eta \cdot (E - E_{thr}) \qquad (5.2)$$

It can be understood from equation (5.2) that the slope η represents a conversion efficiency.

The dependency of the two parameters E_{thr} and η on the distance h between fibre end and stone surface, fibre diameter D and the acoustic properties of the liquid that determine the parameter ξ are presented and evaluated in the following sections. First the acoustic properties are tabulated below.

medium	ρ (kg/m^3)	c (m/s)	ρc ($\cdot 10^6$ kg/m^2s)	ξ_{21}	ξ_{31}	ξ
quartz [1)]	2500	6000	15	-	-	-
stone [1)]	2500	3000	7.5	-	-	-
glycerol [2)]	1060	1770	1.88	4.0	8.0	2.7
water [1,2)]	1000	1500	1.5	5.0	10.0	3.3
silicone oil [2)]	850	1000	0.85	8.8	17.6	5.9

Table 5.1. Acoustic properties of the respective media; [1)] reference ([37]), [2)] measured values (see appendix F).

5.2 Water

We first concentrate on the slopes η.

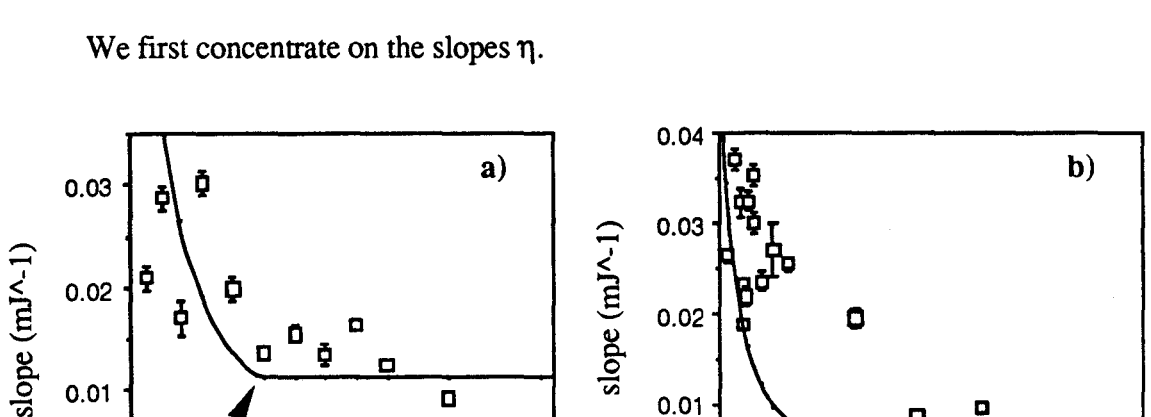

Figure 5.3. Slope η as a function of normalized distance between fibre and stone. a) 320 µm fibre; b) 600 µm fibre.

The qualitative trend implies that η can be proportional to the total acoustic impedance R_{tot}. The full line represents a fit of both formulae (3.12b) and (3.14) where the transition appears in the point indicated with an arrow. One has to realize that forcing the theoretical model on the fit procedure leaves us with only one fit parameter, viz. a proportionality factor.

If we further assume that the product of slope η and threshold energy E_{thr} is constant E_{thr} is inversely proportional to R_{tot}. This assumption leads to the full lines in the following graphs.

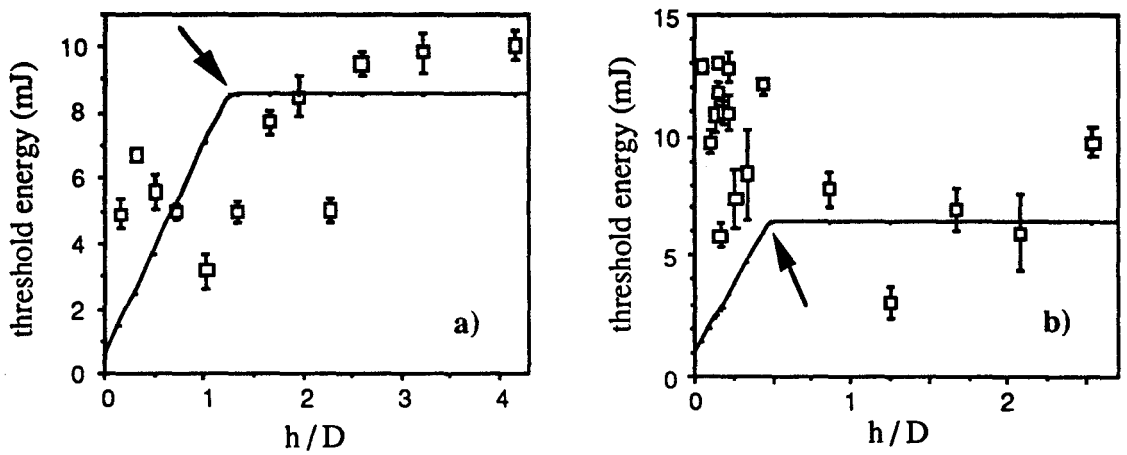

Figure 5.4. Threshold energy E_{thr} as a function of normalized distance between fibre and stone. a) 320 µm fibre; b) 600 µm fibre.

The theory fits the data poorly as the threshold energy definitely increases with decreasing h for h beneath the transition point. If we focus on the regime where $h < (3/2) \cdot D$ and divide the threshold energy by the respective fibre diameter an agreement between the data of both diameters is suggested. The same relation of threshold energy on diameter is implied by the experimental results of van Swol ([23]).

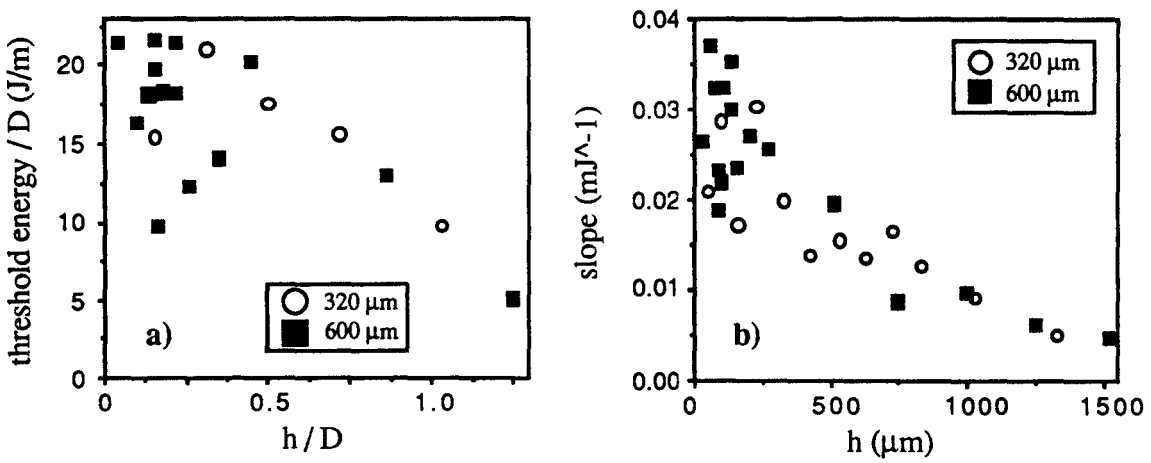

Figure 5.5. a): E_{thr} divided by D as a function of normalized distance h for both diameters. b): slope η as a function of absolute h.

A remarkable agreement between data of both diameters is found in figure 5.5b. where η as a function of absolute distance h is depicted.

5.3 Other liquids

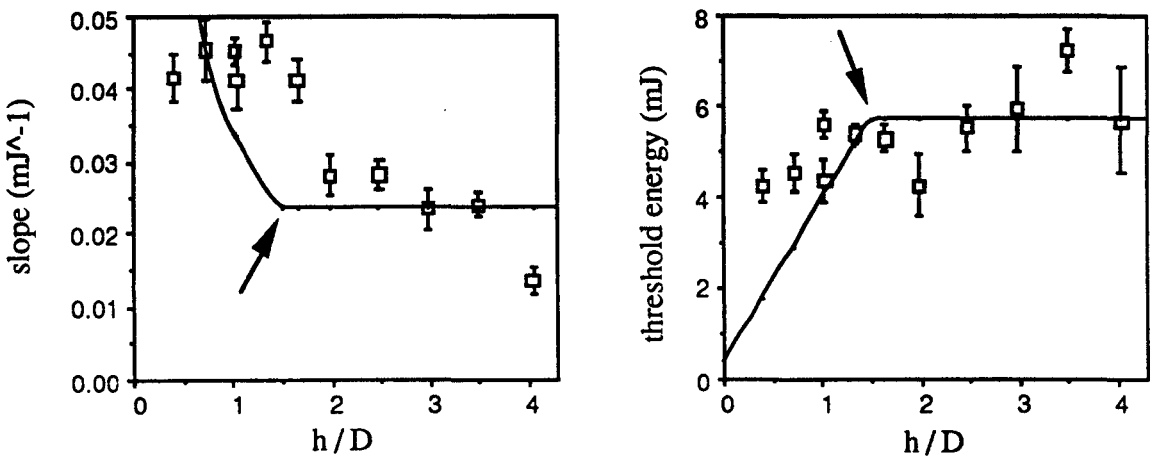

Figure 5.6. Slope η and threshold energy E_{thr} as a function of normalized distance between fibre and stone in glycerol. (D = 320 μm).

In glycerol the threshold energy shows no significant dependence on h/D. With regard to the slope a more explicit trend that qualitatively agrees with the one in water can be distinguished. Identical observations appear from the measurements carried out in silicone oil.

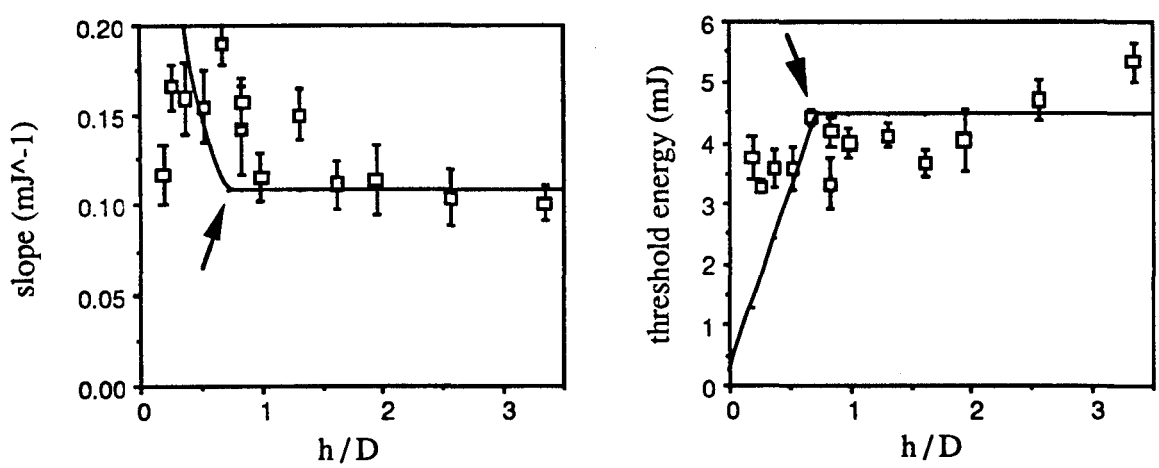

Figure 5.7. Slope η and threshold energy E_{thr} as a function of normalized distance between fibre and stone in silicone oil. (D = 320 μm)

It also appears that the theory manages to fit the data on slope η fairly good.

5.4 Comparison of the three liquid media

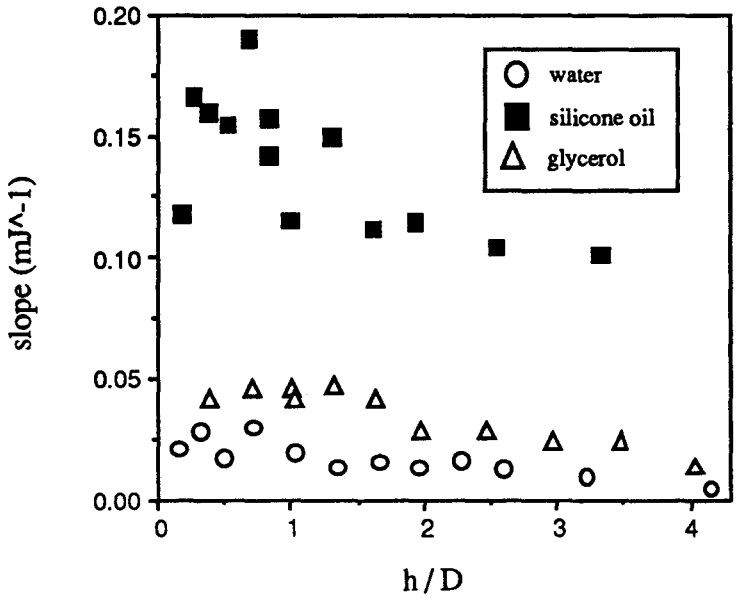

Figure 5.8. Slope η as a function of normalized distance between fibre and stone in all three liquids. (D = 320 μm; error bars have been omitted).

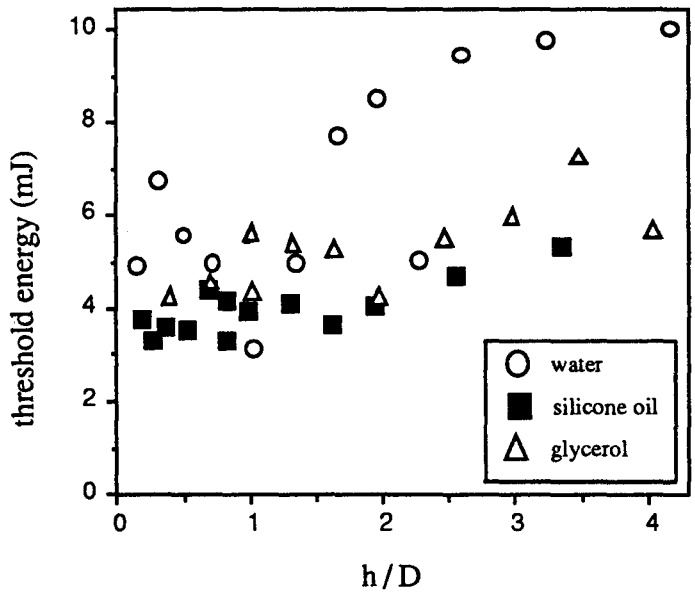

Figure 5.9. Threshold energy E_{thr} as a function of normalized distance between fibre and stone in all three liquids. (D = 320 μm; error bars have been omitted).

When ξ as defined in relation (3.13) is taken as the descriptive parameter of the liquid we can conclude that there is no plain monotonous dependence of both η and E_{thr} on ξ. Glycerol with its minimal value for ξ gives results in between the other two fluids. However one ought to be very cautious with respect to a quantitative comparison of the results on the slope η. The proportionality factor that links η and a function of h, D and ξ is dependent on other experimental parameters as for instance the distance between the source of acoustic effects and the probe beam.

6 DISCUSSION

6.1 On the results

The experiments on the slope η, being in fact a conversion efficiency, show a dependence on h/D. The theoretically modelled mechanism that is supposed to account for this dependency fits the experimental data reasonably well. However one can think of several other functions that will fit the data equally well so a confirmation of the theory cannot be concluded. A remarkable observation is the good agreement of the measurements on η with different fibre diameters. The significance of this fact is difficult to rate as it is unknown which secondary factors play a dominant role in determining η. Without doubt some of these have been different during experiments as is discussed in the next section. Moreover, coincidence cannot be excluded when considering only two diameters.

If from the same experiments the threshold energy E_{thr} is obtained two different regimes seem to arise. The first contains the data of measurements in water. In that case it can be concluded that the threshold energy also depends on h/D. Unfortunately, the two experimental series on different fibre diameters do not lead to an overall trend. It is obvious that the theory cannot fit either series. As it is still possible that the theory describes η properly the additional assumption of the product of η and E_{thr} being constant is probably not valid. An intuitive impression of these rough data is that for values of h/D beneath approximately one an universal function of E_{thr}/D might be distinguished. For h/D larger than unity the threshold energy increases with increasing h and does not depend on D.

The second regime consists of the experimental data obtained in the two viscous media. The results on E_{thr} in this regime do not show any significant dependence on h/D. However one gets the impression that E_{thr} slightly increases with increasing h/D at higher values. A logical explanation seems to be the beam divergence of the light coming out of the quartz fibre which reduces energy and power density at the stone surface. An estimate of this divergence confirms this presumption[1]: a divergence of approximately 7° can account for the average increase of the data.

---

1 The divergence θ leads to an increase of the effective diameter equal to θh (for small θ) so that the energy density or fluence F is given by

$$F = \frac{4E}{\pi D^2} = \frac{4E}{\pi(D_0 + \theta h)^2}$$

In conclusion the results on E_{thr} in the viscous media can best be presented as an average value independent of h/D. This yields values of 5.3 ± 0.6 mJ for glycerol and 4.0 ± 0.3 mJ for silicone oil (the accuracies equal two times the mean deviation σ_m; σ_m is defined in equation (5.1)).

The overview of the results on all three media mainly reveals the fact that no simple monotonous dependence on ξ is found as is expected from theory. Besides, more thorough study learns that this dependence is expected to be quite weak[1]. This evaluation is only true when on the whole the method can be expected to yield results that are independent on other factors.

It is very questionable whether the theoretical approach which is based on linear acoustics is applicable to media such as glycerol and silicone oil. Moreover one can imagine that characteristics other than the acoustic ones are responsible for the difference. Not only acoustic but also optical and thermal properties are essential and it can even be imagined that in case of an essential role for a plasma chemical properties like the polarity of the fluid become important. Hence it is difficult to come to any pertinent conclusions. However the observation that the liquid tends to influence the threshold energy in this unexpected way is in itself a remarkable result in this field.

In table 6.1. values of several properties have been gathered from different sources. One ought to be cautious with the data on silicone oil as most numbers deviate strongly from the analysis form of the supplier.

Demanding F to be independent of parameters at its threshold value F_{thr} leads to

$$E_{thr} = \frac{\pi D_0^2 F_{thr}}{4}\left(1 + \theta\left(\frac{h}{D_0}\right)\right)^2$$

which can be approximated by

$$E_{thr} = E_{thr,0}\cdot\left(1 + 2\theta\left(\frac{h}{D_0}\right)\right)$$

θ is estimated to be 0.12 rad ($\approx 7°$) and $E_{thr,0}$ is estimated to be 3 mJ in silicone oil and 4 mJ in glycerol. Thus at $h/D_0 = 3$ E_{thr} is expected to be 5 and 7 mJ respectively which agrees with experiments. (Linear regression on the experimental data yields a divergence of about 4°).

1 R_{tot} being proportional to $\xi/(4\xi h/D + 1)$ gives

$$\frac{\partial R_{tot}}{\partial \xi} \sim \frac{1}{(4\xi h/D + 1)^2} > 0$$

This derivative is small for the experimental ranges of ξ and h/D under consideration.

---

	silicone oil (Dimeticonum 350)	water	glycerol (Glycerolum 88 %)
density ρ 1)	0.85 ± 0.07	0.998 ± 0.004	1.06 ± 0.02
(g/cm^3) 2)	0.76 [36]	0.998 [36,37]	1.23 (88%) [37,a] 4)
			1.26 (100%) [36,37]
sound velocity c 1)	1.01 ± 0.03	1.44 ± 0.06	1.77 ± 0.06
(10^3 m/s) 2)	0.79 [36]	1.484 [36]	1.93 (100%) [36]
		1.497 [37]	1.904 (100%) [37]
3)			1.85 (88%) 4)
specific heat c_p			
(10^3 J/kg·K) 2)	1.37 [36]	4.18 [36]	2.43 (100%) [36] 4)
thermal conductivity λ			
(W/m·K) 2)	0.10 [36]	0.60 [36]	0.29 (100%) [36] 4)
thermal diffusivity κ 3)	0.96	1.44	0.95 (100%)
(10^{-7} m^2/s)			1.01 (88%) 4)
dynamic viscosity η 2)	0.49 [36]	1.00 [36]	1500 (100%) [36]
(10^{-3} kg/m·s)			1760 (100%) [37]
			147 (88%) [37]
kinematic viscosity ν 2)	344 [a]		120 (88%) [37]
(10^{-6} m^2/s = cSt) 3)	0.64 !!!	1.00	120
refractive index n_0 2)	-		1.456 [a]
(λ_0 = 589 nm)	-	1.333 [36]	1.469 (100%) [36]
(λ_0 = 687 nm)	-	1.330 [36]	1.466 (100%) [36]
3)	-		1.45 (88%)

Table 6.1. *Relevant properties of the respective liquids.*
1): measured: see appendix F 'Liquid properties';
2): reference values. [a] refers to the data of the supplier;
3): calculated from other quantities;
4): An estimate of the respective quantity Q at 88% is obtained by putting $Q = 0.88 \cdot Q_{glycerol,100\%} + 0.12 \cdot Q_{water}$. *In this way the following values are found:* $\rho = 1.23$; $c = 1.85$; $c_p = 2.64$; $\lambda = 0.33$; $\kappa = 1.01$.

The existence of viscosity and thermal conductivity results in dissipation of energy in pressure waves. Consequently the intensity of an acoustic wave decreases with the distance r traversed. For a spherical wave this implies that the pressure amplitude decays faster than 1/r

which is true for the case of no dissipation. This additional decrease in pressure will occur according to a law exp(-χr) where the absorption coefficient χ is found to be ([21])

$$\chi = \frac{\omega^2}{2\rho c^3}\left[\left(\frac{4}{3}\eta_{vis} + \zeta\right) + \lambda\left(\frac{1}{c_v} + \frac{1}{c_p}\right)\right] \equiv \psi\omega^2 \qquad (6.1)$$

where ω is the angular frequency and η_{vis} and ζ are the dynamic and second viscosity (coefficient) respectively. (This is only valid when the condition $\chi c/\omega << 1$ is satisfied which always appears to be true for liquids). Normally ζ is of the same order of magnitude as η_{vis} ([21]). Thus ψ can be approximated by

$$\psi \approx \frac{1}{2c^3}\left[\frac{7}{3}\nu + \kappa(\gamma - 1)\right] \qquad (6.2)$$

Substitution of numbers from table 6.1. shows two things. First the second term of relation (6.2) accounting for heat conduction is small compared to the influence of viscosity for all fluids. Only in case of glycerol and silicone oil and only at high enough frequencies dissipation becomes significant[1]. As it can be expected that the experimental pressure waves also contain frequencies of the order of 1 to 10 MHz dispersion effects are likely to appear.

6.2 On the method

The Schlieren set-up has already been discussed extensively in section 4.4. Although it appears to be complex to give an exact description of the experimental signal the method in itself is without doubt usable in these experiments. It has become obvious that utmost care must be taken in performing experiments to ensure identical circumstances.

---

1 $\omega_1 = 2\pi \cdot 10^6$ s^{-1} (frequency = 1 MHz) and $\omega_2 = 10\pi \cdot 10^6$ s^{-1} (frequency = 5 MHz).

		ψ (s^{2}m^{-1})	χ (m^{-1})	1/χ (mm)	exp(-χr) (r = 5mm)
silicone oil	ω_1	$8\cdot10^{-13}$	$3\cdot10^{1}$	$3\cdot10^{1}$	0.9
	ω_2		$8\cdot10^{2}$	1	0.02
water	ω_1	$3\cdot10^{-16}$	$1\cdot10^{-2}$	$1\cdot10^{5}$	1
	ω_2		$3\cdot10^{-1}$	$3\cdot10^{3}$	1
glycerol	ω_1	$2\cdot10^{-14}$	$8\cdot10^{-1}$	$1\cdot10^{3}$	1
	ω_2		$2\cdot10^{1}$	$5\cdot10^{1}$	0.9

To overcome most of the high requirements the choice was made to perform threshold measurements. The incomplete understanding of the physical meaning of the experimental signal leads to an arbitrary threshold definition. Qualitative comparison of all experimental series does not bring up reasonable doubt on the threshold criterium. Few series show a slight deviation from a linear trend around the threshold energy as can be seen in figure 6.1. The impression of a gradual decay of the signal can possibly be explained by a stochastic character of the physical interaction ([41]). At pulse energies comparable to the threshold energy not every laser pulse leads to shock wave induction. Hence averaging over ten measurements can lead to this gradual decay.

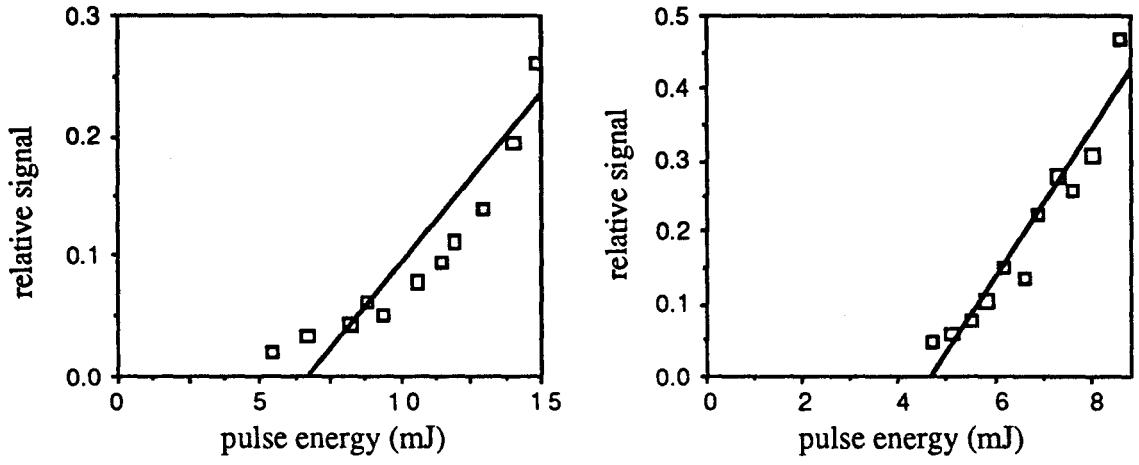

Figure 6.1. Examples of experimental series which imply another trend than a linear one.

It is also possible that all series contain this small effect but that it can only be distinguished when the signals themselves are small.

Convinced that this method is useful to do the threshold measurements a logical question arises: can this method be improved?

A first improvement is acquiring more experimental data. The series presented in this work contain little overlap and in that respect limited knowledge about accuracy in the results is obtained although extensive attention is paid to careful error analysis.

Second a consistent idea about the influence of secondary parameters will certainly lead to improvements. As an example one can think of an experiment where the distance between the source of acoustic effects at the laser spot and the probe beam is varied in a controlled way.

At present no information is found about the regime where the acoustic impedance of the liquid interface exceeds the combined impedance of the solids ($h/D < 1/4\xi$). It is clear that choosing a thicker fibre will enable measurements at smaller values of h/D. However

experimental experience leads to the expectation that acquiring useful data will become impossible.

Although these considerations are plausible they will probably not lead to an essential improvement of the results but mainly of the understanding. One has to be aware of two fundamental restrictions.

The method yields threshold values for acoustic effects at the position of the probe beam which need not be identical to threshold behaviour of the driving physical mechanism. As a consequence of the indirect nature of the method several assumptions and simplifications have to be made for interpretation. Therefore the primary interest is restricted to qualitative demonstration of a dependence on acoustic parameters as described in section 3.4. Clinical and prior laboratory experience shows that the fragmentation efficiency decreases rapidly when the fibre tip is further away from the stone surface ([10]). This implies that acoustic confinement is needed to obtain the desired effect.

The most important limitation of the method is the large spread in the experiments. This is partly due to spread in the experimental parameters but it is probable that the mechanism itself spreads significantly. Experimental circumstances which can vary are numerous.

* the laser pulse energy;
* the relative absorption of the stone surface. Originally the surface is polished. The ablative effect of the pulsed laser can change the optical behaviour of the stone material dramatically;
* the formation of small bubbles and dust has a strong effect on the experimental signal as can be seen from figure 6.2. where the signal after a single pulse is compared to that after the second pulse at the same spot. This effect can largely be reduced by either flushing the stone surface (in water) or shifting the stone with respect to the fibre tip. Disadvantage of the latter is the introduction of an uncertainty in distance h. Especially in the viscous media small persisting bubbles are formed. When these bubbles remain behind between fibre and stone surface the pressure wave signal will almost completely disappear regardless the laser pulse energy. Besides the dust formed by surface ablation is suspended in the viscous liquids and can lead to increased scattering of the probe beam.

As already mentioned an intrinsic stochastic nature of the physical mechanism is presumed ([41]) apart from these experimentally introduced uncertainties.

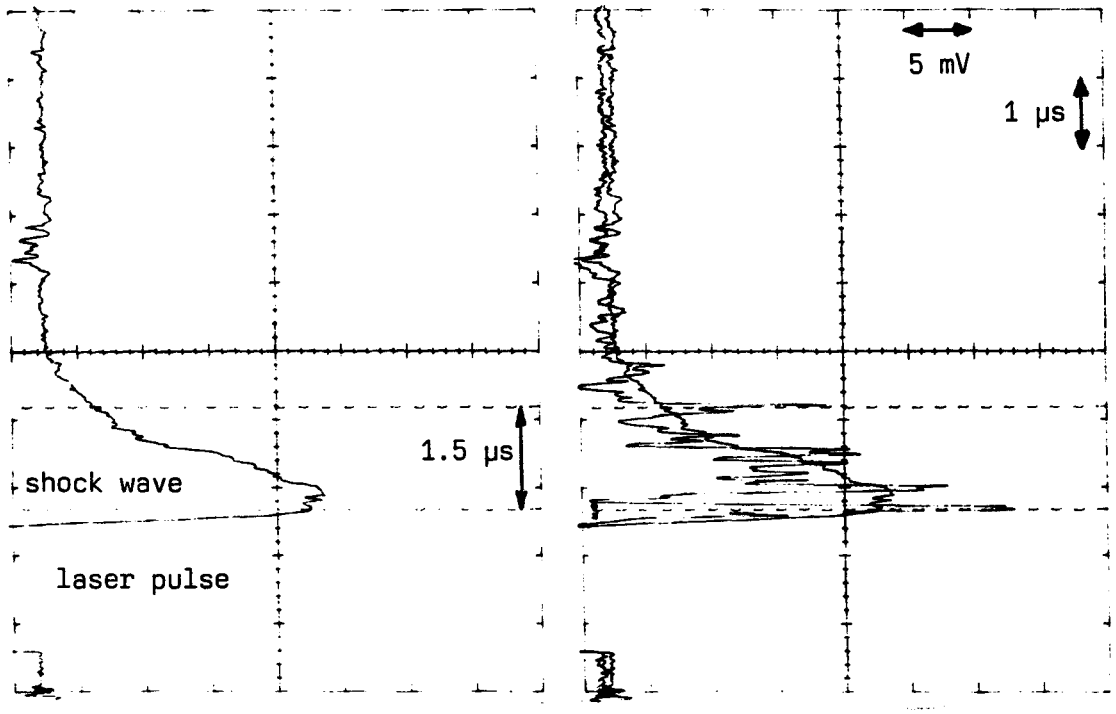

Figure 6.2. Experimental signal after the first and second laser pulse. (in water; 600 µm fibre; pulse energy ≈ 30 mJ).

6.3 On the physical mechanism

The general method for theoretical description of the interaction always contains two distinguishable parts. On one side the flow field of the surrounding liquid is considered. Usually straightforward acoustics is applied and complications only appear to arise when a realistic geometry has to be implemented.

The characteristic part for the interaction is the laser induced formation of a vapor bubble and its side effects like pressure waves. Evaluation of this part is meant to yield a description of how the laser pulse energy is (partially) converted to the energy of the vapor bubble. In the review of section 1.2 the two current mechanisms are presented. The plasma-mediated approach assumes almost total absorption of the laser light by an opaque plasma neglecting the initial plasma formation. The second analysis or hot particle flux mechanism takes explosive dissociation or ablation of the hot stone material to be responsible for the energy input.

The principle imperfection of both models is that they ignore the liquid medium in the analysis of the bubble formation. As already mentioned before the liquid will influence the initial stage of the interaction between stone material and laser light. The strongly simplified

analysis of chapter two confirms this idea. The results of this chapter justify a reconsideration of the main assumptions of existing theory.

* When merely heating of solid material in thermal contact with water is considered one should be aware of the strong dependence on both the optical absorption length δ and the relatively high thermal conductivity properties of water. The latter can appear to be of negligible influence as an insulating vapor layer is formed almost immediately but at low power densities e.g. in sub threshold tissue ablation it can become determining for certain processes;
* Second the possibility of explosive formation of an insulating water vapor layer alters the general idea on the assumptions of steady state ablation. Application of this principle is already disputable as McKenzie's model ([31]) is meant for description of ablation in air. In the realistic situation the ablation and subsequent expansion will have to take place against a considerable dynamic pressure that determines most parameters originally taken to be constant.

Finally the conception of a threshold effect is rather poor in existing theory. Lo ([27]) only concludes that a certain amount of energy is needed for plasma formation and that it concerns a small fraction of the total pulse energy.

Van Swol ([23]) and Wiersma ([22]) consider the energy required to raise the temperature of the stone material to its dissociation value to be the threshold energy. This can be expressed mathematically by

$$E_{thr} = \frac{\pi D^2}{4}\int_0^{\tau_d} \Phi \, dt' = \frac{\pi D^2}{4} \rho c_v \delta \, \Delta T \qquad (6.3)$$

Substitution of numerical values[1] leads to results that give rise to the supposition that the measured thresholds are not identical to this threshold criterium.

The same concept is found in a treatise on breakdown by Weyl but then a second stage is distinguished ([39]). Again at first heating during a time τ_d is supposed to take place until the vaporization temperature is reached. Thereafter a thermal runaway develops which can be understood as follows. Directly after the heating phase steady state ablation as described in equation (1.5) starts (The heating term $\mu c_v \Delta T$ is omitted). Certain constituents in the vapor with a relatively low ionization poten[illegible] will be partially ionized in the temperature regime under consideration. Subsequent inverse Bremsstrahlung (IB) absorption

---

1 Take δ to be between 1 and 10 μm in accordance with the results found by Sterenborg et al. ([38]). Take ΔT to be 2000 K and ρ and c_v given as in table 2.1. Then threshold values of 0.3 - 3.0 mJ (300 μm fibre) and 1.2 - 12.0 mJ (600 μm fibre) are found

by the free electrons will raise the temperature of the vapor which in its turn leads to more ionization and increased IB absorption. Thus the conditions for a thermal runaway have been created. Weyl succeeds in deriving a characteristic time τ_{vbr} that is required for vapor breakdown. Conclusively a threshold criterium is formulated by the requirement that the sum of τ_d and τ_{vbr} at least equals the laser pulse duration t_L. Implicitly the laser intensity is assumed constant over this time t_L. As this analysis concerns breakdown of vapor at a free surface certain adaptations are necessary. The confinement of the vapor by the surrounding liquid (and fibre) will probably have a favourable effect on the total interaction as it leads to an increase in vapor pressure and temperature. Thus a plasma initiating mechanism is found.

Mainly out of curiosity the experiment was also conducted in air. It appears to be possible to detect considerable pressure waves as can be seen from figure 6.3. This need not lead to the conclusion that the confinement concept is false as a reasonably flat stone phantom is used and the fibre is put onto the stone. Besides this observation holds no information on the damage to the stone surface which can also be strongly dependent on the (confinement of the) surrounding medium.

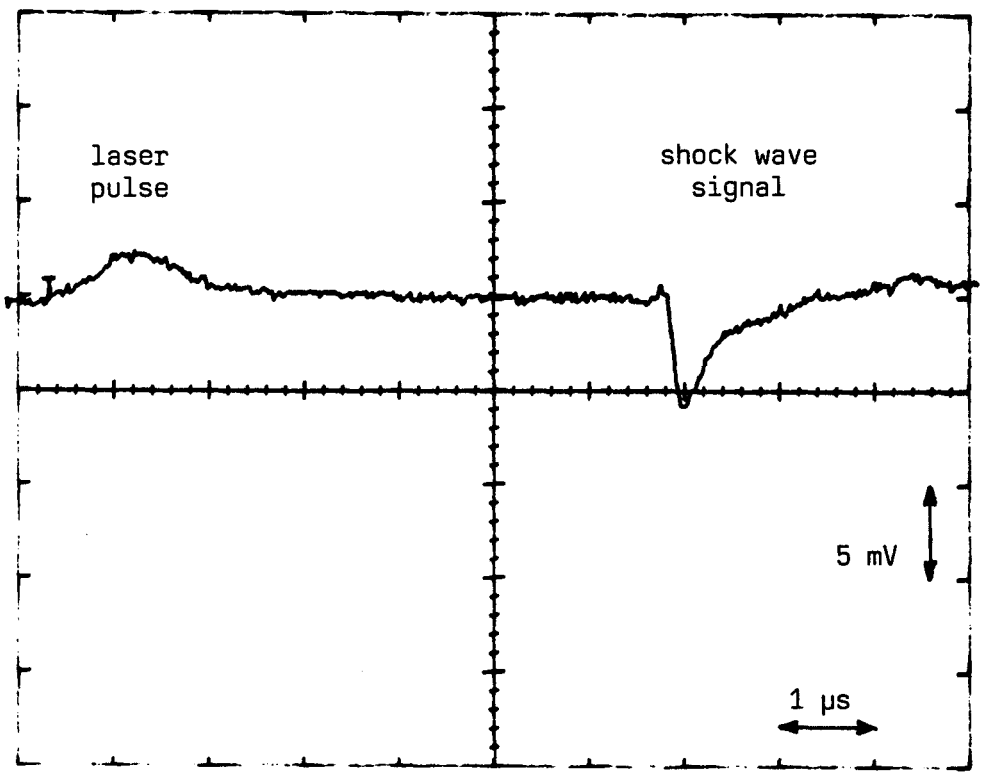

Figure 6.3. Example of an experimental result in air. (320 µm fibre; pulse energy unknown).

7 CONCLUSIONS

Calculations on thermal effects show that the influence of the optical absorption length δ in relation to the thermal diffusion length $\sqrt{(\kappa t)}$ cannot simply be neglected. Further it appears that the presence of water is likely to be more important than has been assumed up till now. A simple calculation on vaporization of water leads to fast and reasonably large pressure effects with an order of magnitude of 50 bars on a time scale of 10 ns. It is necessary to evaluate the consequences of the surrounding liquid thoroughly.

Considering the optical detection method and the developed threshold criterium it can be concluded that both are well applicable for the threshold measurements performed. It is also thinkable that the same set-up or principle is used for detection of comparable pressure waves in other physical and clinical regimes.

The experimental results on slope efficiency η show to be dependent on the distance h between fibre tip and stone surface. It is possible that η is proportional to the total acoustic impedance of the vapor/medium interfaces involved.

No significant dependence on the fibre diameter D is found.

The measurements on threshold energy E_{thr} in both glycerol and silicone oil do not yield a significant dependence on geometrical parameters h and D. The average threshold energies are found to be 4.0 ± 0.3 mJ (silicone oil) and 5.3 ± 0.6 mJ (glycerol) respectively. The accuracies equal two times the mean deviation ($p = 0.95$).

The results on threshold energy E_{thr} in water give the impression of a dependency on h and D. For values of h/D smaller than one E_{thr} increases with diminishing h while for h/D exceeding unity E_{thr} tends to increase with increasing h. Ignoring this possible trend the average for all measurements (29) in water can be calculated to be 8 ± 1 mJ (accuracy two times the mean deviation). This agrees with the result of the acoustic threshold measurement of Wiersma ([22]) which is 7 ± 2 mJ.

With respect to the acoustic impedance of the surrounding fluid it can be concluded that results on both η and E_{thr} do not show the expected monotonous relation with ξ. First the large viscosity of glycerol and silicone oil makes the applicability of linear acoustic theory questionable. Besides, the presumption arises that in addition to the acoustic properties other

characteristics are also important. The possibility of the liquid being an important factor in the bubble formation has been neglected in current theory.

In all liquids the proposed one dimensional flow field model based on linear acoustic theory cannot fit the results. This theoretical model only explains the coupling of the pressure waves into the respective media. It is possible that the interaction process responsible for generation of the pressure waves also depends on the parameters under consideration. When this is the case the simple theory is concealed by the total dependency on parameters.

Finally, in evaluating the physical process of laser lithotripsy it is necessary to consider basic processes first before studying complicated mechanisms and subsequent theory. Such may well lead to a satisfactory description and will in any case improve the understanding of the total process.

ACKNOWLEDGMENTS

Two years ago I had to choose the physical discipline for my graduation work. Only a short conversation was sufficient for Rini van Dongen to push me in the right direction. With the aid and widespread contacts of dr. Massen I visited several hospitals and gradually the specific choice became more difficult although the direction had become clear.

I also met Dick Sterenborg who had to cancel two double appointments, how typical! Dick became my coach. Above all things I want to thank him for the (unintentional ?) liberty that enabled working in the independent way I like. At the same time it strengthened my self-reliance as a physicist. Together with Geert Gijsbers, Niek van Wieringen and Jan Wiersma we had a weekly meeting (the 'bubble club') where profound discussions were combined with fantastic suggestions. Also lots of thanks to the rest of the Laser Centre for the pleasant atmosphere and the sincere interest in work and person. Johan and Peter thanks for the 'graphical' support and many thanks to Arie Steenbeek for his time and technical assistance in straightening out several annoying defects.

During the second half of my training an essential part of this work was supported by people from the University of Technology in Eindhoven. Thanks to David Smeulders for lending me the pressure transducers and Jan Willems for his constructive interest and the trouble of getting me a quadrant photodiode. Special thanks to Mico Hirschberg for the help with the analysis of the Schlieren method and the critical reading of the subsequent chapter. Special thanks also to Rini van Dongen who together with Mico supplied the basis for the theoretical work of chapter two, invested a lot of precious time and did all that with a catching enthusiasm.

Finally thanks to my mediator dr. Massen who read this report critically and gave me the opportunity to develop my organizing talents. According to him thanking him would equal admission of putting up a job... Last but not least thanks to Niav O'Daly who made my English gooder.

DANKWOORD

Twee jaar geleden diende ik een afstudeerrichting te kiezen. Het was Rini van Dongen die mij in een kort gesprekje een flinke duw in de juiste richting gaf. Via de wijdverbreide contacten van dhr. Massen kon ik in meerdere ziekenhuizen een kijkje nemen en hoewel de richting inmiddels duidelijk vorm had aangenomen werd de eigenlijke keuze allengs moeilijker.

Zo kwam ik ook in contact met Dick Sterenborg die en passant nog even twee andere dubbele afspraken moest afzeggen. Dick werd mijn directe afstudeerbegeleider. Waar ik hem bovenal voor wil bedanken zijn de (onbedoelde ?)vrijheid die mij in staat stelde te werken op de door mij geliefde zelfstandige manier. Tegelijkertijd kwam het mijn zelfvertrouwen als fysicus ten goede. Samen met Geert Gijsbers, Niek van Wieringen en Jan Wiersma vormden wij een werkgroepje (de "bellenclub") waarin naast diepgaande discussies ruimte was voor (achteraf ?) de meest fantastische ingevingen. De rest van het Laser Centrum allen zeer bedankt voor de prettige sfeer en de oprechte interesse in elkanders werk en persoon. Dank aan Johan en Peter voor de "grafische" ondersteuning. Arie Steenbeek zeer bedankt voor de geweldige technische hulp en tijd om de nodige euvelen te verhelpen.

In de tweede helft van mijn stage werd een essentieel deel van het werk ondersteund door mensen van de Technische Universiteit Eindhoven. David Smeulders leende mij de pressure transducers. Jan Willems bedankt voor het lospraten van een kwadrantendiode en de interesse in mijn werk. Speciale dank aan Mico Hirschberg voor de hulp bij de analyse van de Schlieren methode en de correctie van het betreffende hoofdstuk. Ook speciale dank aan Rini van Dongen die samen met Mico de fundamenten aanleverde voor het theoretische werk van hoofdstuk twee, daar veel kostbare tijd in investeerde en dit alles deed met een zeer aanstekelijk enthousiasme.

Tenslotte dank aan dhr. Massen die dit rapport kritisch heeft bekeken en mij graag mijn organisatorische kwaliteiten liet ontplooien. Hem bedanken zou gelijk staan aan het toegeven van een doorgestoken kaart. Last but not least Niav O'Daly bedankt voor het onder de loep nemen van mijn Engels.

REFERENCES

[1] D.C. Emmony, M.W. Sigrist, F.K. Kneubühl, 'Laser-induced shock-waves in liquids', Appl. Phys. Lett. **29** (1976) 547-549.

[2] P. Harris, H.N. Presles, 'Reflectivity of a 5.8 kbar shock front in water', J. Chem. Phys. **74** (1981) 6864-6866.

[3] P. Teng, N.S. Nishioka et al., 'Acoustic studies of the role of immersion in plasma-mediated laser ablation', IEEE J. Qu. El. **23** (1987) 1845-1852.

[4] R.S. Dingus, B.P. Shafer, 'Laser-induced shock wave effects in materials', SPIE Vol. **1202** 'Laser-Tissue Interaction' (1990) 36-45.

[5] A.G. Doukas, R. Birngruber, T.F. Deutsch, 'Determination of the shock wave pressures generated by laser-induced breakdown in water', SPIE Vol. **1202** 'Laser-Tissue Interaction' (1990) 61-70.

[6] P. Teng, N.S. Nishioka et al., 'Microsecond-long flash photography of laser-induced ablation of biliary and urinary calculi', Lasers in Surg. & Med. **7** (1987) 394-397.

[7] P. Teng, N.S. Nishioka et al., 'Optical studies of pulsed-laser fragmentation of biliary calculi', Appl. Phys.B **42** (1987) 73-78.

[8] S. Thomas, J. Pensel et al., 'The pulsed dye laser versus the Q-switched Nd:YAG laser in laser-induced shock-wave lithotripsy', Lasers in Surg. & Med. **8** (1988) 363-370.

[9] P. Teng, N.S. Nishioka et al., 'Mechanisms of laser-induced stone ablation', SPIE Vol. **712** 'Lasers in Medicine' (1986) 161-164.

[10] H.J.C.M. Sterenborg, C.R. Erkens et al., 'Laser lithotripsy with a 504 nm pulsed dye laser: in vitro fragmentation related to stone weight and pulse energy', Lasers in Med. Science **5** (1990) 65-69.

[11] P. Teng, N.S. Nishioka et al., 'Mechanism of laser-induced fragmentation of urinary and biliary calculi', Lasers in the Life Sciences **1** (1987) 231-245.

[12] U. Drees, 'Ein Beitrag zur Dichtegradientenmessung in Überschallströmungen mit Hilfe eines quantitativen Laser-Schlierensystems', (1981) dissertation Technische Hochschule Aachen.

[13] E.W. Marchand, 'Gradient index optics', (1978) Academic Press, New York.

[14] J.G. Kirkwood, 'Shock and detonation waves', ed. by W.W. Wood, (1963) Univ. of Cal., Los Alamos.

[15] Y.B. Zel'dovich, S.B. Kormer et al., 'A study of the optical properties of transparent materials under high pressure', Soviet Phys.-Doklady **6** (1961) 494-496.

[16] M.H. Rice, J.M. Walsh, 'Equation of state of water to 250 kilobars', J. Chem. Phys. **26** (1957) 824-830.

[17] M. Born, E. Wolf, 'Principles of optics' 5th ed., (1975) Pergamon Press, Oxford.

[18] E. Hecht, A. Zajac, 'Optics', (1974) Addison-Wesley Publ. Comp., Reading.

[19] H.C.W. Beijerinck, 'Lasers in fysische experimenten 3P140', (1987) syllabus Technische Universiteit Eindhoven.

[20] M.G.M. Ferguson-Hessler, 'Statistische methoden in de natuurkunde voor N1.2', (1985) syllabus Technische Universiteit Eindhoven.

[21] L.D. Landau, E.M. Lifshitz, 'Fluid Mechanics' 2nd ed. from 'Course on theoretical physics' Vol. **6** (1987) Pergamon Press, Oxford.

[22] J. Wiersma, 'Bubble formation in laser lithotripsy - a mathematical description', (1990) internal report, Laser Centre, AMC, Amsterdam.

[23] C.F.P. van Swol, 'Some physical aspects of laser lithotripsy', (1990) internal report, Laser Centre, AMC, Amsterdam.

[24] B. Ward, D.C. Emmony, 'Conservation of energy in the oscillations of laser-induced cavitation bubbles', J. Acoust. Soc. Am. **88** (1990) 434-441.

[25] G.M. Watson, J.E.A. Wickham, 'The use of a laser for fragmenting ureteric calculi', in 'Lasers in de geneeskunde' ed. by M.J.C. van Gemert, T.A. Boon, (1987) 222-231.

[26] M.J.C. van Gemert, W.M. Star, 'Fysische achtergronden van klinisch lasergebruik' in 'Lasers in de geneeskunde' ed. by M.J.C. van Gemert, T.A. Boon, (1987) 52-74.

[27] E.Y. Lo, H. Petschek, D.I. Rosen, 'A hydrodynamic model for the laser-induced fragmentation of calculi', Lasers in the Life Sciences **3** (1990) 233-244.

[28] G. Weyl, T. Tucker, 'Penetration of plasma radiation in tissue', Lasers in the Life Sciences **3** (1989) 125-138.

[29] A. Hirschberg, 'Shock tube determination of the heat conductivity of non-ionized and partially ionized argon', (1981) dissertation Technische Hogeschool Eindhoven.

[30] M. Brugmans, 'Temperature response of water, polyacrylamide and biological tissues to non-ablative pulsed CO_2 radiation', (1990) internal report, Laser Centre, AMC, Amsterdam.

[31] H.S. Carslaw, J.C. Jaeger, 'Conduction of heat in solids', 2nd ed. (1986) Clarendon Press, Oxford.

[32] A.L. McKenzie, 'How far does thermal damage extend beneath the surface of CO_2 laser incisions ?', Phys. Med. Biol. **28** (1983) 905-912.

[33] M. Abramowitz, I.A. Stegun, 'Handbook of mathematical functions', (1965) Dover Publications Inc. NY.

[34] P.J. Vrugt, 'Shock tube study of the coefficient of thermal conductivity of helium, neon, argon, and krypton', (1976) dissertation Technische Hogeschool Eindhoven.

[35] N. van Wieringen, 'Rapid expanding and imploding gas bubbles caused by a XeCl excimer laser used in laser angioplasty', (1991) internal report, Laser Centre, AMC, Amsterdam.

[36] 'BINAS, informatieboek VWO-HAVO voor het onderwijs in de natuurwetenschappen', (1986) Wolters-Noordhoff, Groningen.

[37] 'Handbook of Chemistry and Physics', 56th ed. (1975) ed. by R.C. Weast, CRC Press, Cleveland.

[38] H.J.C.M. Sterenborg, C.F.P. van Swol et al., 'Laser lithotripsy with a pulsed dye laser, correlation between the threshold energy and the optical properties', SPIE Biomed. Opt. 91 (1991) 1724-1728.

[39] G.M. Weyl, 'Physics of laser-induced breakdown: an update' in 'Laser-induced plasmas and applications', ed. by L.J. Radziemski, D.A. Cremers (????) 44-52, M. Dekker Inc., New York.

[40] T.F. Irvine, P.E. Liley, 'Steam and gas tables with computer equations', (1984) Academic Press, NY.

[41] H.J.C.M. Sterenborg, 'A theoretical analysis of stone fragmentation rates', internal paper (1991).

[42] H.J.C.M. Sterenborg, 'Pressure build-up on a surface in front of a fibre', internal paper (1990).

BACKGROUND READING

[43] B. Zysset, J.G. Fujimoto, T.F. Deutsch, 'Time-resolved measurements of picosecond optical breakdown', Appl. Phys. B **48** (1989) 139-147.

[44] K.K. Boyarskii, A.P. Galtsev et al., 'Wave-front distortion in light passage through a shock wave', Opt. Spectrosc. (USSR) **64** (1988) 859-861.

[45] G.S. Bushanam, F.S. Barnes, 'Laser-generated thermoelastic shock wave in liquids', J. Appl. Phys. **46** (1975) 2074-2082.

[46] C.E. Bell, J.A. Landt, 'Laser-induced high-pressure shock waves in water', Appl. Phys. Lett. **10** (1967) 46-48.

[47] H. Schöffmann, H. Schmidt-Kloiber, E. Reichel, 'Time-resolved investigations of laser-induced shock waves in water by use of polyvinylidenefluoride hydrophones', J. Appl. Phys. **63** (1988) 46-51.

[48] N.C. Anderholm, 'Laser-generated stress waves', Appl. Phys. Lett **16** (1970) 113-115.

[49] M.W. Sigrist, F.K. Kneubühl, 'Laser-generated stress waves in liquids', J. Acoust. Soc. Am. **64** (1978) 1652-1663.

[50] A.J. Campillo, R.D. Griffin, P.E. schoen, 'Reflective probing of laser generated multi-kbar compressional shocks in water', Opt. Comm. **57** (1986) 301-306.

[51] H. Schmidt-Kloiber, E. Reichel, H Schöffmann, 'Laserinduced shock-wave lithotripsy (LISL)', Biomed. Technik **30** (1985) 173-181.

[52] R.D. Griffin, B.L. Justus et al., 'Interferometric studies of the pressure of a confined laser-heated plasma', J. Appl. Phys. **59** (1986) 1968-1971.

[53] H. Schmidt-Kloiber, E. Reichel, 'Die Abhängigkeit der Druckamplitude einer Stoßwelle von der Feldstärke beim laserinduzierten Durchbruch in Flüssigkeiten', Acustica **54** (1984) 284-288.

[54] R. Wrobel, P. Bernage et al., 'XeCl laser in biliary calculus fragmentation: fluence threshold and ablation products', IEEE Transact. on Biomed. Eng. **36** (1989) 1202-1208.

[55] W. Shi, T. Papaioannou et al., 'Fragmentation of biliary stones with a 308 nm excimer laser', Lasers in Surg. & Med. **10** (1990) 284-290.

[56] K.M. Bhatta, D. I. Rosen et al., 'Acoustic and plasma guided lasertripsy (APGL) of urinary calculi', J. of Urology **142** (1989) 433-437.

[57] K.M. Bhatta, D.I. Rosen, S.P Dretler, 'Acoustic and plasma-guided laser angioplasty', Lasers in Surg. & Med. **9** (1989) 117-123.

[58] R.K. Luneburg, 'Mathematical theory of physics', (1966) Univ. of Cal. Press, Los Angeles.

[59] W.K. Blake, 'Mechanisms of flow-induced sound and vibration' Vol. 1, (1986) Academic Press, New York.

[60] W. Hentschel, W. Lauterborn, 'Acoustic emission of single laser-produced cavitation bubbles and their dynamics', Appl. Sci. Res. **38** (1982) 225-230.

[61] A. Vogel, W. Lauterborn, 'Time-resolved particle image velocimetry used in the investigation of cavitation bubble dynamics', Appl. Opt. **27** (1988) 1869-1876.

[62] R. Hickling, M.S. Plesset, 'Collapse and rebound of a spherical bubble in water', Phys. of Fluids **7** (1964) 7-14.

[63] A. Shima, K. Nakajima, 'The collapse of a non-hemispherical bubble attached to a solid wall', J. Fluid Mech. **80** (1977) 369-391.

[64] A. Vogel, W. Lauterborn, R. Timm, 'Optical and acoustic investigations of the dynamics of laser-produced cavitation bubbles near a solid boundary', J. Fluid. Mech. **206** (1989) 299-338.

[65] W. Lauterborn (ed.), 'Cavitation and inhomogeneities in underwater acoustics', (1980) Springer-Verlag, Berlin.

[66] S.J. Gitomer, R.D. Jones, 'Laser-produced plasmas in medicine', SPIE Vol. **1202** 'Laser-Tissue Interaction' (1990) 118-132.

[67] S.M. Jones, P.L. Carson et al., 'Simplified technique for the calibration and use of a miniature hydrophone in intensity measurements of pulsed ultrasound fields', J. Acoust. Soc. Am. **70** (1981) 1220-1228.

[68] R.C. Preston, D.R. Bacon et al., 'PVDF membrane hydrophone performance properties and their relevance to the measurement of the acoustic output of medical ultrasonic equipment', J. Phys. E: Sci. Instrum. **16** (1983) 786-796.

[69] R.G. Kepler, R.A. Anderson, 'Piezoelectricity and pyroelectricity in polyvinylidene fluoride', J. Appl. Phys. **49** (1978) 4490-4494.

[70] A.J. Coleman, J.E, Saunders et al., 'Acoustic cavitation generated by an extracorporeal shockwave lithotripter', Ultrasound in Med. & Biol. **13** (1987) 69-76.

[71] A.J. Coleman, J.E, Saunders, 'A survey of the acoustic output of commercial extracorporeal shock wave lithotripters', Ultrasound in Med. & Biol. **15** (1989) 213-227.

[71] H.M. Gijsman, 'Thermodynamica', (1986) syllabus Technische Universiteit Eindhoven.

[72] M.J.C. van Gemert, A.J. Welch, 'Time constants in thermal laser medicine', Lasers in Surg. & Med. **9** (1989) 405-421.

APPENDIX A
Reflectivity of a shock front

After having decided upon whether the shock waves should be detected acoustically or optically, the different principles for an optical detection method were taken into consideration. Besides transmission of a probe beam reflectivity seemed a promising option.

Assuming that a shock front gives rise to a steep increase in pressure, and as a result, the refractive index, we studied this possibility quite thoroughly. The modelling calculations were based on a publication of Harris & Presles ([2]) who take the following equation as a starting point. Locally, for a given angle of incidence $\theta(z)$, the differential amplitude of the reflected ray is given by

$$\frac{dE_r}{E(z)} = \left(\frac{dn}{n(z)}\right)\left(1 \mp \tan^2 \vartheta(z)\right) \qquad (A.1)$$

where dn is the differential change in local index of refraction, and the (-,+) denotes the parallel and perpendicular polarizations respectively to the plane of incidence. E(z) is the given field strength at a given depth z.

After assuming zero absorption and the application of Poynting's theorem and Snell's law, this equation can be rearranged in order to yield

$$\left|\frac{E_r}{E_0}\right| = \sin\left\{\frac{1}{2n_0}\int_0^{\infty}\left(\frac{\partial n}{\partial z}\right)\left(1 \mp \tan^2\vartheta(z)\right)\cos\left[2\pi\left(\gamma_A - \gamma_B\right)\right]dz\right\} \qquad (A.2)$$

where the subscript 0 denotes initial values and the phase difference $(\gamma_A - \gamma_B)$ may be written as

$$(\gamma_A - \gamma_B) = \frac{2}{\lambda_0}\int_0^{z}\sqrt{\left(n^2(z') - n_0^2\sin^2\vartheta_0\right)}\,dz' \qquad (A.3)$$

where λ_0 denotes the wavelength in vacuum. Equations (A.2) and (A.3), taken together, are a solution of the shock front reflectivity problem for a non absorbing planar shock front. When we restrict ourselves to normal incidence these equations reduce to

$$\left|\frac{E_r}{E_0}\right| = \sin\left\{\frac{1}{2n_0}\int_0^{\infty}\left(\frac{\partial n}{\partial z}\right)\cos\left[2\pi\left(\gamma_A - \gamma_B\right)\right]dz\right\} \tag{A.4}$$

and

$$\left(\gamma_A - \gamma_B\right) = \frac{2}{\lambda_0}\int_0^{z} n(z')\,dz' \tag{A.5}$$

When this result is applied to a constant gradient of the refractive index like Harris & Presles do

$$\frac{\partial n}{\partial z} = \frac{\Delta n}{L} \tag{A.6}$$

the rapid evaluation of dependence of the reflectivity upon pressure amplitude (proportional to refractive index amplitude Δn) and shock front thickness L is possible. Therefore the parameter β, the relative shock front thickness, is introduced

$$\beta = \frac{Ln_0}{\lambda_0} \tag{A.7}$$

In figure A.1. the dependence of equation A.4 upon this parameter is shown:

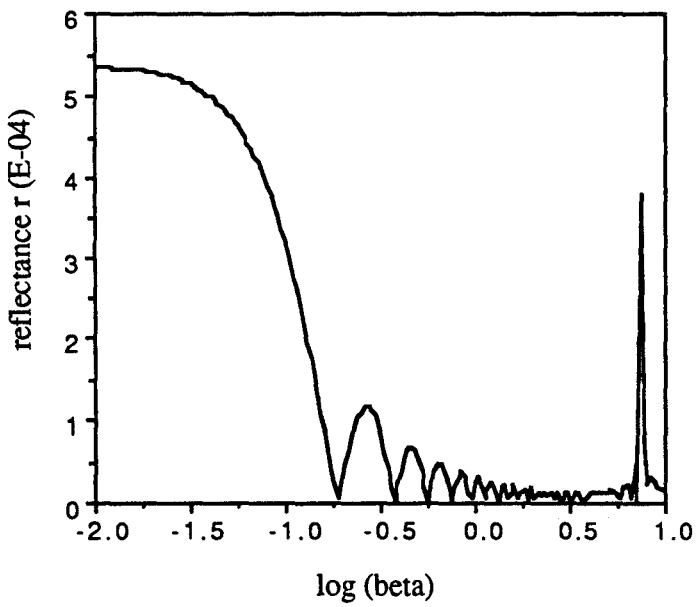

Figure A.1. Shock front reflectivity as a function of the shock front thickness normalized to the wavelength .

We see that for small values of β the reflectance approximates the limiting case of a step change in refractive index[1]. More important is the fact that for shock thicknesses larger than 1/10 of the wavelength the reflectance is very small and strongly dependent on β due to interference effects. For this reason the measuring principle of reflectivity is rejected.

1 $\Delta n = 0.00144$ (this value corresponds with a pressure change of 100 bar) and n_0 is 4/3.
For normal incidence a transition between two medium of different refractive index leads to reflectance of $(n_1 - n_2)/(n_1 + n_2)$ ([18]) which relation equals $5.4 \cdot 10^{-4}$ in this case.

APPENDIX B
Evaluation of the acoustic flow field

1 Fluid dynamics ([21])

The flow of an ideal, inviscid and compressional fluid is described by equating the conservation of mass and the momentum ([21])

$$\text{mass}: \quad \frac{\partial \rho}{\partial t} + \operatorname{div}(\rho \underline{v}) = 0 \tag{B.1}$$

$$\text{momentum}: \quad \frac{\partial \underline{v}}{\partial t} + (\underline{v}.\operatorname{grad})\,\underline{v} = -\frac{1}{\rho}\operatorname{grad} p \tag{B.2}$$

where $\underline{v}$ is the velocity, p pressure and ρ the density. Applying the acoustic approximation

$$\rho = \rho_0 + \rho' \quad ; \quad p = p_0 + p' \tag{B.3}$$

yields

$$\frac{\partial \rho'}{\partial t} + \rho_0 \operatorname{div} \underline{v} = 0 \tag{B.4}$$

$$\frac{\partial \underline{v}}{\partial t} + \left(\frac{1}{\rho_0}\right) \operatorname{grad} p' = 0 \tag{B.5}$$

Further we use the fact that a sound wave in an ideal fluid is adiabatic

$$p' = \left(\frac{\partial p}{\partial \rho_0}\right)_s \rho' \tag{B.6}$$

where the subscript s denotes constant entropy. After introducing the velocity potential ϕ by defining $\underline{v} = \operatorname{grad} \phi$ and the sound velocity c by defining $c^2 = (\partial p/\partial \rho_0)$ the equations (B.4) and (B.5) taken together yield a wave equation for ϕ

$$\frac{\partial^2 \phi}{\partial t^2} - c^2 \Delta \phi = 0 \tag{B.7}$$

2 Spherical symmetry ([21])

Reworking equation (B.7) for spherical coordinates yields

$$\frac{\partial^2(r\phi)}{\partial t^2} - c^2 \frac{\partial^2(r\phi)}{\partial r^2} = 0 \qquad \text{(B.8a)}$$

or equivalently

$$\frac{\partial^2\phi}{\partial t^2} - c^2 \frac{1}{r^2}\frac{\partial}{\partial r}\left(r^2 \frac{\partial\phi}{\partial r}\right) = 0 \qquad \text{(B.8b)}$$

The general solution of this equation is given by

$$\phi(r,t) = \frac{f_1(ct - r)}{r} + \frac{f_2(ct + r)}{r} \qquad \text{(B.9)}$$

where the first term represents a wave moving away from the origin and the second term a wave travelling towards it. We restrict ourselves to an outgoing wave, in other words $f_2 = 0$. Expressing the pressure and velocity fluctuations around the ambient conditions in terms of ϕ yields for the spherical case

$$- p'(r,t) = -\rho_0 \frac{\partial\phi}{\partial t} \qquad \text{(B.10)}$$

$$u(r,t) = \frac{\partial\phi}{\partial r} \qquad \text{(B.11)}$$

After substituting (B.9) putting f_1 equal to f we get

$$p(r,t) = -\frac{\rho_0 c}{r} f' + p_0 \qquad \text{(B.12a)}$$

$$u(r,t) = -\left(\frac{f}{r^2} + \frac{f'}{r}\right) \qquad \text{(B.12b)}$$

where f' denotes the derivative of f with respect to its argument (ct - r).

3 Imposed continuity at the bubble interface ([27])

In order to couple the bubble dynamics to the surrounding acoustic flow field continuity of velocity and pressure is imposed at the bubble interface, i.e. r = a(t). The bubble wall velocity is given by

$$\frac{da}{dt} = u|_{r=a(t)} = -\left(\frac{f}{a^2} + \frac{f'}{a}\right)\Big|_{r=a(t)} \tag{B.13}$$

Re-expressing this using (B.12a) and writing radius a(t) in terms of volume V(t) yields

$$\frac{1}{4\pi}\frac{dV}{dt} = -f|_{r=a(t)} + \frac{1}{\rho c}\left(\frac{3V}{4\pi}\right)^{2/3}(p - p_0) \tag{B.14}$$

Which after differentiation with respect to t gives

$$\frac{d^2V}{dt^2} = -4\pi\frac{df}{dt}\Big|_{r=a(t)} + \frac{1}{\rho c}(48\pi^4)^{1/3}\frac{d}{dt}\left[V^{2/3}(p - p_0)\right] \tag{B.15}$$

Applying the chain rule for differentiation to df/dt at r = a(t), and using equation (B.12a) we get

$$\begin{aligned}\frac{d}{dt}f(ct - r)|_{r=a(t)} &= \left(c - \frac{da}{dt}\right)f'|_{r=a(t)} = \\ -\frac{1}{\rho c}&\left[c - \left(\frac{1}{36\pi V^2}\right)^{1/3}\frac{dV}{dt}\right]\left(\frac{3V}{4\pi}\right)^{1/3}(p - p_0)\end{aligned} \tag{B.16}$$

Substituting this into equation (B.15) finally yields the second order equation for V(t)

$$\frac{d^2V}{dt^2} = \frac{(48\pi^2)^{1/3}}{\rho}V^{1/3}(p - p_0) + \frac{(36\pi)^{1/3}}{\rho c}\left[\frac{1}{3}V^{-1/3}(p - p_0)\frac{dV}{dt} + V^{2/3}\frac{dp}{dt}\right] \tag{B.17}$$

APPENDIX C
Basic considerations on thermal effects

For very little is known about relevant parameters like pressure and temperature a few basic processes concerning thermal effects where studied more thoroughly. The principle problem was reduced severely to enable rather simple calculations. These calculations will be presented and commented on in this section.

1 Thermal properties

All calculations can only yield numeric values when the thermal properties of the media, i.e. stone and water, are known. Values for density ρ, specific heat c_p and thermal conductivity λ and sound velocity c are needed. Here the following values will be used:

	ρ (kg/m^3)	c_p (J/kg.K)	λ (W/m.K)	c (m/s)
water	1000	4200	0.60	1500
stone	2500	920	2.60	3000

Table C1. Thermal properties ([31,36,37)

The numbers for stone material are the mean of values for marble, granite, sandstone and gypsum found in references [31], [36] and [37] except for the sound velocity which value is an estimate based on reference values.

2 General definition of the problem

Three general assumptions are made throughout the following sections:

* The problem can be described in one dimension;
* The media are considered to be semi-infinite with their boundary plane located at $x = 0$;

* The dissipated energy per unit area per unit time, the so called irradiance or flux Φ_0, is considered constant during the nominal laser pulse time t_L.

Then the following procedure as outlined in Carslaw & Jaeger ([31]) is performed. For each medium the following general relation is valid

$$\rho c_p \frac{\partial T}{\partial t} - \frac{\partial}{\partial x}\left(\lambda \frac{\partial T}{\partial x}\right) = Q_s \qquad \text{(C.1)}$$

where Q_S represents a source and T a temperature change. We assume λ to be constant and Q_S independent with time for the stone material and equal to zero for water. Rearrangement of relation (C.1) leads to

$$\frac{\partial^2 T_1}{\partial x^2} - \frac{1}{\kappa_1}\frac{\partial T_1}{\partial t} = 0 \qquad \text{(C.2a)}$$

$$\frac{\partial^2 T_2}{\partial x^2} - \frac{1}{\kappa_2}\frac{\partial T_2}{\partial t} = \frac{-Q_s(x)}{\lambda_2} \qquad \text{(C.2b)}$$

where κ_i equals

$$\kappa_i = \frac{\lambda_i}{\rho_i c_{pi}} \qquad \text{(C.3)}$$

and is called the thermal diffusivity.

These two coupled relations can be solved by performing Laplace transformations and defining initial and boundary conditions for each specific problem. Here a few different cases where studied: the stone material was considered either insulated or in thermal contact with water and the laser energy dissipation was considered to be either in the boundary plane or described by Beer's law.

3 Surface heat dissipation; insulated stone material

This case is fully described by Carslaw & Jaeger ([31]) and Brugmans ([30]). The solution of equation (C.2b) for a semi-infinite medium at $x > 0$ with boundary condition

$$\frac{\partial T_2}{\partial x} = 0 \quad , x = 0 \qquad \text{(C.4)}$$

and

$$Q_s(x) = \Phi_0 \ [W/m^2] \qquad \text{(C.5)}$$

is

$$T_2(x,t) = \frac{2\Phi_0}{\lambda_2}\left\{\sqrt{\frac{\kappa_2 t}{\pi}}\exp\left(\frac{-x^2}{4\kappa_2 t}\right) - \frac{x}{2}\operatorname{erfc}\left(\frac{x}{2\sqrt{\kappa_2 t}}\right)\right\} \qquad \text{(C.6)}$$

where the function erfc has been introduced. This function is defined as

$$\operatorname{erfc}(z) = \frac{2}{\sqrt{\pi}}\int_z^\infty \exp(-\zeta^2)\,d\zeta = 1 - \operatorname{erf}(z) \qquad \text{(C.7a)}$$

$$\operatorname{erf}(z) = \frac{2}{\sqrt{\pi}}\int_0^z \exp(-\zeta^2)\,d\zeta \qquad \text{(C.7b)}$$

$$\operatorname{erf}(\infty) = 1,$$
$$\operatorname{erf}(-z) = -\operatorname{erf}(z)$$

erf(z) is the so called error function.
For the stone surface at x = 0 equation (C.6) reduces to

$$T_2(0,t) = \frac{2\Phi_0}{\lambda_2}\sqrt{\frac{\kappa_2 t}{\pi}} \qquad \text{(C.8)}$$

Because of the linearity of Laplace transformation the solution when taking the finite laser pulse time t_L into account can be found rather easily. One adds a second term that declares the thermal response to an equally large step source function at time t_L of opposite sign, i.e. $-\Phi_0$. The full solution for the stone surface is

$$T_2(0,t) = \frac{2\Phi_0}{\lambda_2}\sqrt{\frac{\kappa_2}{\pi}}\left(\sqrt{t} - \sqrt{t - t_L}\,H(t - t_L)\right) \qquad \text{(C.9)}$$

where the Heaviside or unit step function $H(z - z_0)$ is introduced

$$H(z - z_0) = \begin{cases} 0 & , z < z_0 \\ 1 & , z \geq z_0 \end{cases} \qquad \text{(C.10)}$$

4 Surface heat dissipation; thermal contact with water

We now have two semi-infinite media, the region x < 0 containing water (index 1) and the region x > 0 containing stone (index 2). The boundary conditions for this problem are

$$T_1(0,t) = T_2(0,t) \tag{C.11a}$$

$$\lambda_1 \frac{\partial T_1}{\partial x} = \lambda_2 \frac{\partial T_2}{\partial x} \quad , x = 0 \tag{C.11b}$$

Intuitively a solution of the following form is expected

$$T_1(x,t) = \frac{2\alpha_1 \Phi_0}{\lambda_1} \left\{ \sqrt{\frac{\kappa_1 t}{\pi}} \exp\left(\frac{-x^2}{4\kappa_1 t}\right) + \frac{x}{2} \operatorname{erfc}\left(\frac{-x}{2\sqrt{\kappa_1 t}}\right) \right\} \tag{C.12a}$$

$$T_2(x,t) = \frac{2\alpha_2 \Phi_0}{\lambda_2} \left\{ \sqrt{\frac{\kappa_2 t}{\pi}} \exp\left(\frac{-x^2}{4\kappa_2 t}\right) - \frac{x}{2} \operatorname{erfc}\left(\frac{x}{2\sqrt{\kappa_2 t}}\right) \right\} \tag{C.12b}$$

where α_i is a number between zero and one. Boundary condition (C.11a) then leads to

$$\frac{\alpha_2}{\alpha_1} = \left(\frac{\lambda_2}{\lambda_1}\right) \sqrt{\frac{\kappa_1}{\kappa_2}} = \alpha \tag{C.13}$$

and requiring $\alpha_1 + \alpha_2 = 1$ yields

$$\begin{aligned} \alpha_1 &= \frac{1}{1+\alpha} \\ \alpha_2 &= \frac{\alpha}{1+\alpha} \end{aligned} \tag{C.14}$$

The full solution for the interface is then given by a slightly modified version of relation (C.9)

$$T_1(0,t) = T_2(0,t) = \left(\frac{\alpha}{1+\alpha}\right) \frac{2\Phi_0}{\lambda_2} \sqrt{\frac{\kappa_2}{\pi}} \left(\sqrt{t} - \sqrt{t - t_L}\, H(t - t_L) \right) \tag{C.15}$$

With the values as tabulated in section 1 a value for α_2 of about 0.6 is found. In other words, the thermal contact with water leads to a decrease in temperature of 40 %. However one has to realize that this case is rather pathological as the water will start to evaporate at 100 ^{0}C or a temperature change of approximately 80 K. When a vapor layer has been formed between stone and water it behaves as an almost perfect insulator compared to water and the solution of the surface temperature will approximate the one given in equation (C.9).

5 Optical absorption length δ; insulated stone material

When instead of total absorption at the surface the light flux is assumed to obey Beer's law

$$\Phi(x) = \Phi_0 e^{-(x/\delta)} \tag{C.16}$$

The dissipated energy is given by

$$Q_s(x) = -\frac{d\Phi(x)}{dx} = \frac{\Phi_0}{\delta} e^{-(x/\delta)} \tag{C.17}$$

which is still constant with respect to time. Again boundary condition (C.4) is valid. Laplace transformation of equation (C.2b) after the appropriate substitutions gives

$$\frac{d^2\overline{T_2}}{dx^2} - \frac{s}{\kappa_2}\overline{T_2} = -\frac{\Phi_0}{\lambda_2\delta s}e^{-(x/\delta)} \qquad (C.18)$$

for $T_2(t=0)$ equals zero. The boundary condition remains exactly the same for the transformed function. The solution of linear differential equation (C.18) is then given by

$$\overline{T_2}(x,s) = \frac{A\kappa_2 e^{-(x/\delta)}}{s\left(s-\frac{\kappa_2}{\delta^2}\right)} - \frac{A\kappa_2 e^{-q_2 x}}{\delta q_2 s\left(s-\frac{\kappa_2}{\delta^2}\right)} \qquad (C.19)$$

where $A = \Phi_0/(\lambda_2\delta)$ and $q_2 = \sqrt{(s/\kappa_2)}$. The first term represents the particular solution while the second is the homogeneous one. After separation of the second term in two simpler ones relation (C.19) can be transformed back to the time domain, e.g. with the aid of Carslaw & Jaeger ([31]). The solution is, dropping the subscripts for simplicity

$$T(x,t) = \frac{\Phi_0\delta}{\lambda}e^{-(x/\delta)}\left(e^{(\kappa t/\delta^2)}-1\right) -$$

$$\frac{\Phi_0\delta}{\lambda}\frac{1}{2}e^{(\kappa t/\delta^2)}\left\{e^{-(x/\delta)}\operatorname{erfc}\left[\frac{x}{2\sqrt{\kappa t}}-\sqrt{\frac{\kappa t}{\delta^2}}\right] - e^{(x/\delta)}\operatorname{erfc}\left[\frac{x}{2\sqrt{\kappa t}}+\sqrt{\frac{\kappa t}{\delta^2}}\right]\right\} +$$

$$\frac{2\Phi_0}{\lambda}\left\{\sqrt{\frac{\kappa t}{\pi}}\exp\left(\frac{-x^2}{4\kappa t}\right) - \frac{x}{2}\operatorname{erfc}\left(\frac{x}{2\sqrt{\kappa t}}\right)\right\} \qquad (C.20)$$

The last term equals the solution for surface heating in relation (C.6). The surface temperature change can, again, be found by filling in zero for x

$$T(0,t) = \frac{\Phi_0\delta}{\lambda}\left\{\frac{2}{\delta}\sqrt{\frac{\kappa t}{\pi}} + e^{(\kappa t/\delta^2)}\operatorname{erfc}\left(\sqrt{\frac{\kappa t}{\delta^2}}\right) - 1\right\} \qquad (C.21)$$

Looking qualitatively to this expression it is obviously the solution for surface heating plus a correction. This correction is dependent on $\sqrt{(\kappa t)}/\delta$ which is in fact the ratio of the thermal diffusion length and the optical absorption length. It is interesting to distinguish two limits for this ratio

I. $\sqrt{\kappa t} \ll \delta$ or $\frac{\sqrt{\kappa t}}{\delta} \ll 1$

Series expansion of the respective terms of equation (C.21) ([33]) and using (C.7) yields

$$e^{z^2}\,\mathrm{erf}(z) = \frac{2}{\sqrt{\pi}}\left(z + \frac{2}{3}z^3 + \frac{4}{15}z^5 + \ldots\right)$$

$$e^{z^2} - 1 = \left(z^2 - \frac{1}{2}z^4 + \frac{1}{6}z^6 - \ldots\right)$$

where z is of course $\sqrt{(\kappa t)}/\delta$. Neglecting terms of an order higher than two leads to a strongly simplified temperature change

$$T(0,t) \approx \frac{\Phi_0\delta}{\lambda}\left(z^2 + \frac{2}{\sqrt{\pi}}z - \frac{2}{\sqrt{\pi}}z\right) = \frac{\Phi_0\kappa t}{\lambda\delta} \qquad \text{(C.22)}$$

so initially the temperature increase is proportional to time t.

II. $\sqrt{\kappa t} \gg \delta$ or $\frac{\sqrt{\kappa t}}{\delta} \gg 1$

Again using Abramowitz ([33]) learns us that

$$e^{z^2}\,\mathrm{erfc}(z) \to 0 \quad \text{for} \quad z \to \infty$$

so that T(0,t) reduces to

$$T(0,t) = \frac{\Phi_0\delta}{\lambda}\left(\frac{2}{\sqrt{\pi}}\sqrt{\frac{\kappa t}{\delta^2}} - 1\right) \approx \frac{2\Phi_0}{\lambda}\sqrt{\frac{\kappa t}{\pi}} \qquad \text{(C.23)}$$

which is identical to the solution for surface heating (C.8). Especially this limit can be understood intuitively: when the thermal diffusion length is much larger than the optical absorption length the dimension of the latter becomes less important, in other words the heat dissipation takes place in a relatively diminishing layer.

Whether this limit will be reached taking κ as a constant is strongly dependent on the optical absorption length δ. We therefore calculated the surface temperature for different values of δ as a function of time, at the same time taking the finite duration of the laser pulse into account. The thermal properties and state of the stone are assumed to be constant which is rather pathological for one can expect changes of state at temperatures of about 3 to 4000 degrees Kelvin where the peak temperature in case of superficial absorption is found to be about 35 000 K. However, these calculations give a coarse estimate of maximum temperatures possible. All secondary effects like thermal contact with and subsequent losses to a liquid, changes of state, changes in thermal properties lead to a reduction in possible temperatures.

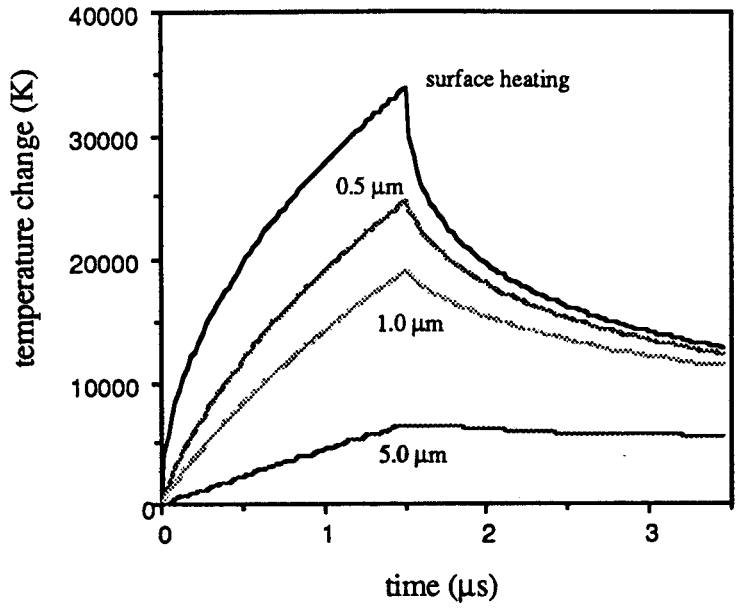

Figure C.1. *Temperature change as a function of time for different optical absorption lengths. Irradiance $\Phi_0 = 6.0 \cdot 10^{10}$ W/m^2 which corresponds to a 25 mJ laser pulse out of a 600 µm diameter fibre.*

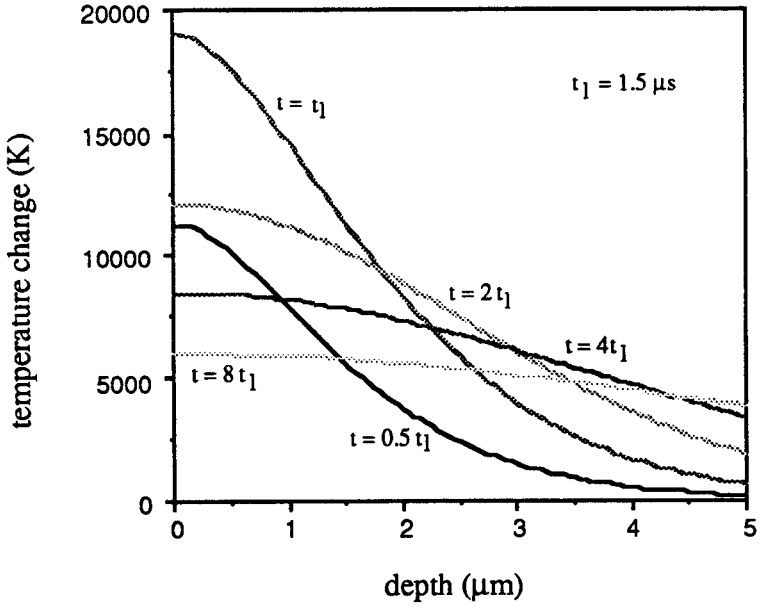

Figure C.2. *Temperature as a function of space for the same parameters. Optical absorption length δ is taken to be 1 µm..*

6 Thermal expansion

We take the conservation of mass as a starting point

$$\frac{\partial \rho}{\partial t} + \frac{\partial}{\partial x}(\rho u) = 0 \qquad \text{(C.24)}$$

Integration with respect to x and some rearrangement gives us the velocity u

$$u = -\frac{1}{\rho}\int \left(\frac{\partial \rho}{\partial T}\right)_p \frac{\partial T}{\partial t} dx \qquad \text{(C.25)}$$

Eventual density changes as a consequence of pressure effects are neglected: only thermal expansion is considered. We recognize the thermal expansion coefficient in relation (C.25)

$$-\frac{1}{\rho}\left(\frac{\partial \rho}{\partial T}\right)_p = a_T \qquad \text{(C.26)}$$

Substituting this and using equation (C.2a) dropping all subscripts yields

$$u = a_T \kappa \int \frac{\partial^2 T}{\partial x^2} dx = -a_T \kappa \left(\frac{\partial T}{\partial x}\right)_{x=0} = \frac{a_T \kappa}{\lambda}\Phi_0 = \frac{a_T}{\rho c_p}\Phi_0 \qquad \text{(C.27)}$$

Next we consider two semi-infinite media whose boundary plane has a velocity u_0. The total velocity in one medium is then given by

$$u_i = u_0 + \frac{a_{Ti}}{\rho_i c_{pi}}\Phi_{0i} \qquad \text{(C.28)}$$

where subscript i refers to the different media and the sign of Φ_{01} is opposite to that of Φ_{02}. The pressure change is then given by

$$p = -\rho_1 c_1 u_1 = \rho_2 c_2 u_2 \qquad \text{(C.29)}$$

The interface velocity can be eliminated by working out the equality at the right hand side. Resubstituting the solution then yields for the pressure p

$$p = \frac{Z_1 Z_2}{Z_1 + Z_2}\left(A_2\Phi_{02} - A_1\Phi_{01}\right) \qquad \text{(C.30)}$$

where Z_i is the acoustic impedance $\rho_i c_i$ and A_i is deduced from equation (C.28)

$$A_i = \frac{a_{Ti}}{\rho_i c_{pi}} \qquad (C.31)$$

For the respective expansion coefficients the following values are deduced from literature values ([37])

$$\begin{aligned} &\text{stone:} && a_{T1} = 9\cdot10^{-6}\ K^{-1} \\ &\text{water:} && a_{T2} = 2.5\cdot10^{-4}\ K^{-1} \end{aligned} \qquad (C.32)$$

We found as a result in section 4 that stone material in thermal contact with water absorbs 60 % of the total deposited heat and the remainder diffuses into the water. When all the numbers are substituted in relation (C.30) we get

$$p = (3.3\cdot10^{-4})\cdot\Phi_0 \quad [Pa] \qquad (C.33)$$

which means for an incident irradiance Φ_0 of $6.0\cdot10^{10}$ W/m^2 a pressure change of approximately 20 bar.

7 Water vaporization

7.1 Definition of the problem

The basic assumptions and conditions are outlined in section 2.3 of this report.

* The vapor layer is supposed to be mainly insulating. We therefore take semi-infinite liquid water at 373 K (100 °C) and force a temperature change ΔT_w as calculated in section 5 of this appendix at its boundary. The optical absorption length δ and irradiance Φ_0 are taken to be 1 μm and $6.0\cdot10^{10}$ W/m^2 respectively.
* A heat flux q that is small compared to the total laser light flux or irradiance Φ_0 exists over the vapor layer. This heat flux is assumed spatially constant over the layer and described by

$$|q| = \lambda_v \frac{dT}{dx} = \lambda_v \frac{\{T_w(t) - T_d(p)\}}{d} \qquad (C.34)$$

where λ_v is the supposed constant heat conductivity of the vapor, d the thickness of the vapor layer and $T_d(p)$ the saturated vapor temperature at x = d. The dependency of T_d on pressure is linearized based on data from steam tables ([40]).

* At the vapor-liquid interface the flux q supplies the latent heat L required for vaporization. The energy needed to heat the liquid is neglected. The vapor is supposed to expand instantaneously by a factor ρ_l/ρ_v which is the ratio of liquid and vapor density. This yields a second relation for q

$$|q| = L\rho_v \frac{d}{dt}(d) \qquad (C.35)$$

The dependency of vapor density ρ_v, latent heat L and their product on pressure can also be derived from steam tables ([40]). Their product is again linearized.

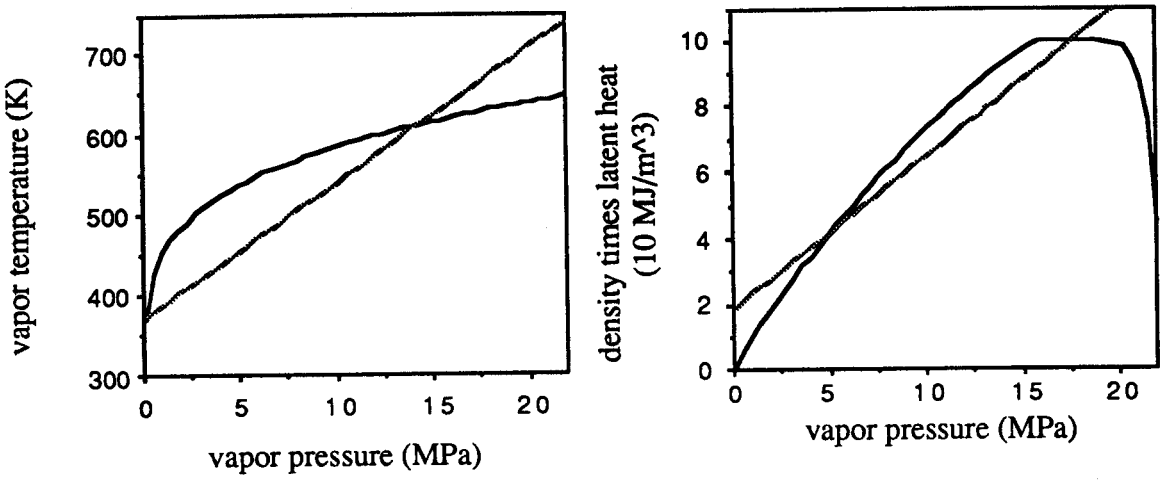

*Figure C.3. Temperature and L*ρ as a function of vapor pressure p.*

* Equating q from relations (C.34) and (C.35) yields a relation between pressure p and layer thickness d.

$$\rho_v L d\frac{d}{dt}(d) = \lambda_v \{T_w(t) - T_d(p)\} \qquad (C.36)$$

A second differential equation of p and d is found from basic acoustic theory

$$p - p_{ref} = \rho_l c \frac{d}{dt}(d) \qquad (C.37)$$

Besides we express both T_d and $\rho_v L$ in terms of $(p-p_{ref})$

$$\begin{aligned} T_d(p) &= T_{ref} + S\cdot(p - p_{ref}) \\ \rho_v L(p) &= P + Q\cdot(p - p_{ref}) \end{aligned} \qquad (C.38)$$

Subsequent substitution leads to a non-linear differential equation for thickness d alone

$$\rho_l c Q d\left(\frac{d}{dt}(d)\right)^2 + \left(\lambda_v \rho_l c S + Pd\right)\cdot\frac{d}{dt}(d) - \lambda_v(T_w(t) - T_{ref}) \qquad (C.39)$$

7.2 Initial conditions

The major problem of the analysis is the tendency of heat flux q, layer velocity and pressure p to approximate infinity at small values for time t and layer thickness d. If relation (C.37) is substituted directly for d(d)/dt in equation (C.36) we get

$$d = \frac{\rho_l c \lambda_v}{p - p_{ref}} \frac{\{T_w(t) - T_d(p)\}}{\rho_v(p) L(p)} \tag{C.40}$$

For sufficiently small times ρ_v, L and T_d can be approximated by evaluation with respect to pressure p and omitting the higher order terms

$$d = \frac{\rho_l c \lambda_v}{(p - p_{ref})} \frac{\{T_w(t) - T_{do} - T_{dop}(p - p_{ref})\}}{\{\rho_{vo} + \rho_{vop}(p - p_{ref})\}\{L_o + L_{op}(p - p_{ref})\}} \tag{C.41}$$

where subscript p denotes derivation with respect to $(p-p_{ref})$ and subscript 0 implies values at $p = p_{ref}$. Working out this result gives

$$d = \frac{\rho_l c \lambda_v}{\rho_{vo} L_o} \left\{ \frac{(T_w(t) - T_{do})}{(p - p_{ref})} - T_{dop} \right\} \left\{ 1 - \frac{\rho_{vop}}{\rho_{vo}}(p - p_{ref}) - \frac{L_{op}}{L_o}(p - p_{ref}) \right\} \tag{C.42}$$

where the last factor appears to be almost equal to unity and can thus be neglected. Rearrangement and substitution of equation (C.37) yields

$$d\frac{d}{dt}(d) + \frac{\rho_l c \lambda_v}{\rho_{vo} L_o} T_{dop} \frac{d}{dt}(d) = \frac{\lambda_v}{\rho_{vo} L_o} \{T_w(t) - T_{do}\} \tag{C.43}$$

Integration gives as a final result

$$\frac{1}{2}d^2 + \frac{\rho_l c \lambda_v}{\rho_{vo} L_o} T_{dop}(d) = \frac{\lambda_v}{\rho_{vo} L_o} \int_0^t \Delta T_w(t')\, dt' \tag{C.44}$$

The integral over time of the boundary temperature change can be calculated from equation (C.21). Integration of the three separate terms is trivial except for the second one. The outcome of that integration is

$$\frac{\Phi_0\delta}{\lambda}\int_0^t e^{(\kappa t'/\delta^2)}\,\mathrm{erfc}\left(\sqrt{\frac{\kappa t'}{\delta^2}}\right)dt' =$$
$$\frac{\delta^2}{\kappa}\left\{\frac{\Phi_0\delta}{\lambda}\left[\frac{2}{\delta}\sqrt{\frac{\kappa t}{\pi}} + e^{(\kappa t/\delta^2)}\,\mathrm{erfc}\left(\sqrt{\frac{\kappa t}{\delta^2}}\right) - 1\right]\right\} = \frac{\Phi_0\delta t}{\lambda} \qquad \text{(C.45)}$$

where the second step follows from equation (C.22) as $\sqrt{(\kappa t)} \ll \delta$. As this result compensates for the third term of the integral the total result is simply given by

$$\int_0^t \Delta T_w(t')\,dt' = \frac{4\Phi_0}{3\lambda}\sqrt{\frac{\kappa}{\pi}}\,t^{3/2} \qquad \text{(C.46)}$$

So now d can be approximated for small times and subsequently velocity d(d)/dt and pressure change ($p-p_{ref}$) can be found. A well-chosen set of these parameters can serve as the initial conditions for equation (C.39).

7.3 Numerical solution

Thickness d and its first derivative with respect to time are expanded in a Taylor series

$$d(t) = d|_{t=t_0} + \frac{d}{dt}(d)|_{t=t_0}(t - t_0) + \frac{d^2}{2dt^2}(d)|_{t=t_0}(t - t_0)^2$$
$$\frac{d}{dt}(d(t)) = \frac{d}{dt}(d)|_{t=t_0} + \frac{d^2}{dt^2}(d)|_{t=t_0}(t - t_0) \qquad \text{(C.47)}$$

Now the basis for a numerical code has been developed. By choosing the respective time intervals small enough to satisfy the criterium

$$\frac{d^2}{dt^2}(d)|_{t=t_0}(t - t_0) \ll \frac{d}{dt}(d)|_{t=t_0} \qquad \text{(C.48)}$$

equation (C.39) can be solved fairly accurately. Some results can be found in section 2.3 of the report. Here the time development of the heat flux is displayed in figure C.4. At the end of this appendix the computer program is reproduced.

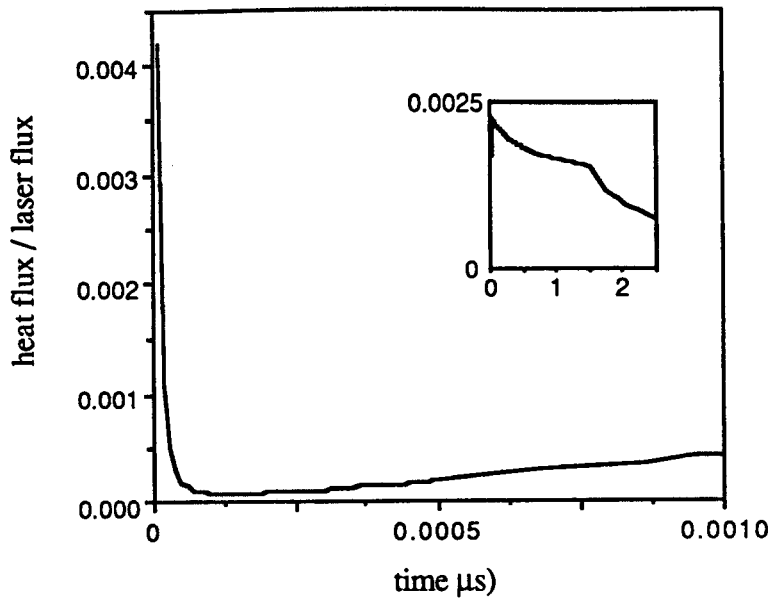

Figure C.4. Heat flux over a water vapor layer as a function of time.

```
verdamping;

uses crt;

const   lambda_vap = 0.02; {W/m*K}
                rho_liq = 1000.0; {kg/m*m*m}
                velo_liq = 1500.0; {m/s}
                cp = 4200.0; {J/kg*K}
                spec_heat = 920.0; {J/kg*K}
                rho_st = 2500.0; {kg/m*m*m}
                lambda_st = 2.6; {W/m*K}
                p_ref = 1.0E05; {Pa}
                T_ref = 372.87; {K}
                pulse = 1.5E-06;
                kappa = (lambda_st/(rho_st*spec_heat));
                delta = 1.0E-06;
                phi = 6.0E10;
                P = 1.921E07;
                Q = 4.592;
                S = 16.761E-06;
                C1 = 2*Q*rho_liq*velo_liq;
                C2 = lambda_vap*rho_liq*velo_liq*S;
                number = 400;

var     i,j,k:integer;
        time,length,speed,druk,secder:array[0..5] of real;
        pres,d,dt,dtt,t,temp,tstep,v:real;
        pres_file:text;
        goed:boolean;

function term1(x:real):real;
begin
  term1:=2*sqrt(kappa*x/pi)
end;

function term2(x:real):real;
var
  z,y:real;
begin
 z:=x;
```

```
 if (z<0.01) then term2:=1-(2*z/sqrt(pi))
 else if (z>100) then term2:=0
 else
 begin
   y:=1/(1+0.3275911*z);
    z:=y*(0.254829592-0.284496736*y+1.421413741*y*y
              -1.453152027*y*y*y+1.061405429*y*y*y*y*y);
  term2:=z
 end;
end;

function T_wall(x:real):real;
var A,b:real;
begin
  b:=kappa/(delta*delta);
  A:=(phi*delta)/lambda_st;
 if (x<(1.0E-04/b)) then T_wall:=A*b*t
 else
 begin
 if (x<pulse)then
   T_wall:=((phi/lambda_st)*term1(x))+(A*(term2(sqrt(b*x))-1))
       else
   T_wall:=((phi/lambda_st)*(term1(x)-term1((x-pulse))))
              +(A*(term2(sqrt(b*x))-term2(sqrt(b*(x-pulse)))))
 end;
end;

procedure taylor(af0,af1,af2,t0:real; var dd,ddt,tt:real);

begin
  dd:=af0+(af1*tstep)+((af2/2)*tstep*tstep);
  ddt:=af1+(af2*tstep);
  tt:=t0+tstep
end;

procedure snelheid(af0,af1,t0:real; var ddt:real);
const crit = 1.0E-06;
var help1,help2,help3:real;
begin
  help1:=(P*af0)+C2;
  help2:=C1*af0;
   help3:=2*help2*lambda_vap*T_wall(t0);
   help2:=help1/help2;
   help1:=help1*help1;
   help3:=help3/help1;
 if (help3<crit) then ddt:=(help2*help3)/2
 else  ddt:=help2*(sqrt(1+help3)-1)
end;

begin
  time[0]:=1.0E-17;t:=time[0];
   length[0]:=1.278821E-21;d:=length[0];
   speed[0]:=0.0001918377;dt:=speed[0];
   secder[0]:=1.918377E13;
  druk[0]:=287.75649226; {[Pa]}
   time[1]:=5.0E-10;time[2]:=5.0E-09;time[3]:=5.0E-08;
   time[4]:=5.0E-07;time[5]:=5.0E-06;
 clrscr;
 assign(pres_file,'c:\jz\filmdruk.dat');rewrite(pres_file);
 for k:=1 to 5 do
 begin
    tstep:=(time[k]-time[k-1])/(50*number);
   for j:=1 to 50 do
   begin
     pres:=dt*rho_liq*velo_liq;{[Pa]}
    temp:=(S*pres);
    writeln(pres_file,t,' ',d,' ',dt,' ',pres,' ',temp,' ',T_wall(t));
    for i:= 1 to number do
    begin
```

```
      goed:=false;
      while NOT goed do
      begin
        snelheid(d,dt,t,v);
         taylor(d,v,dtt,t,d,dt,t);
        dtt:=(dt-v)/tstep;
       goed:=(abs(dt-v)<(dt));
       if (NOT goed) and (tstep>1.0E-15) then
       begin  t:=t-tstep;tstep:=tstep/10.0  end
       else goed:=true;
     end;
    end;
   end;
  end;
  close(pres_file)
end.
```

APPENDIX D
The Schlieren set-up

1 Considerations on alignment

A Gaussian beam of a certain wavelength λ_0 can be described by the waist length L_w for then waist w_0 and divergence α_0 are ([19])

$$w_0 = \sqrt{\frac{\lambda_0 L_w}{n\pi}} \qquad \text{(D.1a)}$$

$$\alpha_0 = \sqrt{\frac{\lambda_0}{n\pi L_w}} \qquad \text{(D.1b)}$$

These and other parameters of a laser beam are explained in figure D.1.

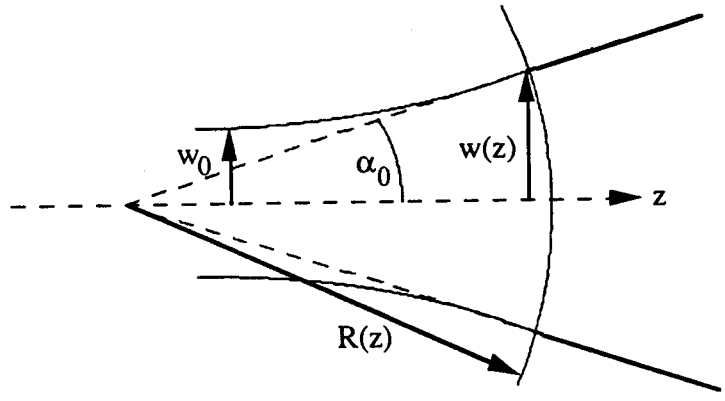

Figure D.1. The propagation properties of a laser beam ([34]).

The passage of a laser beam through an optical system is most conveniently described by means of a complex beam parameter q(z) defined as

$$q(z) = z - jL_w \qquad \text{(D.2a)}$$

or

$$\frac{1}{q(z)} = \frac{1}{R(z)} - j\frac{\lambda_0}{n\pi w^2(z)} \qquad \text{(D.2b)}$$

q(z) is usually referred to as the complex radius of curvature. Passage of an interface of two media leads to the transformation formula

$$q(z^+) = \left(\frac{n_2}{n_1}\right) q(z^-) \tag{D.3}$$

where the minus and 1 denote the side of incidence and the plus and 2 the side of transmittance of the interface. Travelling a distance z_d through a homogeneous medium is described by

$$q(z + z_d) = q(z) + z_d \tag{D.4}$$

So the transition of a focused beam from air through a perspex wall of thickness z_d into water leads to an alteration of the complex radius of curvature mathematically described by

$$q(z_b^+) = q(\{z_a + z_d\}^+) = \left(\frac{n_3}{n_1}\right) q(z_a^-) + \left(\frac{n_3}{n_2}\right) z_d \tag{D.5}$$

The respective quantities are illustrated in figure D.2.

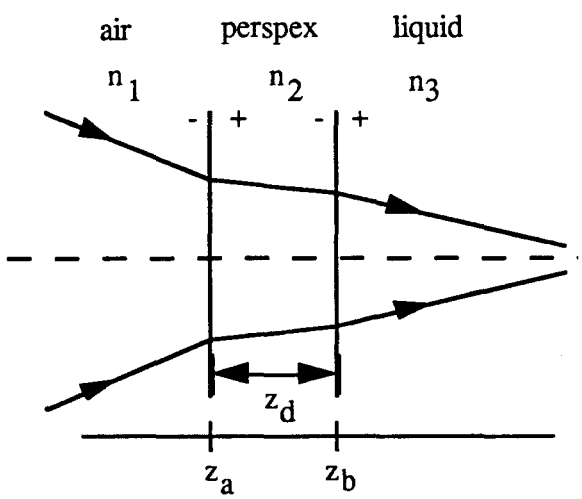

Figure D.2. Illustration of parameters.

It follows from equation (D.5) that waist length, waist and divergence simply transform to respectively

$$\begin{aligned} L_{w3} &= \left(\frac{n_3}{n_1}\right) L_{w1} \\ w_{03} &= w_{01} \\ \alpha_{03} &= \left(\frac{n_1}{n_3}\right) \alpha_{01} \end{aligned} \tag{D.6}$$

where the relation for the divergence α_0 is in fact the paraxial representation of Snell's law. We can use (D.5) also to calculate the required distance between lens and perspex container to obtain the desired position of the focal plane that is in the centre of the container. We then rework (D.5) with the aid of definition (D.2a)

$$q(z_a^-) = \left\{\left(\frac{n_1}{n_3}\right)(z_a + z_d)^+ - \left(\frac{n_1}{n_2}\right)z_d\right\} - jL_{w1} \qquad (D.7)$$

Substitution of the respective values in the real part of $q(z^-)$ leads to

$$\mathrm{Re}[q(z_a^-)] = -78.3 \text{ mm} \qquad (D.8)$$

This is in fact the virtual position of the focal plane with respect to the outer container wall surface that can be realized by putting the lens at (100.0 - 78.3) = 21.7 mm from the container. Because of the symmetry this also holds for the distance between lens and container at the outcoming beam when an object distance of 100 mm is demanded.

2 Determination of beam radii

The intensity profile of a Gaussian beam is described as ([34])

$$I(r,z) = \frac{2P_0}{\pi w^2(z)} e^{-2(r/w(z))^2} \qquad (D.9)$$

where P_0 is the total laser power and w(z) the beam radius as defined in figure D.1.

The value of w(z) was determined experimentally by cutting off the laser beam with a razor blade and measuring the residual transmitted power. See figure D.3. for illustration of this method.

For a certain d the transmitted power P_{tr} is then given by

$$P_{tr}(w(z),d) = \frac{P_0}{2}\left\{1 + \mathrm{erf}\left(\frac{\sqrt{2}d}{w(z)}\right)\right\} \qquad (D.10)$$

The definition of the error function is quoted in appendix C equation (C.7). A computer algorithm was developed to fit experimental data of P_{tr} with varying cut-off parameter d.

In this manner the radius of the assumed parallel beam of the HeNe laser was determined to be 0.42 ± 0.01 mm. Substituting this result in equation (4.12) leads to a theoretical waist behind a 100 mm lens of 48 ± 1 μm. Two measurements yielded values

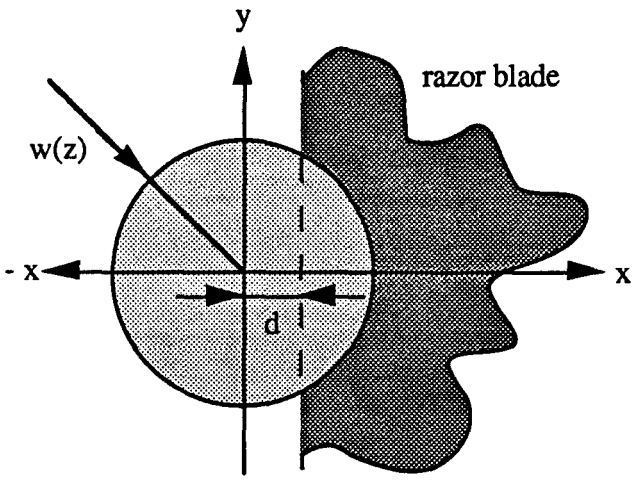

Figure D.3. Determination of a Gaussian beam radius.

of 53 ± 3 and 50 ± 2 μm. Misalignment and the confined validity of the assumed parallellism can account for the slight difference.

3 Sensitivity of the Schlieren set-up

As explained in section 4.2 the sensitivity of the set-up depends on the beam radius at the razor blade. The experimentally obtained value is 4.58 ± 0.01 mm and after setting up the equipment again it showed to be 4.55 ± 0.02 mm.

For the vertical position of the razor blade restricts the measurements to determination of the deflection in the horizontal plane we can only calibrate this deflection. We therefore assume proportional dependency of (now horizontal) deflection φ on the relative signal variation S defined in relation (4.5) as

$$S = \frac{P_{tr} - (P_0/2)}{(P_0/2)} = 2\sqrt{\frac{2}{\pi}}\left(\frac{d}{w(z)}\right) \qquad (D.11)$$

Using relations (4.3) and (4.5) we find

$$\varphi = \left(\frac{w(z)}{2}\sqrt{\frac{\pi}{2}}\right)\left(\frac{f_1}{f_2\,(f_1 - v_1)}\right) S = C \cdot S \qquad (D.12)$$

where the second factor can be understood from figure 4.2. The proportionality constant itself is proportional with beam radius w at the razor blade. We find for the total constant of formula (D.11) $C = 2.72 \cdot 10^{-3}$ rad.

After removal of the positive lens in front of the container the radius at the razor blade has altered to 3.38 ± 0.01 mm and consequently the proportionality constant C changes to $2.01 \cdot 10^{-3}$ rad. The qualitative implication is an increase of sensitivity (of 35 %) for the same deflection induces a larger response signal.

APPENDIX E
Weighted linear regression ([20])

At the basis of normal linear regression on a set of data points (X_i,Y_i) lie the following the conditions:

* The values of X_i are so accurate that the deviation of X_i, σ_x, can be neglected with respect to σ_y

$$\frac{\sigma_x}{|X_{i+1} - X_i|} \ll \frac{\sigma_y}{|Y_{i+1} - Y_i|} \tag{E.1}$$

* The accuracy of the Y_i values is equal for all values.

The second condition is not satisfied in our experiments. Although it appears that the correlation between data points is usually high weighted regression is applied. In this regression method a weight is attached to each data point with the value

$$w_i = \left(\frac{\sigma_{max}}{\sigma_i}\right)^2 \tag{E.2}$$

This implies for the parameters of interest

$$\text{mean :} \quad \overline{X} = \frac{1}{\sum w_i}\sum w_i X_i \quad ; \quad \overline{Y} = \frac{1}{\sum w_i}\sum w_i Y_i \tag{E.3}$$

$$\text{slope :} \quad a = \frac{\sum w_i(X_i - \overline{X})(Y_i - \overline{Y})}{\sum w_i(X_i - \overline{X})^2} \tag{E.4}$$

$$\text{intersection :} \quad b = \frac{\overline{Y}\sum w_i X_i^2 - \overline{X}\sum w_i X_i Y_i}{\sum w_i(X_i - \overline{X})^2} \tag{E.5}$$

$$\text{deviation :} \quad \sigma_a^2 = \left(\frac{1}{\sum w_i(X_i - \overline{X})^2}\right)\sigma_{max}^2 \tag{E.6}$$

$$\text{deviation :} \quad \sigma_b^2 = \left(\frac{\sum w_i X_i^2}{\sum w_i \sum w_i(X_i - \overline{X})^2}\right)\sigma_{max}^2 \tag{E.7}$$

$$\text{and correlation coefficient :} \quad \rho_{xy}^2 = \frac{\left(\sum w_i(X_i - \overline{X})(Y_i - \overline{Y})\right)^2}{\sum w_i(X_i - \overline{X})^2 \sum w_i(Y_i - \overline{Y})^2} \tag{E.8}$$

APPENDIX F
Liquid properties

1 Numbers

The acoustic quantities of the respective liquids are determined experimentally and compared with reference values ([36,37]). The results are given in table F.1.

	silicone oil (Dimeticonum 350)	water	glycerol (Glycerolum 88 %)
density (g/cm^3)			
experiment	0.85 ± 0.07 (8%)	0.998 ± 0.004 (0.4)	1.06 ± 0.02 (2%)
reference [36]	0.76	0.998	1.26
reference [37]	-	0.998	1.26
supplier	-	-	1.23-1.24
sound velocity (10^3 m/s)			
experiment	1.01 ± 0.03 (3%)	1.44 ± 0.06 (4%)	1.77 ± 0.06 (3%)
reference [36]	0.79	1.484	1.93
reference [37]	-	1.497	1.904

Table F.1. Determination of the acoustic properties of the respective liquids.

2 Experimental determination

The density is obtained in the following way. The mass of five empty, dry test-tubes and the complementary caps is obtained with the aid of a precision balance. Then each test-tube is filled with 5.0 ml of the respective liquid. This volume is measured with a pipette. Again the mass is determined and the difference divided by 5.0 yields the density.

The measurement of the sound velocity is performed with the aid of two high-frequency piezo-crystals. These pressure transducers can be applied both as a transmitter and receiver. Two of these transducers are positioned at a certain distance with their flat interfaces parallel to each other within 1 % except for one measurement (3.5 %). The

distance is obtained with a marking gauge before and after the experiment at three different positions at the edge of the flat piezo elements.

Both pressure transducers are totally submersed in the liquid. A control device (Panametrics 5055PR) enables transmitting operation of one transducer and simultaneous receiving operation of the other specimen. Both driving and measured pulses can be obtained at an output entrance of this device. This output signal is analyzed with an oscilloscope (Tektronix 2440). The cursor function of the scope is used to determine time intervals between pulses. For each measurement two time intervals namely between driving pulse and first received pulse and between the first received pulse and a reflected pulse are measured five times. This is done at two different distances between the transducer interfaces for each medium.

3 Discussion

The experimentally obtained values do not agree with reference values for both silicone oil and glycerol.

Compared to water these media are very viscous. This implies that application of a pipette can lead to a systematic error as a relatively large fraction of the liquid will remain behind so that the volume will be overrated. However the resulting density for silicone oil is too high.

Another possibility for explanation of the discrepancy is that glycerol might be very hygroscopic. The glycerol has been exposed to free air for several days. Information of the supplier learns that the requirements for glycerol are $1.229 \leq \text{density} \leq 1.235$ and $0.835 \leq \text{fraction} \leq 0.885$. Dissolving water can never account for the low result on density as this requires a 0.77 water fraction[1]. The most logical explanation still seems to be a systematic error due to the high viscosity.

The measurement of acoustic velocity gives an identical general impression. Agreement for water and none for the viscous media. A few remarks give an inventory of possible complications and explanations for this discrepancy:

* Acoustic theory is not valid for viscous media;
* The measurements are performed with high-frequency signals[2]. This improves the similarity with pressure waves that can be expected in the lithotripsy experiments.

---

1 $1.26 \cdot (1 - x) + 1.00 \cdot x = 1.06 \quad \Rightarrow \quad x \cong 0.77$.

2 Fourier transformation of the driving pressure signals yields a spectrum with a pronounced peak at approximately 5 MHz.

However the velocity of pressure waves is probably frequency-dependent as are eventual damping and dispersion effects.

* It is possible that a certain depth or in other words a certain amount of water above the measuring position is required for proper performance of the experiments.

Lastly the fact that for each medium the discrepancy in both quantities is consistent in terms of its sign should be remarked.

APPENDIX G
Table of the results

Explanation of the respective quantities. For every distance h 10 identical measurements of relative signal S at at least 11 different pulse energies are carried out (110 measurements for each h). At each pulse energy the mean value $\overline{X}$ and mean deviation σ_m are used in for weighted linear regression that gives as a result slope a and intersection b with their respective accuracies and correlation coefficient rho. These results are used to calculate the threshold energy and its deviation in the following manner

$$E_{thr} = \frac{-b}{a};$$

$$|dE| = \left| E - \max\left(\left\{ \frac{-(b - \sigma_b)}{(a + \sigma_a)} \right\}; \left\{ \frac{-(b + \sigma_b)}{(a - \sigma_a)} \right\} \right) \right|$$

The deviation dh is a consequence of the uncertainty in determining the setting of the micromanipulator when h equals zero. This setting is also averaged over at least 10 measurements with the resulting standard deviation being dh.

	h (μm)	dh (μm)	h / D	a (mJ^-1)	da (mJ^-1)	b	db	E (mJ)	dE (mJ)	dE/E	rho
water	27	9	0.045	0.0264	0.0007	-0.34	0.0164	12.87	0.265	0.021	0.959
600 μm	57	20	0.095	0.0371	0.0012	-0.3626	0.0309	9.773	0.525	0.054	0.98
	82	20	0.136	0.0323	0.0016	-0.3511	0.0404	10.86	0.734	0.068	0.906
	90	20	0.15	0.0232	0.0006	-0.2749	0.0159	11.83	0.383	0.032	0.936
	90	20	0.15	0.0188	0.0003	-0.2434	0.0069	12.97	0.195	0.015	0.967
	99	21	0.165	0.0219	0.0009	-0.1286	0.0161	5.861	0.505	0.086	0.926
	107	20	0.178	0.0325	0.001	-0.3566	0.0279	10.98	0.525	0.048	0.984
	132	20	0.22	0.0353	0.0012	-0.4534	0.0371	12.84	0.628	0.049	0.968
	132	20	0.22	0.0301	0.0012	-0.3294	0.0344	10.95	0.737	0.067	0.978
	157	32	0.261	0.0237	0.0011	-0.1756	0.0358	7.411	1.225	0.165	0.959
	207	20	0.345	0.0271	0.003	-0.228	0.0704	8.42	1.869	0.222	0.746
	267	9	0.445	0.0255	0.0008	-0.3088	0.0174	12.09	0.31	0.026	0.974
	517	9	0.861	0.0195	0.001	-0.1514	0.0209	7.768	0.71	0.091	0.887
	749	21	1.248	0.0086	0.0004	-0.0264	0.007	3.061	0.709	0.232	0.877
	999	21	1.665	0.0096	0.0006	-0.0664	0.0123	6.925	0.91	0.131	0.877
	1249	21	2.081	0.0062	0.0005	-0.0374	0.0121	5.993	1.616	0.27	0.954
	1524	21	2.54	0.0048	0.0002	-0.0471	0.0046	9.737	0.601	0.062	0.935

	h (µm)	dh (µm)	h / D	a (mJ^-1)	da (mJ^-1)	b	db	E (mJ)	dE (mJ)	dE/E	rho
water	50	15	0.156	0.0209	0.0012	-0.1029	0.0148	4.913	0.462	0.094	0.889
320 µm	100	15	0.312	0.0286	0.0011	-0.1923	0.0137	6.728	0.216	0.032	0.946
	160	15	0.5	0.0171	0.0017	-0.0956	0.018	5.589	0.546	0.098	0.932
	230	15	0.718	0.0302	0.0011	-0.1506	0.0133	4.989	0.265	0.053	0.969
	330	15	1.031	0.0199	0.0012	-0.0626	0.0132	3.142	0.496	0.158	0.903
	430	15	1.343	0.0137	0.0006	-0.0686	0.0072	4.993	0.318	0.064	0.963
	530	15	1.656	0.0155	0.0007	-0.1199	0.0109	7.738	0.373	0.048	0.929
	630	15	1.968	0.0135	0.0011	-0.1148	0.017	8.497	0.607	0.071	0.965
	730	15	2.281	0.0164	0.0005	-0.0826	0.0089	5.03	0.402	0.08	0.931
	830	15	2.593	0.0126	0.0005	-0.1191	0.0089	9.477	0.352	0.037	0.978
	1030	15	3.218	0.0092	0.0006	-0.0902	0.0111	9.812	0.632	0.064	0.946
	1330	15	4.156	0.005	0.0002	-0.0504	0.0047	10.05	0.486	0.048	0.941
glycerol	128	19	0.4	0.0416	0.0034	-0.1765	0.0271	4.243	0.332	0.078	0.961
320 µm	228	19	0.713	0.0454	0.0043	-0.2058	0.037	4.535	0.424	0.094	0.979
	324	12	1.013	0.0453	0.002	-0.2546	0.0237	5.617	0.282	0.05	0.952
	328	19	1.025	0.0414	0.0044	-0.1801	0.0364	4.348	0.465	0.107	0.976
	428	19	1.338	0.0466	0.0029	-0.251	0.0254	5.391	0.223	0.041	0.942
	528	19	1.65	0.0412	0.0028	-0.2171	0.0265	5.266	0.306	0.058	0.971
	634	12	1.981	0.028	0.0027	-0.1188	0.0287	4.238	0.685	0.162	0.899
	794	12	2.481	0.0281	0.002	-0.1547	0.0234	5.497	0.475	0.086	0.888
	954	12	2.981	0.0234	0.0028	-0.1389	0.0359	5.94	0.925	0.156	0.928
	1114	12	3.481	0.024	0.0016	-0.1736	0.0222	7.244	0.475	0.066	0.967
	1294	12	4.044	0.0136	0.0018	-0.0774	0.0242	5.684	1.186	0.209	0.947
silicone oil	58	15	0.181	0.117	0.016	-0.4391	0.0948	3.755	0.343	0.091	0.931
320 µm	86	23	0.269	0.165	0.0128	-0.5425	0.0598	3.289	0.117	0.035	0.977
	118	15	0.369	0.159	0.0202	-0.57	0.1155	3.584	0.31	0.087	0.923
	168	15	0.525	0.154	0.0197	-0.5503	0.1196	3.573	0.366	0.103	0.864
	218	15	0.681	0.1901	0.0118	-0.8415	0.075	4.426	0.127	0.029	0.953
	266	23	0.831	0.1415	0.0245	-0.4695	0.1293	3.317	0.41	0.124	0.894
	268	15	0.838	0.157	0.0128	-0.6568	0.0869	4.185	0.232	0.055	0.983
	318	15	0.994	0.1151	0.0138	-0.4584	0.0802	3.981	0.25	0.063	0.957
	418	15	1.306	0.1497	0.0139	-0.6169	0.0857	4.121	0.21	0.051	0.928
	516	23	1.613	0.1116	0.013	-0.4086	0.0678	3.662	0.204	0.056	0.944
	618	15	1.931	0.1143	0.0195	-0.4629	0.1281	4.05	0.519	0.128	0.898
	818	15	2.556	0.1042	0.0152	-0.4904	0.0999	4.708	0.317	0.067	0.964
	1068	15	3.338	0.1011	0.01	-0.5395	0.0845	5.335	0.341	0.064	0.926

It can be seen from the table that for all series except one (98 %) the correlation exceeds 0.85. More than half (51 %) even has a correlation of at least 0.95.